UNIVERSITE D'AIX-MARSEILLE

Ecole doctorale 463 – Sciences du Mouvement Humain

IFSTTAR – LBA / LBMC

Thèse présentée pour obtenir le grade universitaire de docteur
Discipline : Sciences du Mouvement Humain
Spécialité : Biomécanique

Audrey CHENEL

Caractérisation morphologique et mécanique du foie humain en vue de l'amélioration d'un modèle éléments finis
Morphological and mechanical characterization of the human liver to improve a finite element model

Soutenue le 03/12/2018 devant le jury :

Pr Rémy WILLINGER	UNISTRA, ICube, Strasbourg	Rapporteur
Pr Yannick TILLIER	CEMEF, Mines ParisTech	Rapporteur
Pr Nicolas CHEYNEL	Hôpital Le Bocage CHRU, Dijon	Examinateur
Dr Aline BEL-BRUNON	LaMCoS – INSA de Lyon	Examinateur
Dr Catherine MASSON	IFSTTAR – LBA	Directrice de thèse
Dr Karine BRUYERE	IFSTTAR – LBMC	Directrice de thèse
Dr Thierry BEGE	AP-HM	Encadrant
Dr Cyril KAHN	IFSTTAR – LBA	Encadrant

Numéro national de thèse/suffixe local : 2018AIXM0721/019ED463

Résumé

Lors des accidents de la voie publique, même si peu de lésions sont dénombrées à l'abdomen en comparaison avec les lésions au niveau de la tête et du thorax, celles-ci sont sévères, mettent la vie du blessé en danger et nécessitent un traitement médical délicat, long et coûteux. Dans ce contexte, il semble important d'offrir une meilleure protection, et ce par une meilleure prévention des lésions abdominales traumatiques. Des modèles numériques de corps humain de plus en plus raffinés ont été développés afin de mieux comprendre les mécanismes de blessure et d'évaluer le risque lésionnel. Les modèles du corps entier tel que HUMOS, THUMS ou GHBMC peuvent reproduire différentes configurations d'impact constatées lors des accidents de la voie publique. La validation de ces modèles nécessite des données expérimentales complémentaires à celles issues d'essais sur corps complets. Ainsi l'objectif de cette thèse est de contribuer au développement d'un modèle numérique de foie humain pour la prédiction de lésions hépatiques en se focalisant sur le choc frontal qui provoque une décélération du foie et des lacérations sur le lobe droit.

Dans un premier temps, une caractérisation morphologique du foie a été réalisée sur soixante-dix-huit scanners de patient sain. La base de données ainsi constituée comprend les caractéristiques de l'anatomie externe du foie comme son volume, sa longueur antéro-postérieure, médio-latérale ou cranio-caudale, des caractéristiques internes, à savoir les volumes des différents segments de Couinaud, des caractéristiques sur les vaisseaux hépatiques, comme le diamètre de la veine cave et de la veine porte, ou encore des caractéristiques sur sa position au sein de la cage thoracique. Une étude statistique nous a permis de mettre à jour l'existence de quatre morphotypes qui peuvent être liés à la morphologie de l'individu.

En vue de valider les modèles numériques du foie, des essais sur organes isolés sont utiles pour compléter les essais sur corps complet. Ils permettent de mieux maitriser les conditions aux limites et offrent la possibilité d'observer plus facilement l'organe. De plus, la fiabilité des modèles numériques demande de connaitre le comportement jusqu'à la rupture des tissus dans un état le plus physiologique possible. Or l'essentiel des essais expérimentaux proposés dans la littérature ont été réalisés sur échantillons de tissu hépatique ou sur foies non pressurisés. Deux campagnes d'essais ont été ainsi menées. L'objectif de la première était d'évaluer les déformations de la capsule de Glisson par corrélation d'image 3D en fonction de différents niveaux de pressurisation. Elle nous a permis de mettre en évidence l'influence non négligeable de la pressurisation des vaisseaux sur la déformation initiale de capsule. La seconde avait pour but d'identifier la déformation à rupture locale lors d'un choc frontal grâce à des tests de décélération. Les

mesures de champ de déformation ont alors permis d'identifier le mécanisme de rupture de la capsule.

Enfin, un modèle numérique générique de foie a été construit et utilisé pour simuler les essais de décélération réalisés dans la partie expérimentale. Les quatre morphotypes identifiés ont été implémentés dans le modèle générique montrant l'importance de la morphologie dans la réponse des modèles numériques.

Mots clés : Foie, Morphotype, Corrélation 3D, Pressurisation, Décélération, Modèle numérique

Abstract

In road accidents, even if there are few lesions of the abdomen compared to the lesions of the head or the thorax segment, those lesions are severe, life-threatening, and require a delicate, long and expensive medical treatment. In this context, it seems important to offer a better protection by better prevention of traumatic abdominal lesions. Numerical models of the human body have increasingly been developed to better understand the mechanisms of injury and assess this risk of injury. Models of the whole body such as HUMOS, THUMS or GHBMC can reproduce different impact configurations found in road accidents. The validation of these models requires experimental data complementary to those obtained from whole body tests. Thus, the aim of this thesis is to contribute to the development of a numerical model of the human liver for the prediction of liver lesions by focusing on the frontal shock, which causes a deceleration of the liver and lacerations on the right lobe.

First, a morphological characterization of the liver was performed on seventy-eight healthy patient scanners. The database thus constituted includes the characteristics of the external anatomy of the liver include its volume, antero-posterior, medio-lateral or cranio-caudal lengths; internal characteristics, namely the volumes of the different segments of Couinaud; characteristics on the hepatic vessels, such as the diameter of the vena cava and the portal vein; information on its position within the thoracic cavity. A statistical study allowed us to highlight the existence of four morphotypes that may be related to the morphology of the individual.

In order to validate digital models of the livers, isolated organs tests are useful for completing full body tests. They make it possible to better control the boundary conditions and offer the possibility of observing the organ more easily. Moreover, the reliability of numerical models requires to understand the behavior until rupture of the tissues in a most physiological state as possible. However, most of the experimental tests proposed in the literature were performed on samples of liver tissue or on non-pressurized livers. Two test protocols were thus conducted. The objective of the first one was to evaluate the strain state of the Glisson capsule by 3D digital image correlation according to different levels of pressurization. It allowed us to highlight the significant influence of the pressurization of the vessels on the initial strain state of the capsule. The second was to identify the local ultimate strain during a frontal impact through deceleration tests. The strain field measurements then made it possible to identify the mechanism of rupture of the capsule.

Finally, a generic numerical model of the liver was constructed and used to simulate the deceleration tests performed in the experimental part. The fourth identified

morphotypes were implemented in the generic model showing the importance of morphology in the response of numerical models.

Acknowledgements

I would like to thank my current firm, Newclip Technics and of course Jean-Pierre Podgorski and Grégoire Larché, for their support to help me finish my thesis the fourth year. Most of all, thank you to Philippe Berton for trusting me and welcoming me to his division. Thanks to Avi for having us immediately integrated into the BE. And last but not least thank you to all the BE and especially Sami, Clarisse and Lisa. Sami thank you for your humor that livens up our days; Clarisse thank you for your frankness and your good mood; and Lisa thank you for being my second half even if you gave up the upper limb.

I would like to thank my parents for allowing me to become the woman I am today, for pushing me to always give the best of myself. I would like to thank my brother and all my in-laws for being there all along this journey. Thank you for all the moral support you have given us.

And of course, I would like to thank more than anyone Mathias, the man of my life, who supported me during these four years, who helped me to keep in sight our common goal. Thank you for our little family who is growing up with Miha and Loki. Thank you for being the half that I missed, anger when I no longer have the strength to react; patience when I would like everything to go faster.

Table of contents

List of figures

List of tables

INTRODUCTION

Abdominal trauma is observed following a fall, a shock during road accidents or the penetrations of a sharp object. Road accidents represent the majority of trauma in the abdomen[1]. It is therefore in shock that this part of the body is most often injured, resulting from a simple contusion to a hepatic avulsion[2]. In road accident, even if there are few lesions of the abdomen compared to the lesions of the head or the thorax segment, those lesions are severe, life-threatening, and require a delicate medical treatment. In this context, it seems important to offer a better protection by better prevention of abdominal lesions.

Numerical models of the human body have increasingly been developed to better understand injury mechanisms and quantify injury criteria. Models of the whole body[3] can be used to reproduce different impact configurations of road accidents. Those models tend to be more and more accurate, with the distinction of mains organs and vessels, and some of them include the physiology of the muscles[4]. Moreover, dedicated tools have been developed for their posture and geometry personalization[5]. The validation of these human body models requires experimental data obtained from tests on both whole body and isolated organs

In the abdominal region, the liver is a preponderant organ by its volume and its vital functions. The liver is partially covered by the rib cage, which makes it vulnerable to frontal or oblique abdominal impact or loading with the safety belt. The aim of this thesis is to acquire new knowledge on the variability of the geometry of the liver and on its mechanical behavior to contribute to the development of liver numerical models for injury risk prediction.

When developing numerical models, we faced different issues. First of all, on the geometry of the organ. Indeed, as there is a geometric variability, a personalization of the geometry for each subject can be realized. But for the development of numerical models to assess road injury criteria, generic models need to be considered. It is therefore necessary to target higher risk population and to define liver morphotypes. Finally, on the mechanical behavior. Indeed, the physiological functioning cannot be ignored in the analysis of the mechanical response of the liver. *In vivo*, however, we cannot invasively

---

[1] Abri et al, 2016, Blunt Abdominal Trauma and Organ Damage and Its Prognosis." J. Anal Res Clin Med 4 (4): 228–32.

[2] Tinkoff et al, 2008, "American Association for the Surgery of Trauma Organ Injury Scale I: Spleen, Liver, and Kidney, Validation Based on the National Trauma Data Bank." Journal of the American College of Surgeons 207 (5): 646–55.

[3] HUMOS, THUMBS or GHBMC

[4] Salin et al, 2016, Implementation of reflex loops in a biomechanical finite element model. *Computer methods in biomechanics and biomedical engineering*, *19*(14), 1578-1582.

[5] HUMOS2, PIPER

study this mechanical behavior. It would be interesting to carry out *ex vivo* tests on an isolated organ placed in a physiological situation.

In the part A of the manuscript, after a review of the literature on the liver anatomy, we present the work done to identify liver morphotypes in a population of seventy-eight healthy patients. Characteristics of the external geometry of the liver, of its internal geometry, of the hepatic vessel network, and of the liver position within the thoracic cavity were quantified from scanner imaging and a statistical analysis was performed.

The part B of the manuscript presents the experimental work. Two experimental protocols were conducted. The objective of the first one was to evaluate the strain state of the Glisson capsule by 3D digital image correlation according to different levels of pressurization. The second was to identify the local ultimate strain during a deceleration tests with a frontal impact on the right lobe.

The part C of the manuscript presents the use of a generic numerical model of the liver to simulate the deceleration tests performed in the experimental part. Then to highlight the influence of the geometrical variability of the organ on the its mechanical response to an impact, models corresponding to the previously identified morphotypes were used to simulate the same deceleration test

Finally, a general conclusion of the interest of developing different numerical models according to the morphotype of the liver will be established.

Part A: Morphological characterization of the liver

Knowledge of the liver morphology is very important in many fields: in the clinical field, morphotypes can be used for the development of new surgical instruments, and the implementation in finite elements models for pedagogical purposes; in the trauma field, morphotypes will be important to implement numerical models of the human body with a bio-accurate model of the liver in order to correctly predict the risk of lesions of internal organs.

Do different liver morphotypes can be identified and correlated to the anthropometry of the individuals?

Chapter 1 presents a review of the literature on the anatomy of the liver and the different attempts to determine morphotypes. Chapter 2 presents the database constructed and the parameters studied. Finally, Chapter 3 presents the methodology followed and the results found on the elaboration of different morphotypes of liver.

Chapter 1: Anatomical description of the liver – A review

The following chapter details a review of the literature on the external and internal anatomies of the liver, its location within the ribcage, and the anatomy of the hepatic vessels, and describes the different anatomical variations.

Table of contents

1. General anatomy of the human body

1.1. Anatomical terminology

The terminology expose in this section is proper to anatomist. These terminologies are important to properly understand the scientific work of this report and avoid any ambiguity. By convention, a reference position is used to describe the human body: the standard anatomical position. In this position, a person is standing, feet apace, with palms forward and thumbs facing outward (OpenStax, 2016). The Terminologia anatomica (1998), developed by the Federative Committee on anatomical terminology (FCAT) and the International Federation of Associations of Anatomists (IFAA) is the international standard on human anatomic standard. Thus, to locate the different structures in 3-dimensional space, three planes have been defined, as well as terms to orientate the structure, as shown in Fig A- 1.

Fig A- 1. Anatomical terms of location (Kamina, 2014)

A. Sagittal	C. Transverse	1. Proximal	3. Cranial	5. Anterior	7. Lateral
B. Frontal		2. Distal	4. Caudal	6. Posterior	8. Medial

The sagittal plane divides the body into two parts: left and right. Parasagittal planes are parallel to it. The frontal plane divides the body into posterior (dorsal) and anterior (ventral) portion. The transverse plane separates the inferior (caudal) from the superior (cranial). Some directions are deduced from these planes. Then, "medial" refers to a structure close to the center of the body in opposition to "lateral" which refers to the sides of the body.

1.2. Organization of the body and the abdominal cavity

Cells, which are the basic structural functional and biological units, make up the human body. A lot of different cells can be counted according to their structural or functional role. Thanks to the gathering of cells, different structures can be identified. Tissues like lining cells, connective tissue, nervous tissue and muscle tissue, are defined as cells that act with the same specialized function. Organs are defined as a collection of cells and tissues with a specific function, as the liver. Then, systems are defined as a network of organs with the same goal, like the digestive systems.

The body maintains its internal organization by means of membrane. Specific membranes divide the body into several cavities as shown in Fig A- 2:

- Dorsal cavity:
  - Cranial cavity enclosed by the skull and containing the brain.
  - Vertebral canal enclosed by the spine.
- Ventral cavity:
  - Thoracic cavity enclosed by the ribcage. This cavity protects sensitive organs like the heart and the lung.
  - Abdominopelvic cavity:
    - Pelvic cavity enclosed by the pelvis and containing the reproductive system
    - Abdominal cavity, enclosed by the ribcage and the pelvis, this cavity is containing the digestive organs as the liver.

Fig A- 2. Human body cavities (OpenStax, 2016)

The abdominopelvic cavity can be divided in nine regions thanks to horizontal and vertical lines as shown in Fig A- 3:

- Horizontal lines:
    - Subcostal line is the horizontal line from the subcostal arch (tenth rib).
    - Intertubercular line is between the two rough tubercles[1]
- Vertical lines:
    - Right line cut the intertubercular line at the ileocecal valve[2].
    - Left line corresponds to the inner edge of the descending colon.

Fig A- 3. Nine-abdominal-region scheme (OpenStax, 2016)

The major part of the abdominal wall is constituted from a serous membrane: the parietal peritoneum. Moreover, the viscera are covered by visceral peritoneum. Parietal peritoneum and visceral peritoneum define the peritoneal cavity, which contains the greater part of the digestive system such as the spleen, the kidney and the liver. A peritoneal fluid lubricates the surface of tissues and decreases the friction between organs and abdominal wall. The normal peritoneal fluid volume rarely exceeds 5 mL in men and 18 mL in women (Balfe et al., 2009).

---

[1] Tubercle: Round nodule, small eminence or warty outgrowth found on external or internal organs.
[2] Ileocecal valve: Sphincter muscle valve which separates the small and the large intestine.

2. Liver anatomy

2.1. Gross anatomy

The liver is located in the upper right quadrant of the abdomen right below the diaphragm[1]. It takes the whole right hypochondriac region and extends itself in the anterior part of the epigastric region, in front of the stomach (Chevallier et al., 2011) up to the left hypochondriac region (Rouiller, 1964). It is highly recovered by the ribcage. Moreover, the position of the body seems to influence the location of the liver. On one hand, there is little difference in the sagittal plane and the transverse plane between the supine and the seating position. On the other hand, there is a difference of 34 ± 16 mm in the frontal plane (Beillas et al., 2009; Howes et al., 2013).

The human liver is wedge-shaped with a big right extremity and a slender left extremity. It is the largest gland and the heaviest internal organ of the abdomen. It measures approximately 28 cm in the medio-lateral direction, 8 cm in the cranio-caudale direction and 15 cm in the anteroposterior direction (Cuilleret and Bouchet, 1991). It weight is around 1.5 kg that is 2-3% of the body mass (Guyton, 1976). The liver is highly vascularized; indeed, it contains permanently 450 mL of blood, which gives it its dark reddish-brown color (Castaing et al., 2006). A quarter of the cardiac supply is received by the portal vein and the hepatic artery and restored through the heart by the inferior vena cava (Neviere, 2005). The hepatic vasculature is surrounded by a brittle parenchyma, covered by a fibrous capsule: the Glisson's capsule.

From an external viewpoint, the liver presents three faces shown in Fig A- 4 & Fig A- 5:

- The diaphragmatic surface covers the convex shape of the diaphragm. The liver is covered by a thin double-layer membrane, the peritoneum, which folds back on itself to form the falciform ligament and the right and left triangular ligaments.
- The visceral or inferior surface is uneven and concave and fit closely the viscera below it (Williams at al., 1989). A left anteroposterior fold contains the round ligament, and a deeper transversal dip protects the porta hepatis (Vitte and Chevallier, 2006). The four lobes are visible on the surface: the right, left, caudate and quadrate lobe.
- The posterior surface is vertically. Two folds are visible for the vena cava and the ligament of ductus venosus.

---

[1] Diaphragm: internal skeletal muscle which separates the thoracic cavity from the abdominal one.

Fig A- 4. Anterior view of the liver (Netter, 2014)

Fig A- 5. Inferior view of the liver (Netter, 2014)

2.2. Environment of the liver

The liver is fixed by the vena cava thanks to the hepatic veins and some adhesion of the parenchyma. It is also maintained by the porta hepatis, which contains the hepatic artery, the portal vein and bile[1] ducts; and by the different ligaments[2], which link the liver to the diaphragm, the stomach and the umbilicus.

The different ligaments, presented in Fig A- 6 & Fig A- 7, are the following:

- The coronary ligament joins the diaphragmatic surface of the liver to the diaphragm. It is divided into two layers, which merge to form the triangular ligaments.
- The falciform ligament is vertical on the diaphragmatic surface. It is extended by the round ligament.

---

[1] Bile: Dark green to yellowish brown fluid produced by the liver which aids the digestion of lipids in the small intestine.
[2] Ligament: Refer to a fold of peritoneum or other membranes.

- The lesser omentum is a double layer, which links the liver to the stomach and the first part of the duodenum.

Moreover, the liver is maintained by other organs since its posterior surface lies on the right kidney, and the visceral surface is in contact with the viscera, the duodenum[1], the pancreas and the transverse colon. Finally, the diaphragmatic face is protected by the ribcage, especially from the sixth to the tenth ribs (Melvin, 1988).

2.3. Vascularization and associated classification

2.3.1. Vascularization of the liver

The distinctive feature of the liver is that it receives a dual blood supply from the hepatic portal vein and the hepatic artery. The flow in this vein is about 1000 mL/min and the blood pressure is around 10 mmHg (Abdel-Misih and Bloomston, 2010; Guyton, 1976; Ottensmeyer et al., 2004). In the hepatic artery, the blood flow is about 280 mL/min and the blood pressure between 80 and 120 mmHg (Guyton, 1976; Ottensmeyer et al., 2004; Rouiller, 1964; Zoli et al, 1999). Two groups of vessels can be defined:

- The afferent[2] ones, known as the portal triad, gathered (Fig A- 6):
  - The portal vein which carries the blood from the gastrointestinal tract and spleen to the liver. It measures between 15 and 20 mm for a diameter of 9 mm (Castaing at al, 2006). Thanks to this vein, all the blood rich in nutrients extracted from the food is filtered;
  - The hepatic artery which supplies oxygenated blood to the liver;
  - The biliary tract.

Fig A- 6. The portal triad on a ventral view of the liver (Sobotta, 2006)

---

[1] Duodenum: First section of the small intestine.
[2] Afferent: Conveying towards the liver.

- The efferent[1] ones are the hepatic veins. They are divided in three major veins which drain the right, middle and left regions of the liver and merge in the inferior vena cava (Fig A- 7).

Fig A- 7. The hepatic veins on a ventral view of the liver (Sobotta, 2006)

2.3.2. Classification of the liver

In the anatomical description of the liver, there are two schools of thought: the morphological anatomy and the functional anatomy. From the morphological anatomy point of view, four lobes are made out through surface characteristics (Skandalakis, 1989; 2004) as shown in Fig A- 4 & Fig A- 5. The left and right lobes are separated by the falciform ligament. The caudate lobe is on the postero-superior surface of the liver, upon the portal triad, between the inferior vena cava and the ductus venosus. The quadrate lobe is below the portal triad between the gallbladder and the umbilical vein. This classical description does not take account of the internal vascularization. For example, the quadrate lobe morphologically comes from the right lobe, but is functionally close to the left lobe (Rutkauskas et al, 2006).

From the 50s, different classifications of functional anatomy of the liver have been proposed and are presented in Table A- 1. Healey and Schroy (1953) are the first to divide the liver into functional parts, based on the biliary ducts and the branches of the hepatic artery. Goldsmith and Woodburne (1957) proposed a classification based on the portal vein and the hepatic veins. Nevertheless, no distinction is done between the inferior and superior part, which becomes mandatory with the development of surgical technique. Thus, Couinaud (1957) took over this classification and proposed eight subsegments as shown in Fig A- 8. Nowadays, Couinaud's classification is widely used in Asia and Europe (Rutkauskas et al, 2006).

---

[1] Efferent: Conveying away from the liver.

Fig A- 8. Couinaud's classification (Bismuth, 1982)

Bismuth (1982) took over the work of Couinaud, Goldsmith and Woodburne and distinguished the fourth subsegment into two 4a and 4b (Fig A- 9). This classification is popular in Europe and America as it corresponds to the need of surgeons and radiologists.

Fig A- 9. Bismuth's classification (Smithuis and de Lange, 2015)

In 1998, the IHPBA (International Hepato-Pancreato-Biliary association) (Strasberg, 2005) establishes a committee to unify the terms used for classification. No classification has been proposed but only a nomenclature as followed:

- First-order division: Hemiliver (right and left hemiliver)
- Second-order division: Section (right anterior and posterior sections, left medial and lateral section)
- Third-order division: Segment (Segments 1-9).

Table A- 1. The different classification of the liver (Rutkauskas et al., 2006)

Part	Classification									
	J.E. Healey and P.C. Schroy (1953)		N. Goldsmith and R. Woodburn (1957)		C. Couinaud (1957)		H. Bismuth (1982)		FCAT (Whitmore, 1999)	
	Segment	Sub-segment	Segment	Sub-segment	Part	Segment	Part	Segment	Part	Segment
Dorsal	Caudal	Right	Caudal lobe		Caudal lobe	I	Caudal lobe	I	Caudal lobe	Posterior, I
		Left								
Left	Lateral	Superior	Lateral	Superior	Lateral	II	Posterior	II	Lateral	Posterior, II
		Inferior		Inferior	Para median	III	Anterior	III		Anterior, III
	Medial	Superior	Medial	Superior		IV		IVa, IVb	Medial	Medial, IV
		Inferior		Inferior						
Right	Anterior	Inferior	Anterior	Inferior	Para median	V	Antero-medial	V	Medial	Anterior, V
		Superior		Superior		VIII		VIII		Posterior, VIII
	Posterior	Inferior	Superior	Inferior	Lateral	VI	Postero medial	VI	Lateral	Anterior, VI
		Superior		Superior		VII		VII		Posterior, VII

Finally, Fasel et al. (2010) studied the classification of the liver and proposed a new concept "1-2-20", in which the liver can be divided into levels. First, the whole liver, then the hemilivers, and finally an average of 20 bifurcations marked out 20 areas. The Couinaud's approach is in accordance with the classification of Fasel et al. (2010) as the segments are a merging of areas. So, it's highly recommended to use the Couinaud's classification while keeping in mind the high number of areas.

2.4. Microanatomy of the liver

The liver consists of epithelial[1] and mesenchymal[2] elements arranged in repetitive microscopic units (Krishna, 2013).

2.4.1. Main components

The main structural components of the liver are presented in Fig A- 10. The elementary structure of the liver is the hepatocytes. They are polygonal and measure 25 to 40 μm. The hepatocytes normally are arranged in cords and separated by sinusoids. Sinusoïds are channels through which blood flows from portal tracts to hepatic venule. A portal tract comes from the hilum, and gathers bile duct and ductules, hepatic artery, portal vein, lymphatic vessels, nerve fibers and a few inflammatory cells.

---

[1] Epithelium: One of the four basic types of animal tissue with connective tissue, muscle tissue and nervous tissue.

[2] Mesenchyme: Also known as mucous connective tissue or mucoid connective tissue is a type of connective tissue.

All the hepatic venules merge in one hepatic vein. Blood flows from the portal tract to the venules with a decreasing oxygen and nutrient gradient.

Fig A- 10. Photomicrograh which illustrates the periportal (PP), the midlobular (MZ) and the centrilobular (CL) zones, with the portal tracts (PT) and the hepatic venule (CV/THV), from Krishna (2013)

2.4.2. Hepatic lobule

The microscopic structure of the liver can be conceptualized in two points of view. The first traditional point of view is the hepatic lobule, which are hexagonal and consist of a central vein, a hepatic venule, and surround by portal tracts at each angle (Fig A- 11). The lobules measure 0.8 mm high and have a diameter of 2 mm (Guyton, 1976).

Fig A- 11. Scheme of a hepatic lobule (Kamina, 2014)

The second point of view; which places the small portal tract at the center and the terminal hepatic venule, locates at the periphery, is named acinus.

2.5. Morphological variation

2.5.1. Variation of the external shape of the liver

2.5.1.1. Opposition slender and stocky morphologies

The global morphology of the liver can vary from one person to another. The development of each lobe depends of the overall morphology of the person. Two morphotypes have been proposed by Caix and Cubertafond (1978), according to the morphology of the subject.

- In the slender morphology, the thoracic-abdominal region is narrow and the sternal angle[1] is closed. The height of the diaphragmatic dome and the depth of hypochondrium are small. In this configuration, the hepatic parenchyma is deformed towards the right and the front. The left lobe is minimal while the right lobe has the maximum development. The liver has a dorsal-sagittal shape. It is only partially protected by the rib cage (Fig A- 12b).
- In the stocky morphology, the thoracic-abdominal region is large, and the sternal angle is open. The height of the diaphragmatic dome and the depth of hypochiondrium are important. Then, the left lobe of the liver spreads in the left hypochondriac and covers the abdominal esophagus. The development of the right lobe is only moderate. The liver has a ventral-frontal shape. It is almost completely protected by the rib cage (Fig A- 12a).

Fig A- 12. a. Stocky morphology; b. Slender morphology (Caix and Cubertafond, 1978)

---

[1] Sternal angle: It is the angle formed by the articulation of the manubrium (the broad upper part of the sternum) and the body of the sternum.
Sternum: Long flat bone which connects to the ribs, forming the front of the ribcage.

2.5.1.2. Different morphotype aspects

Since Caix and Cubertafond (1978), other researchers looked into the morphotypes of the liver. Thus, Nagato et al. (2011) classify the liver into nine groups:

- Six nurtures[1] ones:
  - Normal liver
  - Liver with lingular process[2]
  - Costal liver with a very small left lobe and deep impressions
  - Liver with deep renal impression and "corset" type constriction
  - Liver with biliary vesicle invading the diaphragmatic face
  - Liver with diaphragmatic impressions
- Three congenital[3] ones:
  - Liver with a right lobe very much smaller than the left
  - Transversal liver with a large left lobe
  - Liver with total atrophy of the left lobe

2.5.1.3. Pathological cases

Contrary to the variations, anomalies of the hepatic morphology are unusual (Champetier et al, 1985; Fraser, 1952; Vinnakota and Jayasree, 2013). This statement is in accordance with the study of Nagato et al. (2011) since the congenital abnormality represent less than 10% of the case. It is usually the consequence of an excessive development or the lack of development of one of the lobes. Some cysts can be noted and more rarely an additional lobe (Fraser, 1952).

2.5.2. Variation of the vascularization

In this part, the variation of vascularization is studied for the arteries and veins into the liver parenchyma. The variation of the superior vena cava will not be exposed.

2.5.2.1. Variation of the portal vein

The portal vein is usually divided into three branches in the liver, the right branch, the left branch and the cystic vein[4] (median branch). The bifurcation of the portal vein exists in 70 to 80% of the case (Lafortune et al, 2007). The main variation (15-20% of the cases) is the lack of trunk of the right portal branch. This can be due to a trifurcation in 10% of the

---

[1] Nurture: A disease or a physical abnormality developed with time.
[2] Lingular process: Prolongation of one of the liver lobes.
[3] Congenital: A disease or a physical abnormality present from birth.
[4] Cystic vein: It drains the blood from the gall-bladder and usually ends in the right branch of the portal vein.

cases. In some cases, the right part of the liver is irrigated by a bifurcation ahead or a bifurcation on the left portal branch.

2.5.2.2. Variation of the hepatic artery

The hepatic artery proper is a branch of the hepatic artery. It bifurcates into three branches, such as the portal veins, the right and left hepatic arteries and the cystic artery[1]. The branches of the hepatic artery run close to the portal veins. The main variation comes from the bifurcation between the right and left hepatic arteries. These variations are presented in Fig A- 13.

1	Right hepatic artery
2	Left hepatic artery
2'	Left hepatic artery from the coronary
3	Stomachic coronary
4	Splenic
5	Gastroduodenal
6	Accessory hepatic artery

Fig A- 13. A. and B. Premature division of a unique common hepatic artery; C. and D. embryological placement with three hepatic arteries from the celiac trunk or the mesenteric one. E. Lack of common hepatic artery. F. Hepatic blood supply through the superior mesenteric. G. Hepatic blood supply through the stomachic coronary artery. H. Hepatic blood supply through an artery from the superior mesenteric and one from the coronary. Illustrated from Bouchet and Cuilleret (1991)

2.5.2.3. Variation of the hepatic veins

The vena cava is divided into three hepatic veins in the liver: the left, the median and the right hepatic veins. The left and the median hepatic veins usually have a common core.

The variations of the vena cava are uncommon. It may be the lack of common core of the median and left hepatic veins (15% of the cases), or the presence of a large accessory inferior hepatic vein (15-20% of the cases). A hypoplasia of the right hepatic vein or the splitting into two of the median or left hepatic vein can also be observed (Lafortune et al, 2007).

---

[1] Cystic artery: It supplies oxygenated blood to the gallbladder and cystic duct.

3. Synthesis and problematics

The anatomy of the liver is well known, based on old studies which offer a detailed quantitative description. Moreover, they are rarely challenged. It therefore seems important **to bring new quantitative data describing the morphology of the liver.**

Moreover, some authors highlighted the variability of hepatic anatomy and some suggested the existence of different morphotypes. But the number of morphotypes found in the literature depends on whether the study was performed on *in situ* or *ex vivo* livers. These studies only take into account two characteristic measures to discriminate one morphotype from another or refer to visual characteristics such as costal or diaphragmatic impressions. It seems interesting **to identify if the variability of the hepatic anatomy is due to the existence of different morphotypes**.

Furthermore, only few studies establish a link between the anthropometry of the subject and the morphology of the liver. It seems interesting **to analyze the possible quantitative relationships between the liver morphotype and the anthropometry of the subject.**

In addition, no precise data on the location of the liver regarding other organs and the protection of the ribcage have been found. It seems important **to study the precise location of the liver in the ribcage**, and **to verify the existence of variability**.

As explained previously, just as the parenchyma, the hepatic vessels exhibit some variability. Moreover, these vessels are at the origin of the classification of the liver into segments. Indeed, the Couinaud's classification, which is the most common nowadays, takes into account the path of the vena cava and the portal vein. It seems logical to exclude from the following study the hepatic artery whose path is identical to the portal vein one. So, it will be interesting, in a first step, **to study the variation of the vena cava and the portal vein**. In a second step, it is important **to study the variation of the volume of the segments established by the Couinaud's classification**.

Chapter 2: Quantitative data describing the morphology of the liver

The following chapter describes the methodology to analyze various external and internal geometric characteristics of the liver, its position in the thoracic cage and different geometric characteristics of the associated veins from a database of 78 abdominal CT scans.

Table of contents

1. Study population

This study was carried out on anonymous CT-scans[1] performed on 78 patients of the Mediterranean type at the Department of Medical Imaging and Interventional Radiology at Hôpital Nord in Marseille. This study gathered the CT-scans of 42 women and 36 men. These patients are aged from 17 to 95 years, with no liver disease nor morphological abnormalities of the abdominal organs or the peritoneum. The CT-scans comprised the acquisition of axial, sagittal and cross-section views of the abdominopelvic area over a portal phase for a better observation of the veins. These acquisitions were taken with a Siemens Sensation 64 Cardiac scanner (Erlangen, Germany), set at 120kV, with 400-500-mAs exposure and a 1.2 mm section thickness interpolated at 0.6 mm. Each acquisition was taken 80 seconds after injection of 120 cm³ of an iodinated contrast agent at 350 mg/mL.

2. Geometrical data

2.1. 3D reconstruction

3D reconstructions of the liver, the thoracic cage and the associated veins were performed manually using the 3D Slicer 4.3.1. (Fedorov et al., 2012), an open-source software platform (Fig A- 14). These 3D reconstructions were used to determine a set of geometrical characteristics.

Fig A- 14. 3D reconstruction of the liver, the thoracic cage and the associated veins

---

[1]CT-scan: Digital geometry processing is used to generate a three-dimensional image of the inside of the human body from a large series of two-dimensional radiographic images.

2.2. External geometry of the liver

Geometric data related to the external shape of the liver were taken on CT-scans and are presented in Fig A- 15. These data, representative of the overall geometry of the liver, were previously defined in Serre et al. (2006).

P1: Right triangular ligament	
P2: Insertion of the falciform ligament	
P3: Left triangular ligament	
P4: Insertion of the round ligament	
P5: Hepatic arrowhead	
P6: The most anterior point of the right lobe	
P7: The most posterior point of the right lobe	

P1-P3	Medio-lateral length of the liver
P1-P5	Right height of the right lobe
P2-P3	Medio-lateral length of the left lobe
P2-P4	Height at the falciform ligament
P3-P5	Oblique length of the liver
P6-P7	Antero-posterior length of the right lobe

Fig A- 15. External geometry of the liver: anatomic points and associated dimensions; a), b) illustrated on Netter's view (Netter, 2014); c), d) illustrated on the 3D reconstruction view

In addition to these data, the volume of the whole liver was measured, based on the 3D reconstruction, as well as the volume of the left lobe, which was deduced thanks to the volume of the whole liver and the plane defined by the falciform ligament and the right hepatic vein, as shown in Fig A- 16. The volume of the right lobe was then deduced from these two first volumes. Moreover, the volume ratio of the left lobe relative to the overall volume was collected. A total of 6 characteristic lengths, 3 volumes and 1 volume ratio were added in the database.

Fig A- 16. Left and right lobes defined on the 3D reconstruction of the liver

44

2.3. Geometry of the veins

As the segments of the liver are based on the bifurcations of the veins, geometric data representative of the first two bifurcations were identified. Then, to measure the diameters and the angles presented in Fig A- 17 and Fig A- 18, the 3D reconstructions of the veins were imported in Hypermesh (Altair, MI, USA). A total of 8 diameters and 10 angles were included in the database.

A1	Vena cava and cranio-caudal line angle
A2	Vena cave and left hepatic vein angle
A3	Vena cava and median hepatic vein angle
A4	Vena cava and right hepatic vein angle
A5	Left and median hepatic veins angle
A6	Median end right hepatic veins angle
D1	Diameter of the vena cava
D2	Diameter of the left hepatic vein
D3	Diameter of the median hepatic vein
D4	Diameter of the right hepatic vein

Fig A- 17. Geometrical data of the vena cava illustrated on the 3D reconstruction view

A1	Portal vein and medio-lateral line angle
A2	Portal vein and the left branch angle
A3	Portal vein and the right median branch angle
A4	Portal vein and the right angle
D1	Diameter of the portal vein
D2	Diameter of the left branch
D3	Diameter of the right median branch
D4	Diameter of the right branch

Fig A- 18. Geometrical data of the portal vein illustrated on the 3D reconstruction view.

2.4. Liver segments

A semi-automatic program was implemented in order to divide the liver into the eight segments described by Couinaud (1957), as shown in Fig A- 19. To do so, the 3D reconstructions of the liver and the veins were imported in CAO software, Creo® (PTC, MA, USA) and the planes delimiting the segments were marked out by the veins as described by Smithuis and deLange (2015).

Fig A- 19. Internal geometry of the liver: Couinaud segments identification illustrated on the 3D reconstruction

The volumes of each segment, as well as the volume ratio of these segments relative to the overall volume of the liver, were measured. A total of 8 volumes and 8 volumes ratio were included in the database.

2.5. Location of the liver in the thoracic cage

The cranio-caudal location of the liver was defined by the most caudal and the most cranial vertebrae delimiting the projection of the liver on the spine. To assess the orientation of the liver in the rib cage, reference lines of the rib cage were defined on the CT-slice passing through the epiphysis of the vertebra T11, as shown in Fig A- 20**.** The posterior point corresponds to the epiphysis, the anterior point corresponds to the xiphoid process[1], the medial point corresponds to the most medial ribs visible on the CT-slice and the lateral point corresponds to the most lateral ribs visible on the CT-slice.

---

[1] Xiphoid process: It is a small cartilaginous process of the lower part of the sternum.

Fig A- 20. Reference lines of the rib cage at the T11 vertebra

Then, liver angles were measured using these reference lines and some anatomical points defined on Fig A- 21. These angles are: the angle between the medio-lateral reference line (L2) and the principal direction of the left lobe (P1P5); the angle between the anteroposterior reference line (L1) and the principal direction of the right lobe (P4P5); the angle between the main directions of both lobes. Thus, the location of the liver is defined by 2 vertebral levels and 3 angles.

P1	Most medial point
P2	Most lateral point
P3	Most anterior point
P4	Most posterior point
P5	Falciform ligament
L1	Antero-posterior reference line
L2	Medio-lateral reference line
L2b	Medio-lateral parallel line
A1	Angle between the right lobe and the antero-posterior line
A2	Angle between the left lobe and the medio-lateral line
A3	Angle between both lobes

Fig A- 21. Angles defining the liver orientation in the rib cage

2.6. Trunk anthropometry

As the height and weight of the patient are unknown due to a retrospective study, only trunk anthropometry is taken into account. Anthropometric measurements were measured on the CT-scans, such as the xiphoïd angle[1], the abdominal perimeter at the navel and the thoracic perimeter at the xiphoid process, as can be seen in Fig A- 22. The xiphoïd angle was used to distinguish stocky subjects from slender subjects, as proposed by O'Followell (1908), i.e. 70° for men and 75° for women. The abdominal perimeter was used as the criterion for obesity, according to the recommendation from Chia et al. (2016), i.e. when the perimeter exceeds 88 cm for women and 102 cm for men. Lastly, data such as the subject's age and gender were known.

A1	Costo-xiphoïd angle
P1	Abdominal perimeter at the navel
P2	Thoracic perimeter at the xiphoïd process

Fig A- 22. Anthropometric characteristics measured on CT-scans (illustration from Laval-Jeantet et al., 1988)

3. Validation of the database

Our population shows a variability of the geometrical characteristics of the liver, in accordance with the literature. Table A- 2 summarized the different geometric characteristics of the literature.

---

[1] Xiphoid angle: Angle formed by the floating ribs. At its summit the xiphoid process can be found.

Table A- 2. Synthesis of geometric characteristics of the liver reported in the literature

	Current study N = 78	Vinnakota and Jayasree (2013) N = 58	Verma et al. (2010) N = 116	Gupta et al. (2008) N = 50
Medio-lateral length of the liver (cm)	13.8 – 24.1	11.8 – 20	10.6 – 25.3	13.4 – 26.0
Anteroposterior length of the right lobe (cm)	11.4 – 19.2	NV	6.2 – 20.0	6.0 – 15.8
Right height of the right lobe (cm)	10.1 – 20.1	9 – 24	13.8 – 24.9	11.6 – 17.3
Height at the falciform ligament (cm)	4.5 – 14.0	NV	7.1 – 18.3	7.7 – 12.1

NV: No value

Our measurements of the liver volume are in agreement with those reported by Henderson et al. (1981), Grandmaison et al. (2001), Mazonakis et al. (2002), Geraghty et al. (2004), Farraher et al. (2005), and Beillas et al. (2009), as can be seen in Fig A- 23.

Fig A- 23. Synthesis of liver's volumes in the supine position reported in the literature and in our study

A variation of the Couinaud's volumes is noted and in accordance with the literature. Table A- 3 compared the range of the segments' volumes and proportion from this study to the literature.

Table A- 3. Synthesis of segments' volumes and proportion reported in the literature and in our study

		Current study N = 78		Mise et al. (2013) N = 107	Abdalla et al. (2004) N = 102
Volume (cm³)	**Right lobe**	478 – 2140		493 – 1324	464 – 1881
	Left lobe	108 – 630		154 – 628	205 – 827
	Segment 1	15 – 186		13 – 122	8 – 60
	Segment 2	1 – 357	101 – 520	25 – 187	101 – 490
	Segment 3	23 – 458		46 – 232	
	Segment 4	30 – 544		51 – 262	101 – 429
	Segment 5	28 – 349		41 – 249	NV
	Segment 6	24 – 548		11 – 272	NV
	Segment 7	49 – 696		69 – 501	NV
	Segment 8	40 – 736		101 – 586	NV
Volume ratio (%)	**Right lobe**	45.0 – 93.2		50.3 – 75.5	49 – 82
	Left lobe	6.8 – 55.0		15.3 – 45.3	17 – 49
	Segment 1	1 – 15		1.3 – 10.1	1 – 3
	Segment 2	0 – 19	8 – 30	2.9 – 16.1	5 – 27
	Segment 3	1 – 27		4.1 – 19.8	
	Segment 4	3 – 28		5.1 – 20.9	10 – 29
	Segment 5	3 – 22		4.4 – 20.0	NV
	Segment 6	1 – 28		1.2 – 20.0	NV
	Segment 7	4 – 41		6.0 – 35.8	NV
	Segment 8	3 – 34		11.1 – 38.0	NV

NV: No value

A lot of authors studied the variation of the portal vein and the vena cava (De Cecchis et al., 2000; Fang et al., 2012; Varotti et al., 2004). To the best of our knowledge no one deals with the angles between the portal vein and its three branches and between the vena cava and the three hepatic veins.

The diameter of the portal vein found in this study (13.1 ± 2.1 mm) is in accordance with the literature. Indeed, Weinreb et al. (1982) found an average diameter at 11 ± 2 mm based on a population of 107 individuals; Siddiqui et al. (2014) studied 459 subjects and recorded a portal diameter at 9 ± 2 mm; Stamm et al. (2016) found an average diameter of 15.5 ± 1.9 mm in their study of 191 subjects.

Moreover, the diameter of the vena cava found in this study (16 – 31 mm) is in accordance with the results of Prince et al. (1983), which found a diameter between 13 and 30 mm.

Finally, the diameter of the right hepatic vein is found between 6 and 19 mm and is in accordance with the study of De Cecchis et al. (2000), which recorded a diameter between 7 and 23 mm.

To the best of our knowledge, no study deals with the variation of the location of the liver in the thoracic cage.

Chapter 3: Identification and presentation of the morphotypes

The following chapter describes the statistical analysis set up in order to identify different morphotypes as well as to identify a link between these morphotypes and the trunk anthropometry.

Table of contents

54

1. Identification of the morphotypes

The statistical analysis of this study was performed using the R statistical software (Gordon, 1999).

1.1. Principal Component Analysis

To reduce the number of variables, and to ensure the contribution of the different sets of data (defining the external geometry, the liver segments, the geometry of the veins and the location of the liver) in the analysis, a principal component analysis (PCA[1]) was performed on the logarithm of the data of each set. For each set, we chose to keep the four first axes as new variables, as the fifth dimension did not present a good correlation with the parameters of the study, as showed in Table A- 4 to Table A- 7.

Table A- 4. Correlation between the parameters defining the external geometry of the liver and the five first dimensions of the PCA

		Dimension 1	Dimension 2	Dimension 3	Dimension 4	Dimension 5
Medio-lateral length of the liver (cm)		0.47	0.71	-0.37	-	-
Oblique length of the liver (cm)		0.78	0.34	-	-	-0.30
Antero-posterior length of the right lobe (cm)		0.43	-0.27	0.25	0.77	-
Height at the falciform ligament (cm)		0.50	-	-	-0.43	0.70
Right height of the right lobe (cm)		0.74	-	-	-0.34	-0.39
Medio-lateral length of the left lobe (cm)		0.27	0.69	-0.45	0.27	-
Volume (cm³)	**Liver**	0.91	-	0.32	-	-
	Left lobe	-	0.77	0.61	-	-
	Right Lobe	0.95	-	-	-	-
Volume ratio of the left lobe (%)		-0.67	0.64	0.35	-	-

---

[1] PCA: Statistical procedure which uses an orthogonal transformation to convert a set of observations of possibly correlated variables into a set of values of linearly uncorrelated variables called principal components.

Table A- 5. Correlation between the parameters defining the segments of the liver and the five first dimensions of the PCA

		Dimension 1	Dimension 2	Dimension 3	Dimension 4	Dimension 5
Volume (cm³)	**Segment 1**	-	0.60	0.31	-0.41	-0.42
	Segment 2	-0.43	-	0.60	0.26	0.38
	Segment 3	0.44	0.39	-	0.40	-
	Segment 4	0.36	-	0.61	0.41	-0.45
	Segment 5	0.36	0.33	0.69	-0.30	0.27
	Segment 6	0.78	0.23	-	-	-
	Segment 7	-0.65	0.35	0.25	-	-
	Segment 8	-	-0.69	-	-0.36	-
Volume ratio (%)	**Segment 1**	-	0.64	-	-0.44	-0.45
	Segment 2	-	-	0.52	0.28	0.39
	Segment 3	0.34	0.43	-0.54	0.36	-
	Segment 4	0.33	-0.25	0.42	0.47	-0.62
	Segment 5	0.33	0.42	0.49	-0.44	0.29
	Segment 6	0.74	0.30	-	-	-
	Segment 7	-0.80	0.39	-	-	-
	Segment 8	-	-0.77	-	-0.46	-

Table A- 6. Correlation between the parameters defining the geometry of the veins and the five first dimensions of the PCA

		Dimension 1	Dimension 2	Dimension 3	Dimension 4	Dimension 5
Diameter (cm)	**Portal vein**	0.78	-	-0.30	-	-
	Left branch	0.70	-	-	-0.32	-
	Right median branch	0.62	-	-	-	0.29
	Right branch	0.57	-	-	-	-
	Vena cava	0.59	0.24	-	-	-
	Left hepatic vein	0.55	-	0.41	-	-
	Median hepatic vein	0.58	-	0.47	0.24	-
	Right hepatic vein	0.42	-0.31	0.58	-	0.25

Angle (°)	**Portal vein and medio-lateral line**	-	-0.48	-	0.53	-
	Portal vein and left branch	-	-0.28	-0.41	0.51	-
	Portal vein and right median branch	-	0.35	-	-0.54	-
	Portal vein and right branch	-	0.25	-0.49	0.49	-
	Vena cava and cranio-caudal line	-	0.58	-	0.31	-0.42
	Vena cava and left hepatic vein	-	0.64	-	0.46	-
	Vena cava and median hepatic vein	-	0.73	-	-	0.42
	Vena cava and right hepatic vein	-	0.48	-	-	0.66
	Left and median hepatic vein	-	0.38	-	-	-0.50
	Median and right hepatic vein	-	-	0.49	-	-

Table A- 7. Correlation between the parameters defining the location of the liver and the five first dimensions of the PCA

		Dimension 1	Dimension 2	Dimension 3	Dimension 4	Dimension 5
Position	**Cranial**	0.78	0.33	-	0.50	-
	Caudal	0.66	0.45	-0.48	-0.36	-
Angle (°)	**Right lobe and anteroposterior line**	0.66	0.28	0.67	-	-
	Left lobe and medio-lateral line	-0.68	0.67	-	-	-
	Both lobes	-0.89	0.32	-	-	0.27

1.2. Existence of morphotypes

Before identifying morphotypes, the existence of a conformation effect in the variability of the liver geometry must be checked. To assess this conformation effect, we used the Mosimann method, which is largely used in bio-statistics (Berge, 1986; Darroch and Mosimann, 1985) and which has been assessed by Jungers et al. (1995). They evaluated eleven statistical techniques in reference to one broadly interspecific data set (craniometrics of adults Old World monkeys) and one narrowly intraspecific data set (antropometrics of adult Native American males). They found out that only the Mosimann family of shape ratios allowed to identify different sized individuals of the same shape.

The Mosimann method (1970) is based on the isometric size and on the matrix of conformation associated to the data. An isometric size is computed for each patient and corresponds to the mean of the logarithm of the different variables. The matrix of conformation is the difference between the logarithm of the variable and the isometric size associated to the patient. A correlation per variable is calculated. The strength of the correlation between the isometric size and the data of the matrix of conformations allows to determine the presence of a size or/and a conformation effect.

Regarding the present study, the correlation between the isometric size and the data of the matrix of conformations is significant ($p<0.05$) and the coefficient of determination is under 0.7 for most of the variables. Thus, both size and conformation effects are demonstrated.

1.3. Clustering

After the verification of the existence of a conformation effect, a hierarchical clustering approach was used. To define the optimal number of cluster, 26 statistical methods were first applied using the NbClust function in R (https://cran.r-project.org/web/packages/NbClust/NbClust.pdf). Then the optimal number of cluster was determined according to the majority rule.

The results obtained using these methods are synthetized in Fig A- 24. Most of these methods suggested that four is the optimum number of morphotypes in our population.

Fig A- 24. Frequency of the optimal number of clusters among all indices, i.e. according to the 26 statistical methods

Creating four groups ensures high inertia in each cluster and preserves enough livers per cluster, respectively 23, 11, 30 and 14 livers.

To classify the individuals into morphotypes, the hierarchical clustering[1] with the Ward method was used. To understand which parameters, explain the most each morphotype, an ascending linear model step to step[2] was applied and validated with an Akaike[3] criterion.

The four morphotypes are presented in

---

[1] Hierarchical clustering: It is a method of cluster analysis which seeks to build a hierarchy of cluster.

[2] Ascending linear model step to step: Simple linear regression is a model with a single explanatory variable.

[3] Akaike information criterion: It is measure of the relative quality of statistical models for a given set of data.

Fig A- **25**. The ascending linear model step to step showed that the data which explain the most the four morphotypes are the right height of the right lobe, the volume of the right lobe, the volume ratio of the left lobe, the volume of segment 2, the diameter of the portal vein, the diameter of the left branch of the portal vein, the angle between the portal vein and the median branch and the caudal location of the liver.

Now that we have look at the liver as a whole, it is interesting to detail the external morphology, the morphology of the vessels, the internal morphology and the location of the liver within the rib cage.

A- 25. Presentation of the four morphotypes

2. Characteristics of the identified morphotypes

The qualifiers "small" or "large" are used in a relative way to compare the same characteristics in the 4 morphotypes.

2.1. External geometry

The external geometry of each morphotype is described by the data given in Table A- 8:

The first morphotype corresponds to a liver with a small hepatic volume (average 1312 cm^3) which shows a small right lobe (average 1030 cm^3), and a medium volume ratio of the left lobe (average 21.4 %). Moreover, a large medio-lateral length (average 19.3 cm) as well as a small height at the falciform ligament (average 8.4 cm), are noticed.

The second morphotype corresponds to a liver with a large hepatic volume (average 1802 cm³) which shows a large right lobe (average 1577 cm³), and a small volume ratio of the left lobe (average 12.6 %). Furthermore, a large medio-lateral length (average 19.2 cm) and a large height at the falciform ligament (average 10.3 cm) are noticed.

The third morphotype corresponds to a liver with a large hepatic volume (average 1688 cm³) which shows a large right lobe (average 1366 cm³), and a medium volume ratio of the left lobe (19.4 %). Furthermore, a large medio-lateral length of the liver (average 18.7 cm) and a small height at the falciform ligament (average 8.7 cm) can be noted.

The fourth morphotype corresponds to a liver with a small hepatic volume (average 1217 cm³) which shows a small right lobe (average 887 cm³), and a very large volume ratio of the left lobe (average 28.1 %). In addition, a small medio-lateral length of the liver (average 16.4 cm) and a small height at the falciform ligament (average 7.5 cm) are noticed.

Table A- 8. Means and standard deviations of the parameters defining the external geometry for each liver morphotype

		Morphotype 1 (N=23)	Morphotype 2 (N=11)	Morphotype 3 (N=30)	Morphotype 4 (N=14)
Medio-lateral length of the liver (cm)		19.3 ± 1.7^c	19.2 ± 1.0^e	18.7 ± 2.5^f	$16.4 \pm 1.6^{c,e,f}$
Oblique length of the liver (cm)		22.8 ± 1.9^c	23.5 ± 1.7^e	22.7 ± 1.9^f	$20.6 \pm 1.9^{c,e,f}$
Antero-posterior length of the right lobe (cm)		$13.7 \pm 1.1^{a,b}$	15.6 ± 1.8^a	15.7 ± 1.9^b	14.8 ± 1.2
Height at the falciform ligament (cm)		8.4 ± 1.4^a	$10.3 \pm 1.6^{a,d,e}$	8.7 ± 1.6^d	7.5 ± 1.3^e
Right height of the right lobe (cm)		15.7 ± 2.3	17.4 ± 1.6^e	15.6 ± 2.1	14.0 ± 2.9^e
Medio-lateral length of the left lobe (cm)		9.4 ± 1.5	9.2 ± 1.3	9.8 ± 1.8	8.8 ± 1.3
Volume (cm³)	**Liver**	$1312 \pm 212^{a,b}$	$1802 \pm 242^{a,e}$	$1688 \pm 322^{b,f}$	$1217 \pm 233^{e,f}$
	Left lobe	282 ± 83	$225 \pm 78^{d,e}$	322 ± 76^d	330 ± 144^e
	Right Lobe	$1030 \pm 166^{a,b}$	$1577 \pm 248^{a,e}$	$1366 \pm 300^{b,f}$	$887 \pm 280^{e,f}$
Volume ratio of the left lobe (%)		$21.4 \pm 4.5^{a,c}$	$12.6 \pm 4.8^{a,d,e}$	$19.4 \pm 4.4^{d,f}$	$28.1 \pm 13.3^{c,e,f}$

a Student's t-test was used to compare morphotypes 1 & 2, (p<0.05)
b Student's t-test was used to compare morphotypes 1 & 3, (p<0.05)
c Student's t-test was used to compare morphotypes 1 & 4, (p<0.05)
d Student's t-test was used to compare morphotypes 2 & 3, (p<0.05)
e Student's t-test was used to compare morphotypes 2 & 4, (p<0.05)
f Student's t-test was used to compare morphotypes 3 & 4, (p<0.05)

2.2. Geometry of the veins

The geometry of the veins for each morphotype is described by the data given in Table A-9:

The first morphotype shows a small diameter of the left branch of the portal vein (average 0.9 cm). Moreover, small angles between the portal vein and the left branch (average 66.9°), between the vena cava and the left hepatic vein (average 60.8°) and between the vena cava and the median hepatic vein (average 53.1°) are found.

The second morphotype shows a large diameter of the portal vein (average 1.4 cm). Furthermore, small angles between the vena cava and the cranio-caudal line (average 20.3°), between the vena cava and the left hepatic vein (average 58.2°), and between the vena cava and the median hepatic vein (48.5°) are found.

The third morphotype shows a large diameter of the portal vein (average 1.4 cm) and its left branch (average 1.1 cm). Moreover, large angles between the portal vein and the left branch (average 80.7°), between the vena cava and the cranio-caudal line (average 38.6°), between the vena cava and the left hepatic vein (average 72.2°) and between the vena cava and the median hepatic vein (average 64.1°) are found.

The fourth morphotype shows a small diameter of the portal vein (average 1.1 cm) and its left branch (average 0.9 cm). In addition, a large angle between the portal vein and the left branch (average 91.6°) and a small angle between the vena cava and the cranio-caudal line (average 21.8°) are found.

Table A- 9. Means and standard deviations of the parameters defining the geometry of the veins for each liver morphotype

		Morphotype 1 (N=23)	Morphotype 2 (N=11)	Morphotype 3 (N=30)	Morphotype 4 (N=14)
Diameter (cm)	**Portal vein**	1.3 ± 0.2	1.4 ± 0.2[e]	1.4 ± 0.2[f]	1.1 ± 0.2[e,f]
	Left branch	0.9 ± 0.2[b]	1.0 ± 0.2	1.1 ± 0.2[b,f]	0.9 ± 0.2[f]
	Right median branch	0.9 ± 0.2	1.0 ± 0.2	0.9 ± 0.2	0.8 ± 0.1
	Right branch	0.8 ± 0.1	0.8 ± 0.2	0.9 ± 0.2	0.8 ± 0.2
	Vena cava	2.1 ± 0.2[b]	2.2 ± 0.3	2.4 ± 0.3[b]	2.1 ± 0.3
	Left hepatic vein	0.9 ± 0.2	1.0 ± 0.3	0.9 ± 0.2	0.9 ± 0.2
	Median hepatic vein	0.2	0.9 ± 0.2	1.0 ± 0.2	1.0 ± 0.3
	Right hepatic vein	1.2 ± 0.2[b]	1.3 ± 0.3	1.0 ± 0.3[b]	1.2 ± 0.4

Angle (°)	Portal vein and medio-lateral line	30.1 ± 9.2^c	34.2 ± 8.8	32.6 ± 7.5	37.7 ± 8.5^c
	Portal vein and left branch	$66.9 \pm 16.0^{b,c}$	77.0 ± 16.2	80.7 ± 14.4^b	91.6 ± 12.5^c
	Portal vein and right median branch	122.1 ± 15.0	122.1 ± 11.9	121.8 ± 12.7	116.6 ± 12.1
	Portal vein and right branch	122.0 ± 19.9	110.4 ± 19.2	123.8 ± 16.0	122.6 ± 19.5
	Vena cava and cranio-caudal line	29.8 ± 13.6	20.3 ± 13.3^d	$38.6 \pm 13.5^{d,f}$	21.8 ± 9.0^f
	Vena cava and left hepatic vein	60.8 ± 12.7^b	58.2 ± 17.2^d	$72.2 \pm 15.1^{b,d}$	62.8 ± 15.4
	Vena cava and median hepatic vein	53.1 ± 15.5^b	48.5 ± 9.8^d	$64.1 \pm 14.5^{b,d}$	58.1 ± 16.8
	Vena cava and right hepatic vein	46.2 ± 16.1	45.0 ± 13.0	51.2 ± 18.1	43.8 ± 9.9
	Left and median hepatic vein	50.8 ± 12.3	46.9 ± 11.6	50.0 ± 11.4	44.6 ± 10.1
	Median and right hepatic vein	39.9 ± 7.3	43.0 ± 6.9	39.3 ± 8.6	40.9 ± 8.8

a Student's t-test was used to compare morphotypes 1 & 2, ($p<0.05$)
b Student's t-test was used to compare morphotypes 1 & 3, ($p<0.05$)
c Student's t-test was used to compare morphotypes 1 & 4, ($p<0.05$)
d Student's t-test was used to compare morphotypes 2 & 3, ($p<0.05$)
e Student's t-test was used to compare morphotypes 2 & 4, ($p<0.05$)
f Student's t-test was used to compare morphotypes 3 & 4, ($p<0.05$)

2.3. Liver segments

The segments of each morphotype are described by the data given in Table A- 10:

The first morphotype corresponds to a liver with small volumes and volume ratios of segment 2 (average 50 cm³ & 3.4 %), and segment 6 (average 130 cm³ & 9.7 %), as well as a large volume and volume ratio of the segment 5 (180 cm³ & 13.5 %). Moreover, small volumes of the left liver (average 360 cm³), and the right liver (average 880 cm³) are noticed.

The second morphotype corresponds to a liver with large volumes and volume ratios of segment 2 (average 140 cm³ & 8.0 %) and segment 5 (average 240 cm³ & 13.5 %), as well as a small volume and volume ratio of segment 6 (average 110 cm³ & 5.9 %). Furthermore,

large volumes of the left liver (average 550 cm^3), and the right liver (average 1190 cm^3) are noticed.

The third morphotype corresponds to a liver with large volumes and volume ratios of segment 5 (average 220 cm^3 & 13.3 %) and segment 6 (average 280 cm^3 & 16.5 %), as well as a small volume and volume ratio of segment 2 (40 cm^3 & 2.3 %). Moreover, large volumes of the left liver (average 530 cm^3), and the right liver (average 1090 cm^3) are noticed.

The fourth morphotype corresponds to a liver with small volumes and volume ratios of segment 2 (average 40 cm^3 & 3.7 %), segment 5 (average 90 cm^3 & 7.6 %) and segment 6 (average 130 cm^3 & 10.9 %). In addition, small volumes of the left liver (average 400 cm^3) and the right liver (average 780 cm^3) are noticed.

Table A- 10. Means and standard deviations of the parameters defining the segments for each liver morphotype

		Morphotype 1 (N=23)	Morphotype 2 (N=11)	Morphotype 3 (N=30)	Morphotype 4 (N=14)
Volume (cm³)	**Segment 1**	73 ± 34[c]	62 ± 24	74 ± 26[f]	39 ± 16[c,f]
	Segment 2	47 ± 31[a]	141 ± 91[a,d,e]	40 ± 35[d]	44 ± 41[e]
	Segment 3	164 ± 56[b]	142 ± 86[d]	233 ± 86[b,d]	181 ± 36
	Segment 4	152 ± 62[a,b]	270 ± 126[a,e]	258 ± 83[b,f]	171 ± 58[e,f]
	Segment 5	177 ± 59[a,b,c]	241 ± 70[a,e]	222 ± 59[b,f]	91 ± 45[c,e,f]
	Segment 6	126 ± 42[b]	106 ± 48[d]	277 ± 102[b,d,f]	128 ± 78[f]
	Segment 7	349 ± 110	417 ± 182[d,e]	281 ± 122[d]	251 ± 98[e]
	Segment 8	225 ± 103[a]	423 ± 173[a,d]	303 ± 132[d]	311 ± 96
	Left lobe (S2 & S3)	211 ± 67[b]	283 ± 74	273 ± 100[b]	226 ± 61
	Left liver (S2, S3 & S4)	362 ± 115[a,b]	553 ± 154[a,e]	531 ± 134[b,f]	397 ± 91[e,f]
	Right liver (S5 to S8)	877 ± 170[a,b]	1187 ± 176[a,e]	1094 ± 255[b,f]	781 ± 171[e,f]
	Lateral sector (S6 & S7)	475 ± 113	523 ± 187	558 ± 149[f]	379 ± 97[f]

Volume ratio (%)	Segment 1	5.9 ± 3.1[a,c]	3.3 ± 1.0[a]	4.4 ± 1.5	3.2 ± 1.4[c]
	Segment 2	3.4 ± 2.2[a]	8.0 ± 4.7[a,d,e]	2.3 ± 1.8[d]	3.7 ± 3.3[e]
	Segment 3	12.4 ± 3.8[a]	7.9 ± 4.3[a,d,e]	13.7 ± 4.4[d]	14.9 ± 2.4[e]
	Segment 4	11.5 ± 4.2[b]	14.9 ± 5.9	15.5 ± 4.7[b]	13.9 ± 3.2
	Segment 5	13.5 ± 3.5[c]	13.5 ± 3.6[e]	13.3 ± 3.4[f]	7.6 ± 3.4[c,e,f]
	Segment 6	9.7 ± 2.7[b]	5.9 ± 3.2[d]	16.5 ± 5.0[b,d,f]	10.9 ± 7.6[f]
	Segment 7	26.4 ± 7.0[b]	23.4 ± 10.4	16.6 ± 6.7[b]	20.3 ± 6.5
	Segment 8	17.3 ± 6.8[c]	23.1 ± 7.8	17.6 ± 5.3[f]	25.2 ± 4.9[c,f]
	Left lobe (S2 & S3)	15.9 ± 4.0[b]	15.7 ± 3.4	16.1 ± 4.7[b]	17.9 ± 6.0
	Left liver (S2, S3 & S4)	27.3 ± 6.8[b]	30.5 ± 6.6	31.4 ± 6.0[b]	31.6 ± 5.2
	Right liver (S5 to S8)	66.9 ± 7.1	66.1 ± 6.1	64.0 ± 6.2	62.3 ± 8.7
	Lateral sector (S6 & S7)	36.2 ± 6.4	29.6 ± 11.0	33.0 ± 6.6	29.9 ± 4.5

a Student's t-test was used to compare morphotypes 1 & 2, ($p<0.05$)
b Student's t-test was used to compare morphotypes 1 & 3, ($p<0.05$)
c Student's t-test was used to compare morphotypes 1 & 4, ($p<0.05$)
d Student's t-test was used to compare morphotypes 2 & 3, ($p<0.05$)
e Student's t-test was used to compare morphotypes 2 & 4, ($p<0.05$)
f Student's t-test was used to compare morphotypes 3 & 4, ($p<0.05$)

2.4. Location of the liver

The location of each morphotype is described by the data given in Table A- 11:

The first morphotype corresponds to a liver slightly covered by the thoracic cage (T16 to L22), and a small angle between both lobes (average 83.8 °) is noticed.

The second morphotype corresponds to a liver partially covered by the thoracic cage (T15 to L21), and a large angle between both lobes (average 98.9 °) is found.

As the second morphotype, the third morphotype corresponds to a liver partially covered by the thoracic cage (T15 to L21) and a large angle between both lobes (average 104.6 °) is noticed.

The fourth mophotype corresponds to a liver completely covered by the thoracic cage (T15 to L20) and a large angle between both lobes (average 102.6 °) is noticed.

Table A- 11. Means and standard deviations of the parameters defining the location on the thoracic cage for each morphotype

		Morphotype 1 (N=23)	Morphotype 2 (N=11)	Morphotype 3 (N=30)	Morphotype 4 (N=14)
Position	**Cranial**	$22 \pm 1^{b,c}$	21 ± 1^{e}	21 ± 1^{b}	$20 \pm 1^{c,e}$
	Caudal	$16 \pm 1^{a,b,c}$	15 ± 1^{a}	15 ± 1^{b}	15 ± 1^{c}
Angle (°)	**Right lobe and anteroposterior line**	$19.4 \pm 8.8^{b,c}$	14.7 ± 5.4^{e}	11.7 ± 6.1^{b}	$7.2 \pm 5.5^{c,e}$
	Left lobe and medio-lateral line	$15.5 \pm 9.0^{a,b}$	25.9 ± 12.2^{a}	$27.0 \pm 9.8^{b,f}$	18.3 ± 7.3^{f}
	Both lobes	$83.8 \pm 12.9^{a,b,c}$	98.9 ± 15.4^{a}	104.6 ± 11.7^{b}	102.6 ± 10.7^{c}

a Student's t-test was used to compare morphotypes 1 & 2, ($p<0.05$)
b Student's t-test was used to compare morphotypes 1 & 3, ($p<0.05$)
c Student's t-test was used to compare morphotypes 1 & 4, ($p<0.05$)
d Student's t-test was used to compare morphotypes 2 & 3, ($p<0.05$)
e Student's t-test was used to compare morphotypes 2 & 4, ($p<0.05$)
f Student's t-test was used to compare morphotypes 3 & 4, ($p<0.05$)

To synthetize on the characteristics of the liver morphotypes that have been identified:

Morphoype 1 corresponds to a small liver slightly covered by the thoracic cage, with a moderate development of the left lobe.

Morphotype 2 corresponds to a large liver partially covered by the thoracic cage, with a small development of the left lobe.

Morphotype 3 corresponds to a large liver partially covered by the thoracic cage, with a moderate development of the left lobe.

Morphotype 4 corresponds to a small liver completely covered by the thoracic cage, with a large development of the left lobe.

3. Relationship with the trunk anthropometry

To check the existence of a relationship between the trunk anthropometry of the patients and the different morphotypes, univariate ANOVAs followed by post-hoc Tukey (HSD) tests were performed. The results were considered to be statistically significant for $p<0.05$. Finally, to estimate which anthropometric parameters explain the most the morphotypes, an ascending linear model step to step was applied and validated with an Akaike criterion.

The ascending linear model step to step showed that the anthropometric data which explain the most the morphotypes are the age, the gender, the abdominal perimeter and the thoracic perimeter.

For each liver morphotype, the trunk anthropometry data are summed up in Table A- 12.

Table A- 12. Means and standard deviations of the parameters defining the trunk anthropometry of the subjects for each morphotype

		Morphotype 1 (N=23)	Morphotype 2 (N=11)	Morphotype 3 (N=30)	Morphotype 4 (N=14)
Gender (%)	**Men**	17^b	36^d	$87^{b,d,f}$	14^f
	Women	83^b	64^d	$13^{b,d,f}$	86^f
Age (years)		$34 \pm 17^{b,c}$	$39 \pm 15^{d,e}$	$49 \pm 21^{b,d,f}$	$72 \pm 13^{c,e,f}$
Xiphoïd angle (°)		$62.6 \pm 14.8^{b,c}$	77.1 ± 19.3	83.3 ± 21.0^b	82.7 ± 18.7^c
Subject's morphotype (%)	**Slender**	70^b	45	23^b	29
	Stocky	30^b	55	77^b	71
Abdominal perimeter (cm)		$81.1 \pm 9.4^{a,b,c}$	93.9 ± 8.5^a	91.1 ± 13.1^b	98.2 ± 12.2^c
Obesity (%)	**Healthy**	83^c	55	77^f	$36^{c,f}$
	Obese	17^c	45	23^f	$64^{c,f}$
Thoracic perimeter (cm)		70.3 ± 6.9^b	74.8 ± 8.9	$78.5 \pm 5.7^{b,f}$	70.5 ± 5.5^f
Depth to width ratio of the rib cage		0.68 ± 0.10^c	0.68 ± 0.06^e	0.74 ± 0.07	$0.77 \pm 0.10^{c,e}$
Thoracic perimeter to abdominal perimeter ratio		0.87 ± 0.09^b	0.80 ± 0.11	$0.87 \pm 0.10^{b,f}$	0.72 ± 0.08^f

a Student's t-test was used to compare morphotypes 1 & 2, ($p<0.05$)
b Student's t-test was used to compare morphotypes 1 & 3, ($p<0.05$)
c Student's t-test was used to compare morphotypes 1 & 4, ($p<0.05$)
d Student's t-test was used to compare morphotypes 2 & 3, ($p<0.05$)
e Student's t-test was used to compare morphotypes 2 & 4, ($p<0.05$)
f Student's t-test was used to compare morphotypes 3 & 4, ($p<0.05$)

ANOVAs and post-hoc Tukey (HSD) test showed that:

The first morphotype is mainly found in women under the age of 50, with an abdominal perimeter not exceeding 85 cm, and a thoracic perimeter not exceeding 75 cm.

The second morphotype is mainly found in women under the age of 50, with an abdominal perimeter exceeding 85 cm, and a thoracic perimeter around 75 cm.

The third morphotype is mainly found in men around the age of 50, with an abdominal perimeter exceeding 85 cm, and a thoracic perimeter exceeding 75 cm.

The fourth morphotype is manly found in women over the age of 50, with an abdominal perimeter exceeding 85 cm, and a thoracic perimeter not exceeding 75 cm.

4. Discussion and conclusion

The statistical analysis allowed us to highlight four morphotypes of livers. These morphotypes take into account the external morphology - the shape of the liver – the liver segments – the volumes of the Couinaud's segments – the morphology of the veins and the location of the liver in the thoracic cage.

Studer et al. (2015) defined two liver morphotypes according to the spread of the liver in the left part of the body. These morphotypes are highlighted in our study, as morphotypes 2 on one hand, for which the medio-lateral length is small (16.4 cm), and morphotypes 1, 3 and 4 on the other hand, for which the medio-lateral length is large (19.1 cm).

Furthermore, the study by Studer et al. (2015) showed three spleen morphotypes (flat, convex or concave) and put forward a connection between "cupped" shaped spleens and livers with small overlap on the left part of the thoracic cage. Thus, a compilation of the results from our study and from Studer et al. (2015) suggest elaborating seven models of the abdomen to be morphologically representative of the liver-spleen system, i.e. models with liver morphotypes 2 and a "cupped" shaped spleen, and models with liver morphotypes 1, 3 and 4 with a convex or flat spleen.

Moreover, a relationship between liver morphotypes and the trunk anthropometry is shown. Due to a retrospective selection of the CT-scans, we were not able to gain access to data such as the individual's weight and height. These relationships are partially in line with those obtained by Caix and Cubertafond (1978). As these authors, we observed a greater anteroposterior length in stocky subjects. But, no significant difference in the mediolateral length of the liver and the right height of the right lobe was observed between stocky and slender subjects. Unlike Caix and Cubertafond (1978), who divided the population into slender and stocky, we defined liver morphotypes without preconceptions toward the subjects' morphology.

In our study, all the data were taken on the supine positon. Beillas et al (2009) studied the effect of posture on the position, shape and volume of the liver. Although no statistical difference of volume was found. Moreover, they found a displacement of 34 ± 16 mm along the Z-axis (cranio-caudal direction).

Conclusion

Research question: **Do different liver morphotypes can be identified and correlated to the anthropometry of the individuals?**

In order to answer this question, different questions need to be clarified:

- Is the variability of the liver due to a size effect or a conformation effect?
- Can different morphotypes be identified?
- Can a link between trunk anthropometry and the liver morphology be found?

The risk of hepatic lesions depends on its external geometry but also its location in the rib cage and on the geometry of the hepatic vessels. Moreover, for the creation of pedagogical tools for surgery, it is necessary to know the liver segments, i.e. its classification according to Couinaud. Thus, an extensive study of the morphology of the liver and the associated veins, as well as of the location of the liver in the rib cage was performed. To do so, data were collected from a total of 78 CT-scans. A total of 6 characteristic lengths, 3 volumes (whole liver, right lobe and left lobe) and 1 volume ratio (left lobe) were representative of the external morphology of the liver. The internal geometry of the liver was characterized by 8 volumes and 8 volumes ratio, which described the Couinaud's segments. A total of 8 diameters and 10 angles were used to define the geometry of the vena cava and the portal vein. Finally, 2 vertebra which indicated the location of the liver in the cranio-caudale direction were noted, likewise 3 angles which determined the location of the liver within the rib cage. Those data were gathering in a database behind the statistical analysis.

An initial study of this database showed a great variability of the morphology of the liver, the associated veins and their position within the rib cage. Thus, facing such variability, a first question arose: **Is the variability of the liver due to a size effect or a conformation effect?**

The isometric size of the variables was calculated as well as the matrix of conformation. A linear regression showed that there is indeed a size effect, but this effect is not consistent enough to explain the variability. **Thus, a conformation effect must be taken into account**.

As a conformation effect was pointed out, a second question arose: **Can different morphotypes be identified?**

To answer this question in an unbiased way, a statistical study was necessary. **A hierarchical classification highlighted four morphotypes**.

Now that morphotypes have been highlighted, one more question is raised: **Can a link between trunk anthropometry and the different morphotypes be found?**

Univariate ANOVAs followed by post-hoc Tukey (HSD) tests, allowed us to answer this question. Indeed, **the trunk anthropometry of the subject enabled us to predict the liver morphotype thanks to the age, the gender, the abdominal perimeter and the thoracic perimeter**.

Thus different liver type can be identified and there is a link with the anthropometry of the subjects.

> **To conclude, four morphotypes have been highlighted and will be implemented in a numerical model in Part C.**

Reference

Abdalla, Eddie K., Alban Denys, Patrick Chevalier, Rabih A. Nemr, and Jean-Nicolas Vauthey. 2004. "Total and Segmental Liver Volume Variations: Implications for Liver Surgery." Surgery 135 (4): 404–10.

Abdel-Misih, Sherif R.Z., and Mark Bloomston. 2010. "Liver Anatomy." Surg Clin North Am 90 (4): 643–53. doi:10.1016/j.suc.2010.04.017.

Balfe, Alain, Stan Barry, Ophelia Blake, Dermot Cannon, Martin Healy, Mark Kilbane, Peadar McGing, Ruth O'Kelly, and Paula O'Shea. 2009. "The Biochemistry of Body Fluids." Dr Peadar McGing, Ms Ruth O'Kelly. http://www.acbi.ie/downloads/guidelines-of-body-fluids.pdf.

Beillas, Philippe, Yoann Lafon, and Francis W. Smith. 2009. "The Effects of Posture and Subject-to-Subject Variations on the Position, Shape and Volume of Abdominal and Thoracic Organs." Stapp Car Crash Journal 53 (November): 127–54.

Berge, C. 1986. "Size- and Locomotion-Related Aspects of Hominid and Anthropoid Pelves: An Osteometrical Multivariate Analysis." Hum. Evol. 6: 365–76.

Bismuth, H. 1982. "Surgical Anatomy and Anatomical Surgery of the Liver." World Journal of Surgery 6 (1): 3–9.

Castaing, D., D. Azoulay, and R. Adam. 2006. Chirurgie du foie et de l'hypertension portale. Masson. Techniques chirurgicales digestif.

Cecchis, Lucio De, Marija Hribernik, Dean Ravnik, and Eldar M. Gadzijev. 2000. "Anatomical Variations in the Pattern of the Right Hepatic Veins: Possibility for Type Classification." J. Anat 197: 487–93.

Champetier, J., R. Yver, C. Létoublon, and B. Vigneau. 1985. "A General Review of Anomalies of Hepatic Morphology and Their Clinical Implications." Anatomia Clinica 7 (4): 285–99.

Chevallier, Jean-Marc, Elizabeth Vitte, Christian Cabrol, and Rolland Parc. 2011. ANATOMIE - Le tronc. 2ème ed. Vol. 1. Médecine Sciences Publications.

Chia, Chee W., Michelle Shardell, Toshiko Tanaka, David D. Liu, Kristofer S. Gravenstein, and Eleanor M. Simonsick. 2016. "Chronic Low-Calorie Sweetener Use and Risk of Abdominal Obesity among Older Adults: A Cohort Study." PloS One 11 (11). http://dx.doi.org/10.1371/journal.pone.0167241.

Couinaud, Claude. 1957. Le foie: études anatomiques et chirurgicales. Masson & Cie.

Cuilleret, Monique, and Alain Bouchet. 1991. Anatomie topographique, descriptive et fonctionnelle, tome 2 : Le cou, le thorax. 2e ed. Paris: Editions Masson.

Darroch, J.N., and J.E Mosimann. 1985. "Canonical and Principal Components of Shape." Biometrika 72: 241–52.

Fang, Chi-Hua, Jin-Hua You, Wan Lee Lau, Eric C.H. Lai, Ying-Fang Fan, Shi-Zhen Zhong, Ke-Xiao Li, Zhi-Xiang Chen, Zhong-He Su, and Su-Su Bao. 2012. "Anatomical Variations of Hepatic Veins; Three Dimensional Computed Tomography Scans of 200 Subjects." World Journal of Surgery 36 (1): 120–24.

Farraher, Steven W, Hernan Jara, Kevin J Chang, Andrew Hou, and Jorge A Soto. 2005. "Liver and Spleen Volumetry with Quantitative MR Imaging and Dual-Space Clustering Segmentation." Radiology 237 (1): 322–28. doi:10.1148/radiol.2371041416.

Fasel, Jean H. D., Pietro E. Majno, and Heinz-Otto Peitgen. 2010. "Liver Segments: An Anatomical Rationale for Explaining Inconsistencies with Couinaud's Eight-Segment Concept." Surgical and Radiologic Anatomy 32 (8): 761–65. doi:10.1007/s00276-010-0626-4.

Fasel, Jean H. D., and Andrea Schenk. 2013. "Concepts for Liver Segment Classification: Neither Old Ones nor New Ones, but a Comprehensive One." Journal of Clinical Imaging Science 3 (October). doi:10.4103/2156-7514.120803.

Fedorov, A., R. Beichel, J. Kalpathy-Cramer, F. Fennessy, M. Sonka, J. Buatti, S.R. Aylward, J.V. Miller, S. Pieper, and R. Kikinis. 2012. "3D Slicer as an Image Computing Platform for the Quantitative Imaging Network." Magnetic Resonance Imaging 30 (9): 1323–41.

Fraser, Charles G. 1952. "Accessory Lobes of the Liver." Annals of Surgery 135 (1): 127–29.

Geraghty, E. M., J. M. Boone, J. P. McGahan, and K. Jain. 2004. "Normal Organ Volume Assessment from Abdominal CT." Abdominal Imaging 29 (4): 482–90.

Goldsmith, N. A., and R. T. Woodburne. 1957. "The Surgical Anatomy Pertaining to Liver Resection." Surgery, Gynecology & Obstetrics 105 (3): 310–18.

Gordon, A. D. 1999. Classification. 2nd Edition. London: Chapman and Hall/CRC.

Grandmaison, G. L. de la, I. Clairand, and M. Durigon. 2001. "Organ Weight in 684 Adult Autopsies: New Tables for a Caucasoid Population." Forensic Science International 119 (2): 149–54.

Gupta, D. Madhur, Lavina Sodhi, and T.D. Yadav. 2008. "Morphology of Liver." Indian J. Surg 70: 3–7.

Guyton, Arthur C. 1976. Textbook of Medical Physiology. 5th edition. Philadelphia: W.B. Saunders Company.

Healey, J. E., and P. C. Schroy. 1953. "Anatomy of the Biliary Ducts within the Human Liver; Analysis of the Prevailing Pattern of Branchings and the Major Variations of the Biliary Ducts." A.M.A. Archives of Surgery 66 (5): 599–616.

Henderson, J. M., S. B. Heymsfield, J. Horowitz, and M. H. Kutner. 1981. "Measurement of Liver and Spleen Volume by Computed Tomography. Assessment of Reproducibility and Changes Found Following a Selective Distal Splenorenal Shunt." Radiology 141 (2): 525–27.

Howes, Meghan K., Warren N. Hardy, and Philippe Beillas. 2013. "The Effects of Cadaver Orientation on the Relative Position of the Abdominal Organs." Annals of Advances in Automotive Medicine 57 (September): 209–24.

Jungers, William L., Anthony B. Falsetti, and Christine E. Wall. 1995. "Shape, Relative Size, and Size-Adjustments in Morphometrics." American Journal of Physical Anthropology 38 (S21): 137–61.

Kamina, Pierre. 2014. Petit atlas d'anatomie. 3ème ed. Maloine.

Kim, Seoung Hoon, and Young Kyu Kim. 2013. "Hanging Manoeuver for a Left Hepatectomy Using Glisson's Approach with a Focus on Tape Position in Liver Hilum." HPB (oxford) 15 (9): 681–86.

Krishna, M. 2013. "Microscopic Anatomy of the Liver." Clinical Liver Disease 2: 4–7. doi:10.1002/cld.147.

Lafortune, M., A. Denys, and S. Schmidt. 2007. "Anatomie du foie : ce qu'il faut savoir." J Radiol, 1020–35.

Laval-Jeantet, M., J.P. Lassau, and D. Bastian. 1988. Tomodensitométrie Du Tronc de L'adulte. Atlas Anatomique et Variations. Paris: Masson.

Mazonakis, M., J. Damilakis, T. Maris, P. Prassopoulos, and Gourtsoyiannis N. 2002. "Comparison of Two Volumetric Techniques for Estimating Liver Volume Using Magnetic Resonance Imaging." Journal of Magnetic Resonance Imaging: JMRI 15 (5): 557–63. doi:10.1002/jmri.10109.

Melvin, John W. 1988. "Review of Biomechanical Impact Response and Injury in the Automotive Environment." http://deepblue.lib.umich.edu/handle/2027.42/23.

Mise, Yoshihiro, Shoichi Satou, Junichi Shindoh, Claudius Conrad, Taku Aoki, Kiyoshi Hasegawa, Yasuhiko Sugawara, and Norihiro Kokudo. 2014. "Three-Dimensional Volumetry in 107 Normal Livers Reveals Clinically Relevant Inter-Segment Variation in Size." HPB (Oxford) 16 (5): 439–47. doi:10.1111/hpb.12157.

Mosimann, James E. 1970. "Size Allometry: Size and Shape Variables with Characterizations of the Lognormal and Generalized Gamma Distributions." Journal of the American Statistical Association 65 (330): 930–45.

Nagato, Akinori Cardozo, Marco Aurélio dos Santos Silva, Eduardo Tavares Lima Trajano, Jackson Nogueira Alves, Ana Carla Balthar Bandeira, Tereza Aparecida Ferreira, Samuel dos Santos Valença, and Frank Silva Bezerra. 2011. "Quantitative and Morphological Analyses of Different Types of Human Liver." Braz J Morphol Sci 28 (4): 275–79.

Netter, F.H. 2014. Atlas of Human Anatomy. Sixth edition. Philadelphia: Saunders/Elsevier.

Neviere, R. 2005. "Physiologie Digestive." Cours PCEM 1, Lille.

O'Followell, Ludovic. 1908. Le Corset. Maloine. Paris.

OpenStax. 2016. Anatomy & Physiology. OpenStax CNX. http://cnx.org/contents/14fb4ad7-39a1-4eee-ab6e-3ef2482e3e22@8.26.

Ottensmeyer, Mark P., Amy E. Kerdok, Robert D. Howe, and Steven L. Dawson. 2004. "The Effects of Testing Environment on the Viscoelastic Properties of Soft Tissues." In Medical Simulation, edited by Stéphane Cotin and Dimitris Metaxas, 9–18. Springer Berlin Heidelberg. http://link.springer.com/chapter/10.1007/978-3-540-25968-8_2.

Prince, M.R., R.A. Novelline, C.A. Athanasoulis, and M. Simon. 1983. "The Diamter of the Inferior Vena Cava and Its Implications for the Use of Vena Cava Filters." Radiology 149 (3).

Rouiller, Ch. 1964. The Liver: Morphology, Bio-Chemistry, Physiology. Academic Press. Vol. 2. New-York, NY, USA.

Rutkauskas, Saulius, Vytautas Gedrimas, Juozas Pundzius, Giedrius Barauskas, and Algidas Basevicius. 2006. "Clinical and Anatomical Basis for the Classification of the Structural Parts of Liver." Medicina (Kaunas, Lithuania) 42 (2): 98–106.

Serre, T, C. Brunet, K. Bruyere-Garnier, J-P Verriest, David Mitton, S. Bertrand, W. Skalli, T. Bekkour, and K. Kayvantash. 2006. "HUMOS (Human Model for Safety) Geometry: From One Specimen to the 5th and 95th Percentile, Digital Human Modeling for Design and Engineering Conference." In SAE 2006. Vol. 2006–01–2324. Lyon.

Siddiqui, Tanya Raza, Nushat Hassan, and Pashmina Gul. 2014. "Impact of Anthropometrical Parameters on Portal Vein Diameter and Liver Size in a Subset of Karachi Based Population." Pakistan J. of Medical Sciences 30 (2): 284–388.

Skandalakis, John E., Lee J. Skandalakis, Panajiotis N. Skandalakis, and Petros Mirilas. 2004. "Hepatic Surgical Anatomy." The Surgical Clinics of North America 84 (2): 413–35, viii. doi:10.1016/j.suc.2003.12.002.

References

Skandalakis, Lee John. 2004. Skandalakis Surgical Anatomy: The Embryologic and Anatomic Basis of Modern Surgery 2 Vol. Set. 1 edition. Athens, Greece; London: P.M.P.

Smithuis, Robin, and Eduard de Lange. 2015. "Anatomy of the Liver Segments." Radiology Assistant.

Sobotta. 2006. Atlas of Human Anatomy. 14th ed. Vol. 2. Elsevier.

Stamm, E.R., J.M. Meier, S.S. Pokharel, T. Clark, D.H. Glueck, and K.E. Lind. 2016. "Normal Main Portal Vein Diameter Measured on CT Is Larger than the Widely Referenced Upper Limit of 13 Mm." Abdominal Radiology 41 (10): 1931–36.

Strasberg, Steven M. 2005. "Nomenclature of Hepatic Anatomy and Resections: A Review of the Brisbane 2000 System." Journal of Hepato-Biliary-Pancreatic Surgery 12 (5): 351–55. doi:10.1007/s00534-005-0999-7.

Studer, A.-S., C.J.F Kahn, T. Bege, L. Thollon, A. Londou, K. Chaumoître, S. Coze, S. Berdah, and C. Brunet. 2015. "An Anatomic and Morphometric Analysis of Splenic Variability Using 3D Reconstruction and Spatial Orientation from Computed Tomography." Annals of Anatomy 201: 50–55.

Terminologia Anatomica: International Anatomical Termicology. 1998. New York: Thieme Medical Publishers.

Varotti, G., G.E. Gondolesi, J. Goldman, M. Wayne, S.S Florman, M.E Schwartz, C.M Miller, and Emre Sukru. 2004. "Anatomic Variations in Right Liver Living Donors." Journal of the American College of Surgeons 198 (4): 577–82.

Verma, Sachit K., Kristen McClure, Laurence Parker, Donald G. Mitchell, and Manisha Verma. 2010. "Simple Linear Measurements of the Normal Liver: Interobserver Agreement and Correlation with Hepatic Volume on MRI." Department of Radiology Faculty Papers.

Vinnakota, Sunitha, and Neelee Jayasree. 2013. "A New Insight into the Morphology of the Human Liver: A Cadaveric Study." ISRN Anatomy 2013 (December). doi:10.5402/2013/689564.

Vitte, Elizabeth, and Jean-Marc Chevallier. 2006. Nouvelle Anatomie Humaine - Atlas Médical Pratique. VUIBERT.

Weinreb, Jeffrey C., Sheila Kumari, Gail Philips, and Rubem Pochaczevsky. 1982. "Portal Vein Measurements by Real-Tim Sonography." AJR 139: 497–99.

Whitmore, I. 1999. "Terminologia Anatomica: New Terminology for the New Anatomist." Anat. Rec. 257 (2): 50–53.

Williams, Peter L., Roger Warwick, Mary Dyson, and Lawrence H. Bannister, eds. 1989. Gray's Anatomy. 37 edition. Edinburgh ; New York: Churchill Livingstone.

Zoli, M., D. Magalotti, G. Bianchi, C. Gueli, C. Orlandini, M. Grimaldi, and G. Marchesini. 1999. "Total and Functional Hepatic Blood Flow Decrease in Parallel with Ageing." Age and Ageing 28 (1): 29–33.

Part B: Mechanical characterization of the liver

Accurate knowledge of the ultimate strain of human biological soft tissues is important to improve finite element models in order to realistically predict the risk of traumatic injuries, and to develop surgical tools, in particular for organ prehension. A lot of studies have been carried out on samples in order to quantify the property and material laws and the ultimate strain and stress. These tests on isolated samples of soft tissues raise the problem of the definition of the initial strain state.

Can the ultimate strain of the hepatic capsule be calculated for *in vivo* livers?

In this part, we first review the literature on epidemiological data on road accidents and associated hepatic injuries, as well as a review of the literature on the various methodologies carried out to study the hepatic tissues. These two chapters will allow us to identify our areas of research.

In order to properly define the ultimate strain and to predict the laceration, the third chapter will be dedicating to pressurization tests on different liver state, namely the unpressurized liver, the under pressurized liver, the physiologically pressurized liver, the over pressurized liver and samples. Finally, the fourth and last chapter of this part will be a preliminary study of deceleration tests to create laceration on a specific area of the liver.

Chapter 1: Epidemiologic data in road accident – A review

The following chapter presents a review of the literature on road traffic injuries, injuries to the abdomen and, in particular, the types of injuries found in the liver.

Table of contents

1. Injury classification

In the case of road accidents, most of the accident victims are suffering from polytrauma. Polytrauma represents a set of serious, fatal injuries that without active intensive approach in diagnostics and treatment lead to the undesired end (Bogovic et al., 2014). Victims of major trauma or polytrauma must be treated in trauma centers. When focusing on the liver, its high vascularization can bring serious damage, leading to severe hemorrhages that are difficult to contain, or even death of the patient before rescue. Major trauma patients are defined according to a codification system (Ocak et al., 2009). Thus, codifications have been put in place to classify lesions by gravity. Today, with X-ray tomographic imaging[1], hepatic lesions can be classified more easily (Hoff et al, 2002; Ochsner, 2001).

1.1. Abbreviated Injury Scale

The Abbreviated Injury Scale (AIS) was developed in 1969 and lastly revised in 2015 by The Association for the Advancement of Automotive Medicine and provides an internationally accepted tool for ranking injury severity. It classifies an individual injury by body region according to its relative severity on 6-point scale, as shown in Table B- 1. The AIS score is an estimate of whether or not the injury is fatal. AIS is used for epidemiological records of road traffic injuries.

Table B- 1. Classification of the AIS scores (Champion, 2012)

AIS score	Injury
1	Minor
2	Moderate
3	Serious
4	Severe
5	Critical
6	Maximum
9	Unknown

It described three aspects of the injury by a seven-digit "a b cd ef.g" coding type, location and severity (Association for the Advancement of Automotive Medicine, 2001) :

- a: corresponds to the affected anatomical region (the abdomen is coded by the number 5),
- b: corresponds to the structure type (an internal organ such as the liver is coded by the number 4),

---

[1] Tomography: It is imaging by section or sectioning, through the use of any kind of penetrating wave.

- cd: corresponds to a specific anatomic structure (18 for the liver),
- ef: corresponds to the level of injury (20 for a laceration),
- g: corresponds to the severity of the injuries (AIS score).

Table B- 2 lists the different codes for liver injuries.

Table B- 2. AIS code for the liver (Friedman et al, 1996)

AIS code	Injury description
	Contusion, hematoma
541810.2	Subcapsular[1], ≤ 50 % surface area, Nonexpanding or intraparenchymal ≤ 10 cm in diameter; Minor; Superficial.
541814.3	50 % surface area or expanding; Ruptured subcapsular or parenchyma, Intraparenchymal > 10 cm or expanding; Blood loss > 20 % by volume; Major; Subcapsular.
	Laceration
541822.2	Simple capsular tears, ≤ 3 cm parenchymal depth, ≤ 10 cm in length; blood loss ≤ 20 % by volume; Moderate.
541824.3	3 cm parenchymal depth; Major duct involvement; Blood loss > 20 % by volume; Moderate;
541826.4	Parenchymal disruption of ≤ 75 % of hepatic lobe or 1-3 couinaud's segments within a single lobe; Multiple lacerations > 3 cm deep; "burst" injury; Major.
541828.5	Parenchymal disruption of > 75 % of hepatic lobe or involving > 3 Couinaud's segments within a single lobe or involving retrohepatic vena cava / central hepatic veins; Massive; Complex.
541830.6	Hepatic avulsion[2] (total separation of all vascular attachments).
541840.4	Rupture Use this code only when a more detailed description is not available.

---

[1] Subcapsular: Situated or occurring beneath or within a capsule.
[2] Avulsion: It is an injury in which the liver is forcibly detached from its normal point of insertion.

Thus, for each region considered, there is a MAIS corresponding to the highest AIS for this region. This score does not take into account the long term-deficit of the injury.

1.2. Injury Severity Score

The injury severity score (ISS) is based on AIS. It provides an overall score for patients with multiple injuries (Baker et al., 1974). It corresponds to the sum of the highest AIS squares in the three most affected areas. For this classification, the body is divided into six zones:

- The head and neck (including cervical spine),
- The face (including the facial skeleton, nose, mouth, eyes and ears),
- The chest (thoracic spine and diaphragm),
- The abdomen (abdominal organs and lumbar spine),
- The extremities (pelvic skeleton),
- The external injuries (burns, abrasions, bruises, …)

Thus, the ISS is coded from 0 to 75, which corresponds to three AIS of 5. If an injury is assigned AIS of 6, the ISS score is automatically assigned to 75, due to the unsurvivable injury.

1.3. Organ Injury Scale

The Organ Injury Scale (OIS) was organized in 1987 by the American Association for surgery in order to classify the injuries according to their severity. A graduation was made public in 1989 for the liver, spleen and kidneys, and subsequently for the other organs.

The OIS is divided into 6 grades. Grade 1 corresponds to the least severe injuries, grade 5 to the most severe injuries, to which the patient can survive, and finally grade 6, injuries with no chance of survival. The OIS is specific to each organ and is associated with a qualitative and quantitative notion.

The different injuries of the liver for each grade are described in Table **B- 3Table B- 3.** Organ Injury Scale for the liver (Tinkoff et al., 2008)

grade	Injury type	Description of injury	AIS
I	Hematoma	Subcapsular, < 10 % surface area	2
	Laceration	Capsular tear, < 1 cm parenchymal depth	2
II	Hematoma	Subcapsular, 10 to 50 % surface area: intraparenchymal < 10 cm in diameter	2
	Laceration	Capsular tear 1 to 3 cm parenchymal depth, < 10 cm in length	2
III	Hematoma	Subcapsular, > 50 % surface area of ruptured subcapsular or parenchymal hematoma; intraparenchymal hematoma > 10 cm expanding	3
	Laceration	> 3 cm parenchymal depth	3

IV	Laceration	Parenchymal disruption involving 25 to 75 % hepatic lobe or 1 to 3 Couinaud's segments	4
V	Laceration	Parenchymal disruption involving > 75 % of hepatic lobe or > 3 Couinaud's segments within a single lobe	5
	Vascular	Juxtahepatic venous injuries, ie, retrohepatic vena cava/central major hepatic veins	5
VI	Vascular	Hepatic avulsion	6

2. Source of epidemiologic data

Epidemiological studies are generally divided into three categories. A descriptive part collects information on the number of cases, in our case, the number of road accidents, likewise the number of death and hospitalized victims. The second part is an analytical part, which makes it possible to understand the causes. In road accidents, alcohol and speed factor are often analyzed. Finally, the latter part is an evaluation to measure the impact on public health and to reduce the number of deaths.

The epidemiological data from road accidents come from different sources:

- The police: Reports are put in place for each road accident. The data are gathered in the National Accident Record maintained by the National Interministerial Road Safety Observatory (ONISR). These data are then archived in the form of a bulletin of analysis of accidents by the Departmental Direction of Equipment (DDE). These data are often incomplete due to the lack of follow-up of hospitalized victims.
- The insurance: These data remain confidential.
- Epidemiological records: In France, the most important one is the Rhône Registry of Road Traffic Accidents (2007). This register is based on medical sources. However, this register is incomplete because it takes into account only hospitalized victims and not victims dead at the accident.

3. Road accidents

Improvements in road accidents have reduced the number of fatal accidents, such as the appearance of seat belts (Jolly and Grebing, 1997; Bohlin, 1967), airbags, radar and alcohol control (ONISR, 2011; ONISR, 2012; ONISR, 2013), but also helmet and equipment recommended for cyclist and motorized two-wheelers. Consequently, the pattern of injuries, have evolved with the evolution of car safety. Thus, Klinich et al, (2010) showed that the percentage of victims with abdominal injuries decrease of 67 % from 2001 to 2009 vehicle users and 1985 to 1992 vehicle users. Moreover, with progress in medical imaging, Arvieux et al (2003), showed that between 1975 and 1979, 13 % of hepatic artery and 6 % of major resection were performed, as between 1995 and 1999, only 3 % of resection and one ligature were performed.

3.1. Type of locomotion

Each year, ONSIR draws up a road safety report in France, recording the number of victims according to the type of locomotion, the age and the geographical area. In 2015, there were 3 616 people killed and 73 384 injured of whom 27 717 were hospitalized (Fig B- 1 and Fig B- 2).

Road accidents account for 30 % of the injuries for children between 1 and 4 years old, and 50 % for the children between 5 and 9 years old (Javouhey and Chiron, 2003). In 2015, in France, 226 minor victims were counted and 3 568 hospitalized minors.

Fig B- 1. Percentage of death in France by type of locomotion in 2015 (ONSIR, 2015)

Fig B- 2. Percentage of hospitalized people in France by type of locomotion in 2015 (ONSIR, 2015)

3.2. Type of accidents

There are different collision scenarios (Fig B- 3):

- Accidents of vehicles alone, linked to a loss of control often generated by a speed that is not adapted to the circumstances, and for which shocks against fixed obstacles, as tree, wall, bridge, are more frequent than for other accidents.
- Accidents of a vehicle against one or multiple pedestrians.
- Collision between two vehicles, frontal shock, in which the speeds of the two antagonistic vehicles add up, side shocks or rear shocks.
- Collisions involving three or more vehicles, like multiple collisions, with various configurations, and chain collision.

Fig B- 3. Percentage of death in France by type of accident in 2015 (ONSIR, 2015)

Accidents with the highest number of fatalities correspond to accidents involving a single vehicle or two vehicles.

3.3. Location of injuries

All gravity combined, pedestrians, cyclists and motor two-wheelers are mainly affected to the limbs (lower and upper). On the other hand, vehicle users are mainly affected at the spine and to a lesser extent, at the thorax and the head (Table B- 4).

Table B- 4. Percentage of victims by segments for all gravity combined, in France from 2007 to 2010 (ONSIR, 2011)

	Vehicle users	Motor 2-Wheelers	Cyclists	Pedestrians
Head	19.9	12.3	15.8	26.8
Face	9.8	6.7	22.5	16.6
Neck	18.1	4.3	3.0	4.2
Thorax	20.7	10.7	7.0	10.4
Abdomen	6.4	6.4	4.3	6.7
Spine	46.2	11.6	7.0	13.5
Lower limb	22.0	43.1	46.3	31.1
Upper limb	17.2	60.6	33.2	63.8

By studying only injuries with an AIS 4 or more, it is observed that vehicle users and motor 2-wheelers mainly have this type of injury at the thorax and the head, and to a lesser extent to the abdomen. It is this kind of injuries which are potentially fatal (Table B- 5).

Table B- 5. Percentage of victims by segments for AIS 4+, in France from 2007 to 2010 (ONSIR, 2011)

	Vehicle users	Motor 2-Wheelers	Cyclists	Pedestrians
Head	47.8	41.7	75.8	71.4
Face	2.9	1.8	1.5	0.8
Neck	0.0	0.0	1.5	0.0
Thorax	57.0	60.5	25.8	42.9
Abdomen	11.6	20.2	6.1	6.8
Spine	10.6	8.5	10.6	3.0
Lower limb	0.0	0.0	0.0	0.0
Upper limb	1.9	4.9	1.5	7.5

Impact between cars and heavy vehicles show weak external lesions and massive internal injuries causing death of the car drivers (Carson and Cook, 2008). These collisions involve high speed with generation of high impact force and high acceleration or deceleration.

Polytrauma are due to road accidents in 65 % of the case. Diagnostic of a wound at the abdomen remain difficult, indeed, clinical exam does not always reveal them (Menegaux, 2003).

3.3.1. Abdominal lesion

When analyzing all abdominal trauma occurrences from March 2012 up to March 2014 in the Iman Reza Hospital, at Tabriz in Iran, Abri et al. (2016) observed that more than 50 % of the traumas are due to a road accident (Fig B- 4).

Fig B- 4. Accident condition in Tabriz (Iran) from March 2012 up to March 2014 (Abri et al, 2016)

Car crash gathered a lot of car crash condition, as the type of collision (frontal, rear …) or the type of vehicle implied (collision between a car and an object, between two cars …). Klinich et al. (2016) studied the injuries in motor-vehicle crashes in the United States between 1998 and 2014. They examine abdominal injuries according to the type of car accidents (Fig B- 5).

Fig B- 5. Abdominal injuries due to car accidents in the United States between 1998 and 2014 – Distribution among accidents type (Klinich et al, 2016)

Among all the abdominal injuries, the hepatic injuries represent 19 % and the splenic injuries represent 27 % (Laumon, 2002). Unlike the spleen, the liver cannot be removed and is essential to the functioning of the human body.

3.3.2. Liver injuries

In the case of liver damage, statistics from the Hôpital Nord of Marseille between 2009 and 2011 (unpublished data) show that 60 % of the liver lesions are caused by road accidents. In 80 % of cases, these lesions are associated with a hemoperitoneum[1]. In 37 % of the cases, the lesions of the liver lead to complications.

There are two types of trauma, penetrating and non-penetrating trauma. These are the result of closed trauma and account for 80 % of abdominal trauma (Tinkoff et al, 2008). Liver lesions can be classified into four groups (Lefèvre et al, 2007):

- Subcapsular hematomas are the result of shearing between the Glisson capsule and the parenchyma. It is assessed as the percentage of area covered. If the capsule breaks, the parenchyma is exposed, and bleeding occurs.
- Bruises are deeper hematomas resulting from a fracture of the parenchyma where the Glisson capsule resisted.
- Fractures are tears or lacerations of the organs open in the peritoneal cavity.
- Lesions of the vascular system correspond to tearing of the vessels causing significant bleeding.

Matthes et al. (2003) studied polytrauma patients from a level 1 trauma center at Berlin from September 1997 to January 2001. The patients had encountered high-velocity or severe blunt body trauma as motor-vehicle accident, fall from a height, pedestrian or bicycle/motorbike accidents. They showed the percentage of injury by liver segments (Fig B- 6).

Fig B- 6. Percentage of injury by liver segments (Matthes et al, 2003)

---

[1] Hemoperitoneum: It is the presence of blood in the peritoneal cavity.

Theses lesions can be initiated by:

- A direct shock, which is the application of an important force not absorbed by the costal grill. The energy is transmitted to the liver by the rib cage in the form of a shock wave. This energy can be dissipated locally by costal fracture or chondro[1]-costal disintegration.
- A deceleration that creates a back and forth movement of the liver, performing dilacerations, multiple lacerations, according to the plane of the right coronary and right triangular ligaments. The right lobe will be dragged forward.
- Shear effects in lateral impact.

Tinkoff et al. (2008) studied the mortality rate of the lesions of the liver. As a result, the average mortality rate with liver damage is 13.6%. The mortality rate increased to 23.9% for lesions of grade IV, 61.7% for lesions of grade V and 91.5% for lesions of grade VI.

In a second step, they exclude all liver lesions associated with brain trauma. A mortality rate of 10.5% is obtained. It increases from 20.8% for a grade IV to 59.6% for a grade V and finally 92.5% for a grade VI.

Finally, they exclude liver lesions with premature death due to this lesion. The mortality rate drops to 2.5%. It increases from 4.9% for grade IV to 13.1% for grade V and to 0% for grade VI.

This means that when liver damage is spread to the blood vessels the mortality rate rises rapidly. In addition, with grade VI lesions, death occurs prematurely in more than 90% of cases.

4. Synthesis and problematic

Although injuries to the abdomen account for only a small part of injuries in road accidents, the high vascularization of the liver causes severe internal bleeding. **Thus, the liver is an organ that is important to protect.**

Moreover, a frontal crash preferentially creates lacerations on segments V, to VIII. These four segments gathered more than 60 % of the injuries. **Thus, it will be interesting to study the mechanism of laceration on the right lobe.**

---

[1] Chondro: It refers to the cartilage.

Chapter 2: Experimental study of the mechanical behavior of the liver – A review

The purpose of the following chapter is to present a review of the literature on the different experimental tests and their application to the liver.

Table of contents

Historically, researchers have been interested in abdominals organs to understand the mechanisms of injury in road accidents and thus to improve the safety of cars. Nowadays, with technical progress, including the development of minimally invasive surgery and numerical models, researchers have turned to the study of abdominal organs subjected to different loads during surgery in order to create surgical simulators.

1. Experimental tests on hepatic tissues

1.1. Compression tests

1.1.1. Tests on samples

1.1.1.1. Quasi-static uniaxial compression tests

Uniaxial test consists on applying a uniformly distributed compression load on the surface of a free sample to expand laterally (Fig B- 7). This test, which is relatively simple to implement, is very much described in the literature (Chui et al, 2007; Raghunathan et al, 2010; Tamura et al 2002; Yeh et al, 2002). The samples used are cylindrical or cubic of the order of one centimeter, for compression speeds ranging from 0.01 to 60 mm / s. The compression is in most cases followed by a relaxation phase. The authors then attempt to measure the effects of deformation level and deformation velocity level on observed behaviors.

Fig B- 7. Uniaxial compression test on cylindrical porcine samples of 19 mm in diameter and 10 mm thick (Raghunathan, 2010)

In order to avoid lateral stresses, some authors lubricate the plates prior to the tests (Gao et al, 2010; Kiss et al, 2004; Roan and Vemaganti, 2007; Santago, 2010). Other authors attempted to remove these friction effects by sticking the samples to the plates (Chui et al., 2004, Fu and Chui, 2014, Roan and Vemaganti, 2007, Sakuma et al., 2003).

Roan and Vemaganti (2007) carried out tests under two conditions in order to check the impact of friction during compression tests. The results show a significant difference between these two conditions.

The uniaxial compression tests allow a direct measurement of the stress-strain relationship. On the other hand, the influence of the friction conditions is not negligible and can lead to an overestimation of the stress levels (Wu et al., 2004). In addition, there are problems associated with the cutting of samples (Dan, 1999).

A review of the literature of quasi-static uniaxial compression tests are presented in Table B- 6.

Table B- 6. Review of the literature of quasi-static uniaxial compression tests

Reference	Biological origin	Speed	Tissue preservation	Elastic modulus	Ultimate strain[1] (%)	Ultimate stress[2] (kPa)
Dan (1999)	Human	ND	Fresh	0.338 − 3.027	ND	ND
Tamura et al. (2002)	Porcine	0.05 mm/s	Frozen	ND	43 ± 2,6	123,4 ± 31,4
		0.5 mm/s			42 ± 3,8	135,2 ± 17
		5 mm/s			44 ± 4,0	162,5 ± 27,5
Yeh et al. (2002)	Human	7.1 mm/min	Fresh	ND	ND	ND
Sakuma et al. (2002)	Porcine	50 mm/min	Fresh	ND	ND	ND
Chui et al. (2004)	Porcine	10 mm/min	Fresh	ND	ND	ND
Kiss et al. (2004)	Canine	ND	Fresh	ND	ND	ND
Roan and Vemaganti (2007)	Bovine	ND	Fresh	ND	ND	ND
Raghunathan et al. (2010)	Porcine	ND	Fresh	ND	ND	ND

---

[1] Ultimate strain: It corresponds to the maximum strain at which the material will break.
[2] Ultimate stress: It corresponds to the maximum stress at which the material will break.

Santago (2010)	Human	ND	Fresh	ND	61 ± 5	165,64 ± 41,76
					52 ± 4	158,42 ± 43,10
					46 ± 5	192,60 ± 52,62
					46 ± 5	203,02 ± 33,75
Gao et al. (2010)	Porcine	ND	Frozen	10	ND	ND
Umale et al. (2013)	Human	0.05 mm/s	Fresh	ND	ND	ND
Fu and Chui (2014)	Porcine	ND	Fresh	ND	ND	ND

ND: Not disclosed

1.1.1.2. Dynamic uniaxial compression tests - Kolsky bar

This device consists on a projectile, an "input" bar and an "exit" bar. The sample is then placed between these two bars. The projectile impacts the input bar at high speed (1-50 m / s). The resulting compressive wave propagates in the input bar and in the sample. Part of the wave is reflected at the sample-bar interface and the remainder is transmitted to the output bar. The incident reflected, and transmitted waves are recorded by strain gauges placed on the input and output bars (Fig B- 8). These waves will serve to calculate the axial stress in the sample and the velocity history. The compressibility and shear moduli of the sample tested are deduced therefrom. This dynamic measurement technique has been applied on bovine and porcine liver tissue (Pervin et al, 2011; Saraf et al, 2007a, 2007b). The deformation rates applied are of the order of 1000 s^{-1}. On one hand, Kolsky bar tests allow dynamic measurement and a good repeatability. On the other hand, a problem comes from the compliance of soft tissues whose signal is little transmitted but mainly reflected. A system to compensate the error must then be established (Pervin et al., 2011).

Fig B- 8. (a) Kolsky bar scheme for measuring the modulus of compressibility. (b) View of the tissue confinement device. All measurements are in mm. (Saraf et al., 2007b)

A review of the literature of dynamic uniaxial compression tests are presented in Table B-7.

Table B- 7. Review of the literature of dynamic uniaxial compression tests

Reference	Biological origin	Speed	Tissue preservation	Elastic modulus
Saraf et al. (2007a)	Human	1 to 20 m/s	Frozen	ND
Saraf et al. (2007b)	Human	1 to 50 m/s	Frozen	ND
Pervin et al. (2011)	Bovine	ND	Fresh	20

ND: Not disclosed

1.1.2. Tests on organs

1.1.2.1. Impact tests

Impact tests are intended to recreate the kinetic[1] and kinematic[2] conditions of trauma, and in particular the trauma of road accidents. The stress rates used are between 0.05 and 6 m / s. These tests are mainly performed on human specimens in order to take into account the actual geometry of the organ.

---

[1] Kinetic: Consider the energy that an object possesses due to its motion.

[2] Kinematic: describe the motion of points, objects or groups of objects without considering the mass of each or the forces that caused the motion.

The impactor used can be smaller than the liver (Melvin et al., 1973), the applied stresses can then be controlled; Or greater than the liver (Fig B- 9) to limit edge effects in contact with the organ (Sparks 2007) and it makes it possible to achieve a global compression and observe the overall behavior of the liver (Conte, 2012). In order to re-establish a turgor representative of the *in vivo* state, the livers are pressurized. These tests aim to analyze the lesions induced by these impacts in order to establish a link between the test conditions and the size and depth of the lesion.

Fig B- 9. Experimental set up of uniaxial compression tests on human liver (Conte, 2012)
On one hand, impact tests maintain a good geometry of the organ and a good restitution of the lesions (Sparks, 2007). On the other hand, it is possible to note an influence of the shape of the impactor and a difficult analysis of the stress-strain relationship.

A review of the literature of impact tests are presented in Table B- 8.

Table B- 8. Review of the literature of impact tests

Reference	Biological origin	Speed	Tissue preservation	Elastic modulus	Ultimate strain (%)	Ultimate stress (kPa)
Melvin et al. (1973)	Monkey	5 cm/s	Fresh	ND	$41-59$	$145-293$
		250 cm/s			$44-75$	$234-407$
		500 cm/s			$48-59$	$234-662$
Ozcan et al. (2011)	Human	ND	Fresh	$10-20$	ND	ND
Conte (2012)	Human	0.01 m/s	Embalmed	ND	$42-49$	ND
		1 m/s			$38-53$	
		0.2 m/s			$30-57$	
		80 mm/min			$29-44$	

ND: Not disclosed

1.1.2.2. Motorized endoscopic grasper

The motorized endoscopic grasper (Fig B- 10) allows a more localized compression (Brown et al., 2003a, Rosen et al., 2008).

This method has the advantage of being able to test the liver under various conditions, namely *in-vivo*[1], *in-situ*[2] and *in-vitro*[3], as well as to compare different localization on *in-vitro* livers. It is a motorized grasper developed by the University of Washington's biorobotic laboratory. The motor is capable of producing a gripping force of 26.5N. This instrument is held by hand and can be inserted into the body through standard endoscopic ports. The force sensor directly measures the force of the clamp.

Fig B- 10. Motorized endoscopic grasper (MEG) (Brown et al, 2003b)

A review of the literature of motorized endoscopic grasper tests are presented in Table B-9.

Table B- 9. Review of the literature of motorized endoscopic grasper tests

Reference	Biological origin	Speed	Tissue preservation	Elastic modulus	Ultimate strain (%)	Ultimate stress (kPa)
Brown et al. (2003a)	Porcine	5 mm/s	Fresh	ND	33 – 66	170 – 280
Brown et al. (2003b)	Porcine	8.2, 32.2 & 65.3 mm/s	Fresh	30 – 50	ND	ND
Rosen et al. (2008)	Porcine	ND	Fresh	160 – 280	35 – 60	ND
				220 - 420	30 – 43	

ND: Not disclosed

---

[1] *In vivo*: The liver is tested on the whole living organisms.
[2] *In situ*: The liver is tested on the whole non-living organisms.
[3] *In vitro*: the liver is tested outside the whole living organisms.

1.2. Tensile tests

1.2.1. Tensile tests between two jaws

Tensile tests can be realized by the means of two jaws (Brunon et al, 2010; Lu et al, 2014, Santago, 2010, Untaroiu and Lu, 2013). This method is carried out on specimens of a precise shape named dog bone, which is difficult to obtain on soft tissues. These are uniaxial tensile stress in slow speed ranges from 10 to 76 mm / min. Mounting the test pieces on the machine test is a key step (Fig B- 11).

Fig B- 11. Experimental set up for tensile tests on bovine liver samples (Santago, 2010)

On one hand, these tensile tests allow a good measurement of the strain state as well as the ultimate strain. On the other hand, the fixation of the soft tissues samples is complicated and there is an influence of gravity on the homogeneity of the strain state (Gao and Desai, 2010).

A review of the literature of tensile tests between two jaws are presented in Table B- 10.

Table B- 10. Review of the literature of tensile tests between two jaws

Reference	Biological origin	Frequency or speed of traction	Tissue preservation	Ultimate strain (%)	Ultimate stress (kPa)
Ohara (1953)	Rabbit	ND	ND	46 ± 2.3	23.5 ± 4.9
Uehara (1995)	Porcine	8.33 mm/s	ND	ND	205 ± 28
Stingl et al. (2002)	Human	ND	Fresh	ND	66 – 386

Brunon et al. (2010)	Porcine	0.5 mm/s	Fresh	43.3 ± 25.4	2030 ± 2440
			Frozen	62.9 ± 35.4	1220 ± 1120
	Human		Fresh	32.6 ± 13.8	1850 ± 1180
			Frozen	43.9 ± 24.2	2770 ± 2690
Santago (2010)	Bovine	0.07 s^{-1}	Fresh	33	19
			Frozen	16	23,96
			Fresh, 37°C	26	49,88
			Fresh, 22°C	25	54,79
	Human	0.01 s^{-1}	Fresh	34 ± 12	40,21 ± 21,39
		0.10 s^{-1}		32 ± 5	46,79 ± 24,81
		1.00 s^{-1}		30 ± 10	52,61 ± 25,73
		10.0 s^{-1}		24 ± 7	61,02 ± 24,89
Lu et al. (2014)	Bovine	0.01 s^{-1}	Fresh	35 − 50	30 − 60
			30 days frozen	25 - 45	35 − 55
			60 days frozen	30 − 40	25 − 65
		0.10 s^{-1}	Fresh	30 − 55	35 − 65
			30 days frozen	25 − 40	35 − 70
			60 days frozen	25 − 35	40 − 70
		1.00 s^{-1}	Fresh	30 − 40	30 − 75
			30 days frozen	25 − 35	45 − 80
			60 days frozen	20 − 35	50 − 75

ND: Not disclosed

1.2.2. Tensile tests between two plates

Tensile tests can be realized by the means of two plates. This method (Chui et al., 2007, Gao and Desai, 2010, Gao et al., 2010, Sakuma et al., 2003) requires more compact samples (cylindrical or cubic), which will be glued to the plates. With this method, the rupture is not reached, as an area of stress and strain cannot be localized in samples with a constant section. However, this technique has the advantage of being able to couple tensile and compression tests.

A review of the literature of tensile tests between two plates are presented in Table B- 11.

Table B- 11. Review of the literature of tensile tests between two plates

Reference	Biological origin	Sample		Frequency or speed of traction	Tissue preservation
		Shape	Size (mm)		
Sakuma et al; (2003)	Porcine	Cylindrical	Diameter: 7 Length: 5 to 10	ND	Fresh
Chui et al. (2007)	Porcine	Cylindrical	Diameter: 7 Length: 10	10 mm/s	Fresh
Gao et al. (2010)	Porcine	Rectangular	Length: 25X16	1.25 mm/s	Frozen
Gao and Desai (2010)	Porcine	Rectangular	Length: 25X16	1.27 mm/s	Frozen

ND: Not disclosed

1.3. Indentation tests

The indentation test is used to determine the mechanical properties of the hyper-elastic or elastic behavior of the liver. These tests consist of the application of a load, by means of an indenter, to the surface of the material. As explain by Seifert (2003), it is a rod which comes to bear with a given load in the direction normal to the surface of the material to be characterized. The test conditions are the indenter geometry, indentation depth and indentation speed.

There are three standard shapes for the indentor: cylindrical with rounded end (Carter et al., 2001; Egorov et al., 2008; Samur et al., 2007; Yarpuzlu et al., 2014), cylindrical with flat end (Kim, 2004; Kim et al., 2003; Tay et al., 2006) and needle-shaped (Schwartz et al., 2005; Yarpuzlu et al., 2014), with a diameter ranging from 2 to 12 mm (Fig B- 12). The indentation depth can vary from 0.5 to 20 mm, and the indentation rate is between 0.2 and 48 mm / s, generally between 1 and 10 mm / s.

Fig B- 12. Model of indenters usable *in vivo* (Carter et al, 2001)

The principle of indentation has little changed, but the tools have become more and more complex in order to achieve *in vivo* indentation and to apply a more precise force and duration. A portable indentation system has been developed (Carter et al., 2001; Samur et al., 2007), as well as a robotic system (Kim, 2004; Kim et al., 2003; Ottensmeyer, 2001; Tay et al., 2006) to compensate for the inaccuracy of human force.

This type of test, which is easy to implement and has good reproducibility, has the advantage of being able to obtain a local and non-destructive measurement, which allows the *in vivo* tests, except in the study of Rosen et al. (2008) where the hepatic tissue is indented on both sides until rupture. On the other hand, it requires a prior calibration (Ahn and Kim, 2010) and the dimensions of the sample tested must be large in front of those of the indenter, hence the authors mainly chose to perform the test on an entire organ (Egorov et al., 2008). Thanks to the indentation, the relaxation of the tissues can be observed (Ahn and Kim 2010, Egorov et al 2008), its creep (Kerdok et al., 2006) or its response to a cyclic stress (Kerdok et al., 2006). Finally, the measurement may vary according to the position of the indenter.

The quantities measured are generally the effort and the depth of indentation. From these quantities there are two ways of going back to the properties of the material: either the indentor has a shape such that the radius and surface of the contact zone with the sample and the contact theory is used to determine the mechanical quantities; or the contact area cannot be precisely determined, and an inverse analysis is performed by means of a numerical modeling of the test.

A review of the literature of indentation tests are presented in Table B- 12.

Table B- 12. Review of the literature of indentation tests

Refe-rence	Biologi-cal origin	Type of specimen	Experimental condition	Indenter		Indentation		Tissue preser-vation	Elastic modulus (kPa)
				Shape	Diameter (mm)	Depth (mm)	Speed (mm/s)		
Yokoo and Ko (1951)	Rabbit	Organ	*In vitro*	Flat	5	10	ND	Fresh	5.6
Carter (1998)	Human	Organ	*In vivo*	ND	2.2 to 5	1	ND	Fresh	170
Carter et al. (2001)	Porcine	Organ	*In vitro*	Round	4.5	ND	1	Fresh	490
	Human		*In vivo*			5	3 to 4		270
Ottens-meyer (2001)	Porcine	Organ	*In vivo*	ND	5	0.5	ND	Fresh	10 – 15
Kim et al. (2003)	Porcine	Organ	*In vivo*	Flat	2	ND	ND	Fresh	31.8

Kim (2004)	Porcine	Organ	*In vivo*	Flat	2	2, 4, 6 & 8	ND	Fresh	3.22 ± 0.6
Schwartz et al. (2005)	Cervine	Sample	*In vitro*	Needle	24	Until rupture	2, 6 & 10	Fresh	25
Kerdok (2006)	Porcine	Organ	*In vivo* / *In vitro* perfused / *In vitro*	Flat	6	ND	ND	Fresh	ND
Tay et al. (2006)	Porcine	Organ	*In vivo*	Flat	2	4 / 6 / 8	4 / 6 / 8	Fresh	12.88 ± 2.53
Samur et al. (2007)	Porcine	Organ	*In situ*	Round	4	2 / 4 / 6 / 8	0.2	Fresh	16.9 ± 4.9 / 12.4 ± 4.1 / 10.8 ± 4.7 / 10.0 ± 4.7
Egorov (2008)	Bovine	Sample	*In vitro*	Round	3	ND	ND	Fresh	7.4 – 10
Anh and Kim (2010)	Porcine	Organ	*In vitro*	Flat & round	10	5 & 7	ND	Fresh	ND
Yarpuzlu et al. (2014)	Bovine	Organ	*In vitro*	Round	3 to 6	20	0.5 static & 48 dynamic	5H fresh / 11H fresh / 17H fresh / 29H fresh / 41H fresh / 53H fresh	1.57 ± 1.1 / 1.70 ± 1.1 / 2.95 ± 2.2 / 7.91 ± 1.8 / 20.95 ± 2.9 / 33.60 ± 3.7

ND: Not disclosed

1.4. Shear tests

1.4.1. Shear tests using two plates

Shear tests can be carried out by the means of two plates (Gao et al., 2010, Nicolle et al., 2010). This method is inspired by the rheology[1] tests of polymers. Parallel plate rheometers[2] are used to measure an effort and angles, then a behavior analytical model is used to calculate shear viscoelastic properties in abdominal soft tissues (Nicolle et al., 2010). A sinusoidal loading is then applied on the specimen.

A review of the literature of shear tests between two plates are presented in Table B- 13.

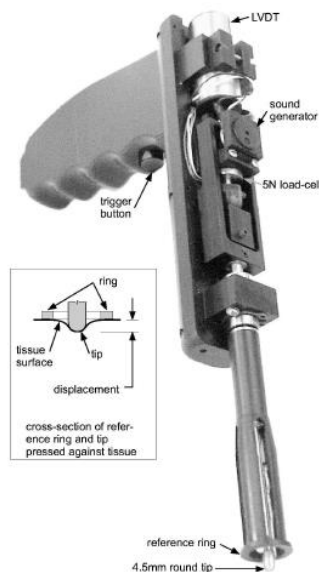**Table B- 13.** Review of the literature of shear tests using two plates

Reference	Biological origin	Speed (mm/s)	Tissue preservation
Gao et al. (2010)	Porcine	0.65 – 0.75 mm/s	Frozen
Nicolle et al. (2010)	Porcine	ND	Fresh

ND: Not disclosed

1.4.2. Shear tests using the Kolsky bar

The second method (Saraf et al., 2007a, 2007b) is implemented within a Kolsky compression bar configuration. In this case, instead of having a cylindrical sample between two elastic bars, there is a system for fixing two paved samples which are surrounded by aluminum plates (Fig B- 13).

---

[1] Rheology: It is the study of the flow matter, primarily in a liquid state, but also as 'soft solids', or solids under conditions in which they respond with plastic flow rather than deforming elastically in response to an applied force
[2] Rheometer: It is a laboratory device used to measure the way in which a liquid, suspension or slurry in response to applied forces.

Fig B- 13. (a) Experimental set up of the Kolsky bar for shear tests; (b) View of the tissue confinement device. All measurements are in mm. (Saraf et al., 2007b)

A review of the literature of shear tests using Kolsky bar are presented in Table B- 14.

Table B- 14. Review of the literature of shear tests using Kolsky bar

Reference	Biological origin	Speed (mm/s)	Tissue preservation	Shear modulus (kPa)
Saraf et al. (2007b)	Human	ND	Frozen	37 – 340

ND: Not disclosed

1.5. Other tests

1.5.1. Deceleration tests

Deceleration tests can be induced by free falls. Thus, some authors (Cheynel 2007, Cheynel et al., 2006) focused their work on the evaluation of the mobility of the liver by directly instrumenting this organ before subjecting trunks to free falls.

1.5.2. Elastography

Elastography tests are based on the Christoffel equation[1] which indicates that the tensor of elasticity of a material is related to the speed of propagation of a plane wave in the environment. In the case of ultrasonic elastography (Maass and Kühnapfel 1999), there is

---

[1] Christoffel equation: It is the mathematical study of how solid objects deform and become internally stressed due to prescribed loading conditions.

therefore a relation between the moduli of elasticity, shear and compressibility and the velocity of sound in the material. This noninvasive technique consists in the transmission of an ultrasound wave in the liver and the measurement of its propagation speed in order to deduce the properties of the material *in vivo*.

1.5.3. Magnetic resonance elasticity

It is a non-invasive technique for which the three-dimensional displacement field induced by the propagation of a shear wave in the tissue is measured by MRI[1]. The viscoelastic properties (conservation and loss modulus), which are written as a function of the deformation, are then deduced (Clarke et al., 2011).

1.5.4. Aspiration

For aspiration tests the hepatic tissue is sucked lightly by creating vacuum in a tube plated on the surface of the organ (Mazza et al., 2008). The induced deformation is recorded and the relationship between the pressure in the tube and the measured peak makes it possible to deduce pseudo material properties.

2. Parameters influencing the mechanical behavior

2.1. Influence of the pressurization on the mechanical behavior

It seems clear that the vascularization of the liver contributes to the incompressible nature of the organ but also to its dependence on the strain rate (Raghunathan et al., 2010). To quantify the influence of this pressurization, some authors (Kerdok et al., 2006) have developed an ex vivo pressurization device for porcine livers (Fig B- 14). By comparing the behaviors measured in vivo, ex vivo with pressurization and ex vivo without pressurization, this device makes it possible to show that a test carried out under perfusion makes it possible to find virtually the behaviors of *in vivo*. They found that the *ex vivo* perfused tissues exhibited similar viscoelastic behavior to the *in vivo* tissues and showed consistency between successive indentations. This study confirms the preponderant role of the vascular tree in the overall behavior of the organ.

---

[1] MRI: Magnetic Resonance Imaging is a medical imaging technique used in radiology to form pictures of the anatomy and the physiological processes of the body.

Fig B- 14. Pressurization device for porcine liver (Kerdok et al., 2006)

2.2. Behavior of the different hepatic tissues

The microscopic structure of the liver may have an influence on its behavior. Indeed, the uniaxial compression of specimens cut at the surface so as to have one of the directions of the sample parallel to the axis of the lobules lead to a transverse isotropic[1] behavior (Chui et al. 2007). In other words, the stiffness of the material is greater when it is stressed along the axis of the lobules. However, on a larger scale, parenchymal samples alone show no anisotropy (Pervin et al., 2011). Finally, Ahn and Kim (2010) show the axi-symmetry of the surface deflection of the liver. These results limit the hypothesis of isotropy to the internal part of the liver observed on the scale of several lobules.

The Glisson capsule can influence the overall behavior of the liver. Even if, cubic sample compression assays with and without capsules (Chui et al., 2007) have shown that locally the presence of the capsule has no influence, at the level of the organ, it is very likely that an intact capsule participates in the cohesion of the structure. To quantify the membrane effect, the authors performed uniaxial tensile tests on capsule samples (Brunon et al., 2010, Dan 1999, Stingl et al., 2002, Umale et al., 2011). To approximate the actual load conditions, some authors have chosen the inflation traction method, which allows multidirectional loading (Brunon et al., 2011). The ultimate strain is then greater in multidirectional loading than in uniaxial loading. This value shows that the capsule is

---

[1] Isotropy: Uniformity in all orientations.

more resistant when it is urged in a multidirectional manner. This confirms the hypothesis according to which the capsule has above all a role of membrane which ensures the cohesion of the organ.

2.3. Influence of the biological origin on the mechanical behavior

For the same trial, the authors observed inter-subject variability (Carter et al., 2001) and an influence of the age and sex of the subject on whom the hepatic tissues were tested (Stingl et al. 2002). On the other hand, the biological origin of the tissue induces variability. Indeed, the hepatic tissue of a diseased liver (cirrhosis, choleastic liver) is twice as rigid as a healthy liver (Carter et al., 2001; Umut Ozcan et al. 2011) and porcine liver tissue, widely used as a substitute for human tissue, shows significant difference of ultimate strain (Brunon et al., 2010).

2.4. Influence of the type of specimen on the mechanical behavior

The anatomical environment in which the liver evolves influences its behavior. For example, full scale tests[1] show that the left lobe is more mobile than the right lobe (Cheynel et al., 2006). It is therefore liable to be subjected to higher deformation levels. Moreover, the shape of the tissue at the time of the test has some influence on the qualitative and quantitative data measured. First of all, the consistency of the liver tissue makes it difficult to cut the samples regularly and causes the experimenter to remove up to 30% of the cut specimens (Dan 1999). In addition, the specimen is an open system, then an irreversible phenomenon is then introduced because of the exudation, even if the latter are negligible at short times (<1 s) (Dan 1999). In their study, Kerdok et al. (2006) realized indentation tests on porcine *in vivo* livers and on porcine *ex vivo* perfused livers. They pointed out the importance of the geometric and physiologic boundary conditions.

2.5. Influence of the tissues preservation conditions

Most authors attempt to perform their tests on fresh tissue as far as possible. But some, for practical reasons, resort to freezing. On one hand, Brunon et al, (2011) and Pukacki et al, (2000) showed that this type of preservation did not significantly influence the behavior of the hepatic parenchyma, Glisson's capsule and vascular tissue of human origin.

---

[1] Full scale test: Those tests are realized on the full body or at least on a body segment.

On the other hand, Ternifi et al. (2013) reported that freezing had a significant effect on the porcine renal tissues and led to a large reduction of standard deviations. Finally, in addition to preservation, tissue dehydration increases their rigidity (Nicolle and Palierne 2010). However, the authors showed that this phenomenon is reversible and that the tissue regains its initial behavior once rehydrated.

3. Synthesis and problematics

Each test presented makes it possible to isolate some characteristics of the **mechanical behavior of the liver**. Experimental work, which can be performed *in vivo* or *in vitro*, at different speeds and under different conditions, gives local or global information.

Thus, before the experimental work it is necessary to point out the type of results we want to record. The purpose of this work is to better understand the liver during road accident. Thus, it is important to realize experimental test on the whole liver. Furthermore, as the liver seems to decelerate most of the time during road accident, **we will reproduce deceleration test on the liver,** to find the ultimate strain of the Glisson capsule.

Then it is important to statue on the initial condition. A lot of studies determine the ultimate strain by carry out tensile tests on samples, but do not allow representing an *in vivo* solicitation. Some tests are performed on the whole liver which allows obtaining mechanical parameters by inverse method. Before deceleration test it seems interesting to **study the difference of behavior between two types of specimen, samples and the hole liver**.

Because of the difference in geometry and on histology, the biological origin can have an influence (Brunon et al, 2010) on the mechanical properties measured, it therefore seems important to perform **experimental work on human liver**.

As Kerdok et al. (2006) found that the *ex vivo* perfused tissues exhibited similar viscoelastic behavior to the *in vivo* tissues the question of the influence of the pressurization of *in vitro* organs can be raised. However, Kerdok et al, (2006) studied porcine liver, and as recall above, significant difference of the ultimate strain can be found between porcine and human liver. Thus, it seems important to **study the influence of the vascularization on human liver**.

Chapter 3: Importance of the initial state of strain for the Glisson's capsule

In order to do experimental tests, it is important to choose the right initial state. This chapter presents the experimental work to point out the importance of the initial state of strain of the Glisson's capsule.

Table of contents

Part B: Mechanical characterization of the liver until ultimate strain

1. Material and methods

1.1. Preparation of the livers

Eight livers were removed from post-mortem human subjects (PMHS) through the French voluntary donation to science program, by a surgeon with particular attention to ensure the entirety of the tissues, namely no tearing of the Glisson capsule, the presence of the portal vein, the hepatic artery, the vena cava, the falciform ligament and the diaphragm.

Five livers, preserved within Winckler solution (Winckler, 1964) were taken off at the Department of Emblaming of the faculty of medicine in Marseille (3 women and 2 men; mean age : 93 y.o.), and three livers preserved within the Safebalm® solution (OGF, France) were taken off at the Department of Anatomy of University of Lyon (1 woman and 2 men; mean age : 91 y.o.) (Table B- 15). The livers preserved with Safebalm® were tested within five days after death. No information is mentioned for livers preserved with Winckler solutions.

Table B- 15. Liver's information for pressurization tests

Liver ID	Age	Gender	Embalming solution
L1	95	Man	Winckler
L2	94	Woman	Winckler
L3	90	Woman	Winckler
L4	NC	Woman	Winckler
L5	NC	Man	Winckler
L6	93	Man	Safeblam ®
L7	91	Woman	Safebalm ®
L8	90	Man	Safebalm ®

After removing, the livers were placed in hermetically sealed boxes and moistened with compresses soaked in PBS[1]. The livers were then kept at +4°C during 24 to 48 hours before testing. One-hour prior testing, livers were put at the room temperature (20±2°C). As Santago et al. (2009) reported no statistical differences for stress and strain values between livers at 24°C (75°F) and livers at 37°C (98°F), no attempt to test the livers at 37°C was made.

Right before testing, in order to approach the physiological condition, the liver was suspended by the diaphragm. To do so, a fixation box as created as shown in Fig B- 15.

---

[1] PBS: Phosphate-buffered saline is a buffer solution commonly used in biological research. It is a water-based salt solution containing disodium hydrogen phosphate, sodium chloride, potassium chloride and potassium dihydrogen phosphate. The osmolarity and ion concentrations of the solutions match those of the human body.

Fig B- 15. Suspension of the liver in the supporting structure

1.2. Pressurization of the livers

A pressurization system (Fig B- 16) has been set up to artificially restore the liver to the *in vivo* condition. PBS column were used to apply a static pressure in the hepatic artery and in the portal vein. In order to keep the liver pressurized, the vena cava was ligatured. To ensure a proper pressurization and avoid air bubble, a purge device has been added.

Fig B- 16. A) Scheme of the pressurization device; B) Picture of the pressurization device

The blood pressure at the portal vein is around 9 mmHg, as explained by Guyton (1976) and there is a pulsatory blood pressure in the hepatic artery between 120 and 80 mmHg ($16*10^3$ and $11*10^3$ Pa) (Rouiller, 1964). Moreover, Abdel-Misih and Bloomston (2010) considered a blood pressure in the portal vein between 3 to 5 mmHg (400 to 667 Pa), and Sparks and Dupaix (2008), have chosen to perfuse the hepatic artery at 100 mmHg ($13*10^3$ Pa) and the portal vein at 9 mmHg ($1,2*10^3$ Pa).

In this study, we chose to apply, four consecutive pressure levels:

- An unpressurized configuration at 0 mmHg in the portal vein and 0 mmHg in the artery;
- An under pressure at 5 mmHg (667 Pa) in the portal vein and at 50 mmHg (6,7*10^3 Pa) in the artery;
- A physiological pressure at 10 mmHg (1,3*10^3 Pa) in the portal vein and at 100 mmHg (13*10^3 Pa) in the artery, as reference state;
- An over pressure at 15 mmHg (2*10^3 Pa) in the portal vein and at 150 mmHg (20*10^3 Pa) in the artery.

During the test, the four levels of pressure were reached progressively every 40 seconds. Each liver was tested three times straight.

For the presentation of the results, in order to study physiological state of the liver, the interval of internal pressure will be reduced to non-pathological pressure.

Thus, the under pressurized state corresponds to a pressure of 8 mmHg (1,1*10^3 Pa) in the portal vein and a pressure of 80 mmHg (11*10^3 Pa) in the hepatic artery. The over pressurized state corresponds to a pressure of 12 mmHg (1,6*10^3 Pa) in the portal vein and a pressure of 120 mmHg (16*10^3 Pa) in the hepatic artery.

1.3. Sample collection

After pressurization and measurement of strain on the whole liver (cf 1.5), samples with parallelepiped shape (close to 120X30X10 mm^3) were taken off from eight right lobes (Fig B- 17). The number of samples for each liver depends on the volume and shape of the right lobe (Table B- 16). A total of eleven samples were collected. A special care was taken to not damage the pattern of the isolated samples, in order to be able to record it.

Fig B- 17. Picture of an isolated sample taken from liver L8

Table B- 16. Information on the isolated samples

ID	Length (cm)	Width (cm)	Estimated Volume (cm³)*	Ratio L/W
L1_LS	12.0	3.0	36.0	4.00
L1_MS	9.5	2.0	19.0	4.75
L2_LS	12.7	2.5	31.8	5.08
L3_MS	9.6	3.6	34.6	2.66
L3_LS	12.8	3.4	43.5	3.76
L4_MS	8.0	4.0	32.0	2.00
L5_LS	11.3	2.8	31.6	4.03
L5_MS	12.2	3.4	41.5	3.58
L6_LS	15.5	4.7	72.9	3.29
L7_LS	11.1	3.0	33.3	3.70
L8_LS	15.5	3.2	49.6	4.80

* The thickness is estimated to 10 mm for all the samples.

1.4. Strain field measurements

In order to measure a strain field, Digital Image Correlation (Palanca et al., 2016) was applied thanks to the VIC3D® software (Correlated Solution, Columbia, SC, USA).

The Glisson's capsule on the right lobe of the liver was covered with a random pattern of black spray-painting, after a thin layer of white cream was put on, in order to have a better contrast, as shown in Fig B- 18. This pattern was used to perform measurement of the strain field by Digital Image Correlation (DIC). The size of the images was 1024x1024 pixels (for a 16x16 cm images, giving a pixel size of 0.15 mm). The software tracks the displacement of a subset area, which has to be large enough to ensure that there is sufficiently distinctive pattern contained in the area used for correlation. The correlation analysis was non-incremental using a subset of 75 pixels and a space resolution of 4 pixels.

It is important to notice that the hydration of the tissues makes it difficult to measure the strain field by DIC because the light of the spotlights is reflected on the wet surface and creates shiny pixels.

Fig B- 18. Random pattern on the Glisson capsule

117

The liver was visualized by two digital high-speed video cameras (Photron, San Diego, CA, USA). The data acquisition frequency was 10Hz (Table B- 17). Both cameras were focused on the right lobe, so as to follow the random pattern during pressurization and after sample cutting (Fig B- 19).

Table B- 17. Information about the digital high-speed cameras

Lenses	60 mm macro
Light	2 spotlights behind the cameras
Frame rate	10 Hz
Shutter	1/50
Aperture	22
Depth of field	Around 10 cm
Working distance	1 m

Fig B- 19. Liver set up for strain field measurements on the Glisson's capsule a) general view of the liver, b) left cameras' views before sample cutting (liver L8), c) right cameras' views after sample cutting (Liver L8)

In order to associate the computed principal strains to anatomical directions, the major or minor principal strain directions were associated to the cranio-caudal or medio-lateral directions. For that, the principal strains with a direction between 80° and 100°, and between -80° and -100° defined the strains in the cranio-caudal direction. Likewise, the principal strains with a direction between 10° and -10°, 170° and 180°, and -170° and -180° defined the strains in the medio-lateral direction (Fig B- 20).

Fig B- 20. Explanatory diagram of post-processing data (e1: major principal direction; e2: minor principal direction)

To determine if the Glisson's capsule strain states on the whole liver and on the isolated samples statistically differ, Wilcoxon tests[1] were performed. Moreover, Wilcoxon test were used to study the intra-liver variability. Furthermore, Wilcoxon tests were performed to verify a potential statistical difference between liver preserved with Winckler and those preserved with Safebalm®. Two states are considered statistically different for a p-value < 0.05.

1.5. Conventional data acquisition and triggering

The pressures were recorded thanks to pressure sensors XP5 (TE Connectivity, Switzerland) with a sampling frequency of 100Hz.

In order to synchronize the conventional data (pressure) to the video, a light emitting diode was placed in the field of the cameras. When the cameras and the pressure sensors are recording, the LED is turned on and a signal is recorded. The cameras and the pressure sensors were triggered at t_0, where the pressure in the vessels was then at 0 mmHg.

---

[1] Wilcoxon test: It is a nonparametric test of the null hypothesis that it is equally likely that a randomly selected value from one sample will be less than or greater than a randomly selected value from a second sample.

2. Results

2.1. Pressurization of the vessels

The set of livers studied shows a similar behavior when the vessels are pressurized. The results of liver L8 are presented below.

For the study, the four pressure levels were applied during around 45s, and these four levels of pressure were applied three times (3 trials). These four levels of pressure are clearly identified on arterial pressure time histories: around 0 mmHg, 50 mmHg, 100 mmHg and 150 mmHg (0 Pa, 6,7*10^3 Pa, 13*10^3 Pa and 20*10^3 Pa) (Fig B- 21) and on the venous pressure time histories: around 0 mmHg, 5 mmHg, 10 mmHg and 15 mmHg (0 Pa, 667 PA, 1,3*10^3 Pa and 2,0*10^3 Pa) (Fig B- 22).

Fig B- 21. Pressurization of liver L8 – Arterial pressure time histories for the 3 trials (P1, P2, P3)

Fig B- 22. Pressurization of liver L8 – Venous pressure time histories for the 3 trials (P1, P2, P3)

As the pressurization device is manual, we observed differences between the 3 pressures time histories.

2.2. Influence of the pressurization on the Glisson capsule strain state

2.2.1. Distribution of the major strains on the whole liver

In order to compare the strain on the Glisson capsule with a quasi *in vivo* condition, the liver pressurized at 10 mmHg (1,3*10^3 Pa) in the portal vein and 100 mmHg (13*10^3 Pa) in the hepatic artery was chosen as the reference state. An example of the strain field obtained on the Glisson's capsule on liver L8 for the three successive trials is shown on Fig B- 23. The distribution of the strain changes for each trial and each pressurization level. In order to quantify this change, statistics will be performed (2.2.b).

Fig B- 23. Typical distribution of the major principal strains of the Glisson's capsule of liver L8 on A) an unpressurized liver, B) an under pressurized liver (arterial pressure at 50mmHg and venous pressure at 5mmHg), C) an over pressurized liver (arterial pressure at 150mmHg and venous pressure at 15mmHg), 1) on the first trial, 2) on the second trial, 3) on the third trial – Reference state: Liver at physiological pressure (arterial pressure at 100mmHg and venous pressure at 10mmHg).

When studying the average major principal strain as a function of the pressure, we observed that the four levels of pressure previously identified lead to a strong increase of the major principal strain (Fig B- 24).

Fig B- 24. Pressurization of liver L8 – Average major principal strain as a function of arterial pressure

Thus, the major principal strain of the liver capsule is related to the internal pressure of the vessels. Moreover, on this graph the preconditioning of the liver tissues does not seem important as all the trial are about the same. A statistical analysis was realized on all the liver of the study to statue on the interest of a preconditioning (see §2.2.2.).

Strain field obtained on the Glisson's capsule on under-pressurized liver at the third trial are shown in Fig B- 25, and on over-pressurized liver at the third trial are shown in Fig B-26. The physiologically pressurized liver is still taken as the reference state. Depending on the morphology of the liver, the highlighted area may be more or less important and impede the DIC. In addition, the costal impressions, which create spans, can also impede the DIC or induces local errors.

Fig B- 25. Distribution of the major principal strains of the Glisson's capsule on under pressurized livers at the third trial – Reference state: Livers at physiological pressure

122

Fig B- 26. Distribution of the major principal strains of the Glisson's capsule on over pressurized liver at the third trial – Reference state: Liver at physiological pressure

2.2.2. Cranio-caudal and medio-lateral strains on the whole liver

The average strains in the cranio-caudal and medio-lateral direction for each liver are presented in Fig B- 27. As expected, as the internal pressure of the liver increases, there is a medio-lateral and cranio-caudal extension of the tissues. Statistical tests (Wilcoxon test) between the three successive trials showed no significant difference of strain in the cranio-caudal and in the medio-lateral directions. Moreover, no difference can be found between livers preserved with Safebalm® and livers preserved with Winckler.

Fig B- 27. Average strains in the cranio-caudal direction (A) and in the medio-lateral direction (B) of the Glisson's capsule on the liver through various pressurization state (T1, T2, T3 means Trials 1, 2 or 3) – Reference state: Physiologically pressurized livers

2.3. Initial strain state on isolated sample

2.3.1. Strain comparison between the whole liver and the restricted area

To study the strain state of a sample, a restricted area much smaller than the area of the whole liver must be analyzed by DIC. In order to compare the DIC results on the same areas, the data corresponding only to the restricted area were collected on the whole liver and compared to the data computed directly on the restricted area (Fig B- 28).

This has been done for 11 restricted areas corresponding to the 11 samples taken from the 8 livers and for each trial of pressurization.

Fig B- 28. Definition of the area of interest of the liver L6 for the study of the strain on: A) the whole liver; B) the restricted area

The mean strains in the cranio-caudal and medio-lateral direction for both methods are presented on the third trial in Fig B- 29.

The choice of the initial area of interest for DIC shows no significant difference in the cranio-caudal direction, but it shows a significant difference in the medio-lateral direction (p-value <0.01, N=33), as values taken on the restricted area on the whole liver showed a bigger compression in the medio-lateral direction than the values taken on the samples. As for both tests, the size of the area on the cranio-caudal direction is approximately the same, but the size of area on the medio-lateral direction is reduced by two on the restricted area, and ss a significant difference is found only on the medio-lateral direction, it is possible to think that this difference is due to an edge effect.

Fig B- 29. Strains in the cranio-caudal direction (A) and in the medio-lateral direction (B) of the Glisson's capsule on the third trial to compare results according to the area of interest selection – Reference state: Physiological pressurized liver

2.3.2. Principal strains of the Glisson's capsule on sample areas and isolated samples

In order to compare the strain of the Glisson capsule on an isolated sample with a quasi *in vivo* condition, the liver with a physiological pressurization (10 mmHg or $1,3*10^3$ Pa in the portal vein and 100 mmHg or $13*10^3$ Pa in the hepatic artery) is still used as reference state.

An example of the strain field of the Glisson's capsule on a sample area from liver L3 is shown in Fig B- 30. As for all cases, a heterogeneous distribution of the strain is noted on the isolated sample.

Fig B- 30. Liver 3 - Distribution of the major and minor principal strains of the Glisson's capsule on A) unpressurized liver, B) under pressurized liver, C) over pressurized liver, D) isolated sample – Reference state: Physiological pressurized liver

2.3.3. Cranio-caudal and medio-lateral strains of the Glisson's capsule on sample areas and isolated samples

The mean strains in the cranio-caudal and medio-lateral directions for each sample area and isolated sample are presented in Fig B- 31.

The strain field of the sample area on unpressurized liver, compared to the sample area on the physiological pressurized liver, shows a significant compression in the cranio-caudal direction (up to 3.2%, p-value < 0.01, N=11). In the medio-lateral direction, no significant compression is found even if 7 samples present preferential compression (up to 7.6%).

The strain field of the sample area on under pressurized liver, with respect to the strain field on the physiological pressurized liver, shows significant compressions in the cranio-caudal direction (up to 1.5%, p-value < 0.01, N=11), and in the medio-lateral direction (up to 1.9%, p-value < 0.03, N=11).

The strain field of the sample area on over pressurized liver, compared to the sample area on the physiological pressurized liver, shows significant extension in the cranio-caudal direction (up to 7.3%, p-value < 0.01, N=11) and in the medio-lateral direction (up to 7.3%, p-value < 0.01, N=11).

The strain field of the isolated samples, with respect to the strain field on the physiological pressurized sample areas, presents a no significant extension in the cranio-caudal direction, even if 7 samples present preferential extension (up to 26.1%). The strain field of the capsule on the isolated samples shows a significant compression in the medio-lateral direction (up to 19.5%, p-value < 0.03, N=11).

We found out that the four samples which present a compression in the cranio-caudal direction have a small ratio Length/Width (around 3), whereas the seven samples which present an extension in the cranio-caudal direction have a large ratio Length/Width (around 4.2).

Even if no significant difference has been found between the average strains obtained on livers embalmed with Winckler and those embalmed with Safebalm®, a higher intra-specimen variation is noted for Safebalm® conservation.

Fig B- 31. Bar graph of the principal strains in the cranio-caudal direction (A) and in the medio-lateral direction (B) of the Glisson's capsule on different state – Reference state: Physiological pressurized liver

3. Discussion
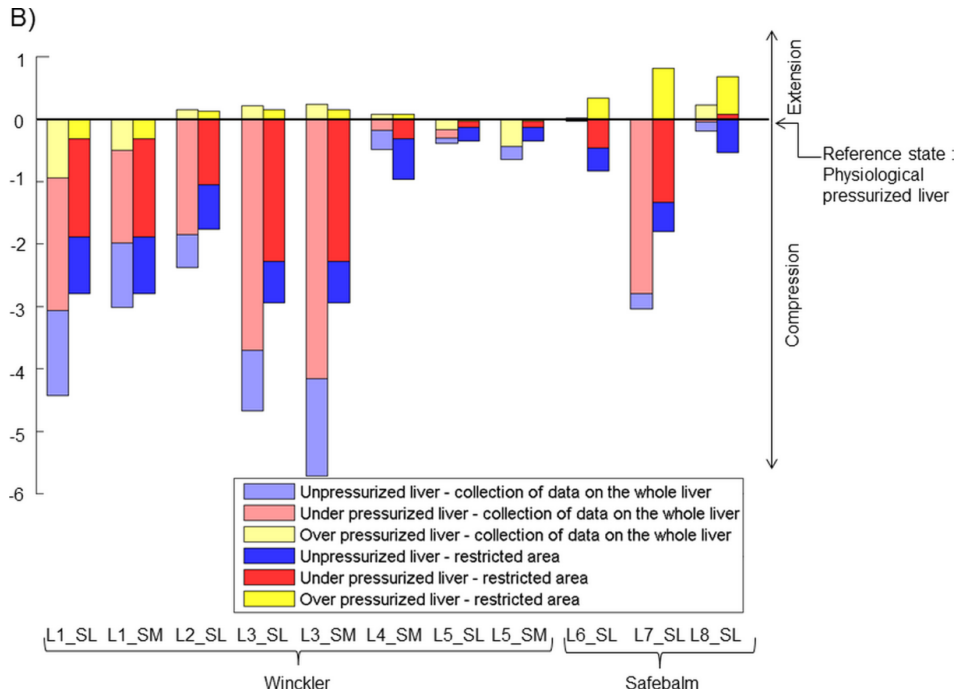
This study highlights the existence of a significant difference between the strain state of the Glisson's capsule on an unpressurized liver, a pressurized liver and on samples. It is therefore important to choose the pertinent reference state according to the types of analysis, and in order to be able to compare the results.

According to Ottensmeyer et al. (2004), the establishment of a system of pressurization of the liver makes it possible to approach the *in vivo* conditions. In this study, we consider that the pressurization of the livers, at 100 mmHg or $13*10^3$ Pa in the hepatic artery and 10 mmHg or $1,3*10^3$ Pa in the portal vein, places them in a quasi *in vivo* condition. This physiologically pressurized state of the liver was used as the reference state for capsule's strain field.

This study questioned the necessity of pre-conditioning before testing soft tissues. Nava et al. (2004), explained that the biomechanical response of organs during surgery does not correspond to a prestressed condition. Even if no prestressed condition is involved during surgery, the pre-strain induced by the blood flow could to be studied. But in our study, the pressurization rate was not applied at the level of the blood flow. Hollenstein et al. (2006) realized 10 loading cycles in order to obtain a stable response. We performed only three trials in our study, because of the fragility of the tissues, notably around the suture zones of the vessels. With 3 trials, the results that we obtained did not justify the necessity of the preconditioning step, as no significant difference was found between them in the medio-lateral and cranio-caudal directions. On another hand, we observed a time of tissue adaptation during the rise in pressure revealing that a delay, around 40 s, is needed so that the perfused tissues reaches a stabilized strain state.

If we consider the isolated samples, Gao and Desai (2010) in their numerical simulation showed that gravity plays on the deformation of samples of very soft tissue under uniaxial tension. In our study, it seems that gravity is not the only effect acting on the isolated samples as a clear compression is observed for 4 samples over 11 in the cranio-caudal direction. It seems that the release of the pre-strain of the capsule on the liver can compensate the effect of the gravity. In the medio-lateral direction, the both effects of gravity and of pre-strain release produce compression.

In their study Jor et al. (2011), highlighted the retraction phenomena of the soft fibrous connective tissues from a preloaded (*in vivo*) and unloaded configuration. They found out that the skin samples retracted 40% in width and 20% in length. Our results are consistent with these findings. Moreover, as Jor et al. (2011) noticed for the skin, we observed a large inter-specimen variability on the average strain of the capsule. If we consider the two different preservation modalities, even if no significant difference has been found between the average strains obtained on livers embalmed with Winckler and those embalmed with Safebalm®, a higher intra-specimen variation is noted for Safebalm® conservation.
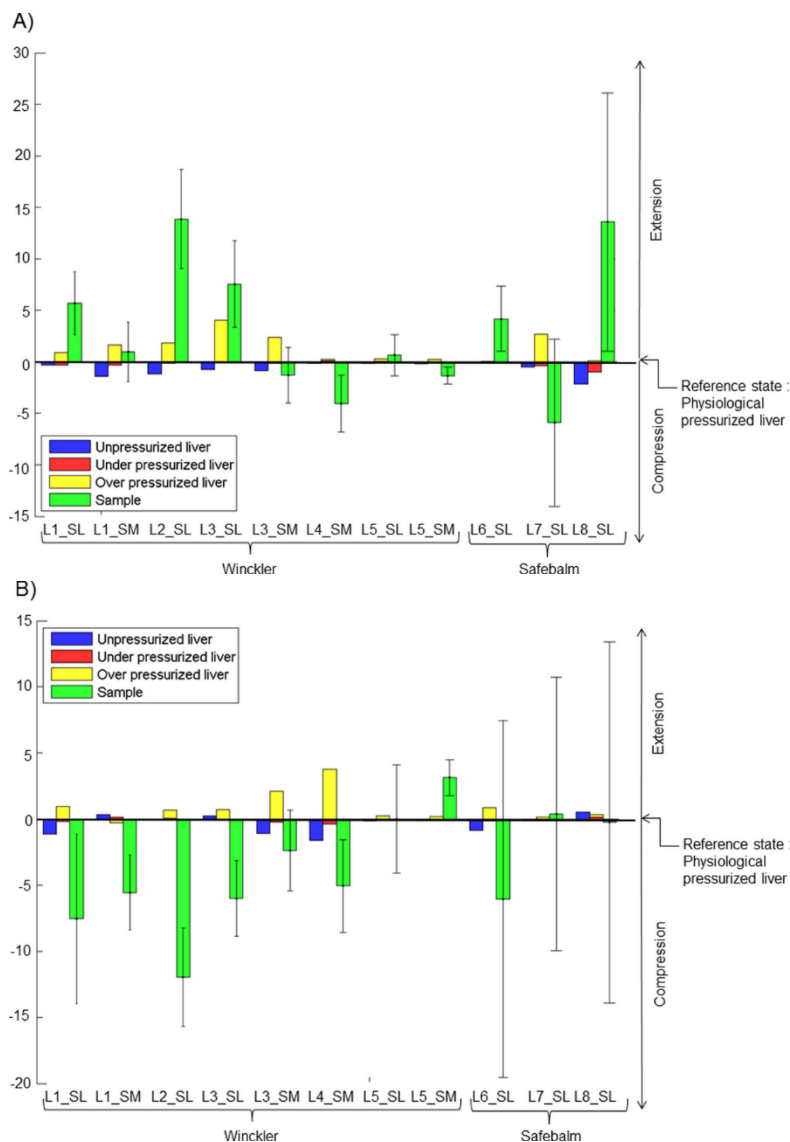
This observation is similar to the one from Ternifi et al. (2013), who reported that freezing had a significant effect on the porcine renal tissues and led to a large reduction of standard deviations. In our study, as preservation with Winckler also led to a reduction of standard deviation, we hypothesize that this preservation solution has a larger influence on the mechanical properties than Safebalm®.

The values of the extension in the cranio-caudal direction of the samples after collection (up to 26.1%) are not negligible compared to the tensile ultimate strain of the capsule through tensile tests on isolated samples obtained by Brunon et al. (2010) or Santago et al. (2009a, 2009b). In such tests, the reference strain state is the isolated sample after collection. Our assessment of the strain state of sample after collection, compared to *in vivo* state, shows that the measured tensile ultimate strains may be underestimated due to the gravity effect for sample with a large ratio Length/Width or overestimated due to *in vivo* pre-strain release, for sample with a small ratio Length/Width. As the samples in the literature have a dog bone shape it will be interesting to study the strain on this type of sample.

Our study was carried out on bodies given to science and therefore does not allow us to have access to livers of young people. Thus, the average age of our study is 92 years old and is thus not representative of the population. However, no liver disease which can cause stiffening of the tissues was revealed during the removal of the organ.

In this study, an experimental work was carried out to show the importance of the initial state of strain of the Glisson capsule. Different states were statistically analyzed to point out this importance. This investigation has shown that it is important to choose the right initial state of strain according to the test performed and the type of analysis. In view of supplying a numerical model of soft organs with ultimate properties, considering the *in vivo* state as the initial strain state should be preferred.

Part B: Mechanical characterization of the liver until ultimate strain

Chapter 4: Deceleration tests

This chapter presents the experimental work to calculate the local ultimate strain on the Glisson capsule through the mechanisms of laceration. This experimental work reproduces a frontal shock, namely a deceleration of the liver in a physiological sate.

Table of contents

In road accidents during frontal impact, there is a deceleration of the liver producing lacerations concentrated on the right lobe. In order to properly understand the mechanisms of laceration, deceleration tests must be set up in physiological conditions, as the strain of the Glisson's capsule depend on the internal pressure.

1. Material and methods

1.1. Preparation of the livers

Four livers were extracted from post-mortem human subjects (PMHS) by a surgeon respecting the same protocol as in Chapter 3.

They were preserved with Safebalm® (OGF, France) and came from the Department of Anatomy of the University of Lyon, through the French voluntary donation to science program (Table B- 18).

Table B- 18. Liver's information for deceleration tests

Liver ID	Gender	Age
L9	Man	92
L10	Man	91
L11	Woman	94
L12	Man	91

After removing, the livers were placed in hermetically sealed boxes and moistened with compresses soaked in PBS. The livers were then kept at +4°C during 24 to 48 hours before testing. One-hour prior testing, livers were put at the room temperature (20±2°C).

Right before testing, in order to approach the physiological condition, the liver was placed in the same condition as in Chapter 3 (Fig B-15). A Plexiglas plate, with a circular hole placed in front of the convex part of the right lobe, was added at the front of the box to create an over pressurized area (Fig B- 32 & Fig B- 33). In order to minimize edge effects, the edges of the hole have been polished.

Fig B- 32. Deceleration tests- fixation with the hole plate

1.2. Pressurization and deceleration of the livers

The same pressurization system as in the Chapter 3 was used to apply a physiological pressure of 10 mmHg ($1,3*10^3$ Pa) at the portal vein and of 100 mmHg ($13*10^3$ Pa) at the artery.

To allow time for the soft tissues to deform under pressure, the pressurization system was left in place for five minutes. Right before deceleration, the pressurization system was clamped near to the sensors, and the PBS columns were disconnected.

The fixation box was then attached to a pendulum. Initially the liver was placed against the Plexiglas plate so that the bulging part of the right lobe was in front of the hole (Fig B-30 & B-31). The pendulum was then dropped to a height varying from 0.10 to 0.50 meters. The fall of the pendulum was stopped by semi-rigid foam, creating the deceleration of the liver against the plexiglass plate. An accelerometer was placed on the pendulum to record its deceleration.

1.3. Displacement and strain field's measurements

The liver was visualized by two digital high-speed video cameras (Photron, San Diego, CA, USA). The data acquisition frequency was 5000Hz (Table B- 19). Both cameras were focused on the hole to measure the strain field during deceleration tests (Fig B- 33). Right before testing, a reference image of the liver was recorded in order to compare the Glisson capsule during the deceleration test to a physiological state.

Table B- 19. Information about the digital high-speed cameras

Lenses	60 mm macro
Light	2 spotlights behind the cameras
Acquisition frequency	5000 Hz
Shutter	1/5000
Aperture	16
Estimated Depth of field	Around 7 cm
Working distance	Around 30 cm

Fig B- 33. Deceleration test - General view

In order to measure displacement and strain fields, Digital Image Correlation (Palanca et al., 2016) was applied thanks to the VIC3D® software (Correlated Solution, Columbia, SC, USA).

As in Chapter 3, the Glisson's capsule was covered with a random pattern of black spray-painting, after a thin layer of white cream was put on, in order to improve contrast. This pattern was used to perform the Digital Image Correlation. The displacement and strain fields were calculated on a specific area delimited by the hole on the Plexiglas plate. Moreover, a random black pattern was applied on the Plexiglas plate around the hole. The marker used to study the movement is attached to the Plate. Thus, the Z-displacements are normal to the plate and the strain is zero on the Plate. The size of the images was 512x512 pixels (for a 8x8 cm images, with a pixel size of 0.15 mm). The software tracks, the displacement of a subset area, which has to be large enough to ensure that there is sufficiently distinctive pattern contained in the area used for correlation. The correlation analysis was non-incremental using a subset of 75 pixels and a space resolution of 4 pixels.

It is important to notice that the hydration of the tissues makes it difficult to measure the strain field by DIC because the light of the spotlights was reflected on the wet surface and creates shiny pixels; this lead to have areas where the computing is not possible. As the error of the computation is maximal on the boundary of the computed areas, a checking of the computed areas gives many points of maximal error (Fig B- 34).

Even if this error is low, it makes difficult to analyze the strain concentration and to relate it to the capsule laceration.

Fig B- 34. Sigma field on the Glisson's capsule of liver L9 (A), liver L10 (B), liver L11 (C) and liver L12 (D).

1.4. Conventional data acquisition and triggering

The pressures were recorded over time thanks to pressure sensors XP5 (TE Connectivity, Switzerland) with a sampling frequency of 10000Hz.

In order to synchronize the conventional data (pressure) to the video, two contact blades were placed at the area of impact. When the impact occurs, a signal is sent to the cameras and pressure sensors to start recording. Thus, the cameras and the pressure sensors were triggered at t0, when the impact occurred.

Data were filtering thanks to a simple moving average at 10.

Moreover, acceleration was recorded thanks to a device fixed on the fixation box.

2. Results

2.1. Case of liver L9

The reference state corresponding to a pressurized liver placed in front of the Plexiglas plate is illustrated in Fig B- 35.

Fig B- 35. Reference state of the liver L9, A) Left camera, B) Right camera

The pressure's recordings showed a peak in the portal vein at 10ms and a peak in the hepatic artery at 15ms. The strain peak occurs at 25ms, approximately at the same time as the maximum deflection of the Glisson's capsule in the over pressurized area (Fig B-36).

Fig B- 36. Deceleration tests – Liver L9 – strain and pressure time-histories

Fig B- 37 presents the maximum deflection of the bulbous part of the capsule during the deceleration test. It corresponds to the point of the bulbous area of the liver farthest from the plate which is taken as a reference and is followed throughout the test.

Fig B- 37. Maximum deflection of the capsule of Liver L9 during time

Even if some lacerations occurred on the right lobe of Lover L9, this liver presented no laceration on the area of interest (Fig B- 38).

Fig B- 38. Presentation of the lacerations on Liver L9

2.2. Case of liver L10

A laceration occurred on the area of interest on Liver L10. The reference state corresponding to a pressurized liver placed in front of the Plexiglas plate is illustrated in Fig B- 39. In this particular case, the Plate was not used as a reference for the Z-displacement.

Fig B- 39. Reference state of the liver L10; A) Left camera, B) Right camera

The study of the pressure and strain of the Glisson capsule showed a peak in the portal vein and in the hepatic artery at 13ms. The strain peak occurs at 25ms (Fig B- 40).

Fig B- 40. Deceleration tests – Liver 10 – strain and pressure time-histories

To highlight an area of concentrated strain, we reduced the scale between 30 and 50% as all the value under 30% are represented in purple and all the values over 50% are represented in red (Fig B- 41).

Fig B- 41. Strain concentration on L10 A) right before the laceration, B) just after the laceration

It seems that one of the concentrated strain areas leads to a laceration. Moreover, this laceration seems to be consistent with the orientation of the major principal strain.

In addition to the laceration on the area of interest, other lacerations occurred on the right lobe (Fig B- 42).

Fig B- 42. Presentation of the lacerations on Liver L10

2.3. Case of liver L11

The reference state (Fig B- 43) corresponds to a pressurized liver placed in front of the Plexiglas plate.

Fig B- 43. Reference state of the liver L11; A) Left camera, B) Right camera

The strain showed a strain peak at 5ms. The pressure peak in the portal vein and in the hepatic artery occurred at 10ms, approximately at the same time as the maximum deflection (Fig B- 44).

Fig B- 44. Deceleration tests – Liver 11 – strain and pressure time-histories

Fig B- 45 presents the maximum deflection of the bulbous part of the capsule during the deceleration test. It corresponds to the point of the bulbous area of the liver farthest from the plate which is taken as a reference and is followed throughout the test.

Fig B- 45. Maximum deflection of the capsule of Liver L11 during time

As the value of sigma is lower than 0,05%, we can hypothesize that there is no artefact. To highlight an area of concentrated strain, we reduced the scale between 30 and 50% as all the value under 30% are represented in purple and all the values over 50% are represented in red (Fig B- 46).

Fig B- 46. Strain concentration on L11, A) right before the laceration, B) just after the laceration

No correlation is calculated around the laceration, only in the upper neighborhood. The peak of strain occurs at the same time as the initiation of the laceration. No concentrated strain area is visible before the laceration, but the orientation of the major principal strain can explain the creation of the laceration.

In addition to the laceration on the area of interest, other lacerations occurred on the right lobe (Fig B- 47).

143

Fig B- 47. Presentation of the lacerations on Liver L11

2.4. Case of liver L12

The reference state corresponding to a pressurized liver placed in front of the Plexiglas plate is illustrated in Fig B- 48.
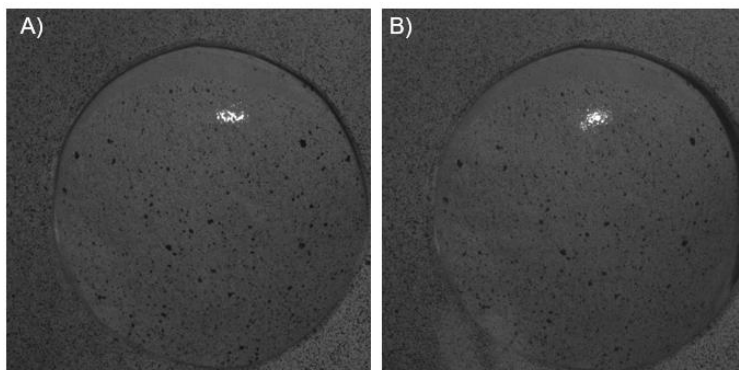

Fig B- 48. Reference state of the liver L12; A) Left camera, B) Right camera

The study of the pressure, strain and deflection of the Glisson capsule showed a strain peak at 5ms. The pressure peak in the portal vein and in the hepatic artery occurs at 10ms, approximately at the same time as the maximum deflection (Fig B- 49).
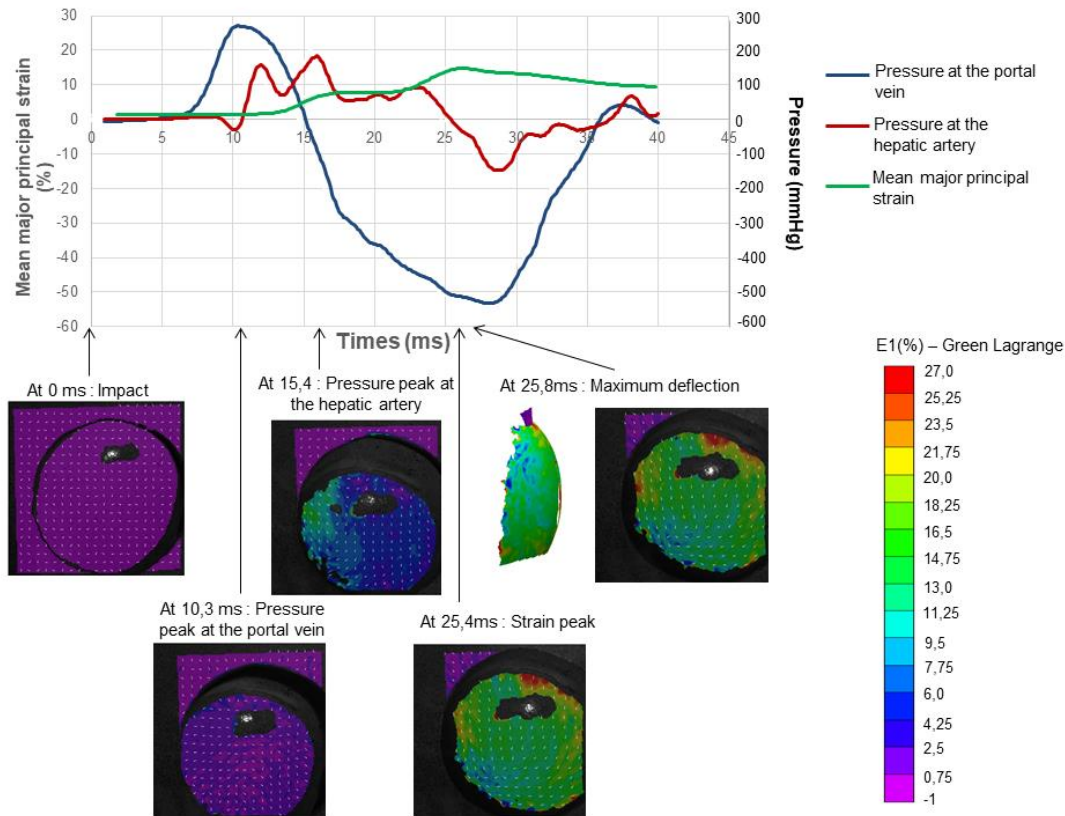
Fig B- 49. Deceleration tests – Liver 12 – strain and pressure time-histories

Fig B- 50 presents the maximum deflection of the bulbous part of the capsule during the deceleration test. It corresponds to the point of the bulbous area of the liver farthest from the plate which is taken as a reference and is followed throughout the test.
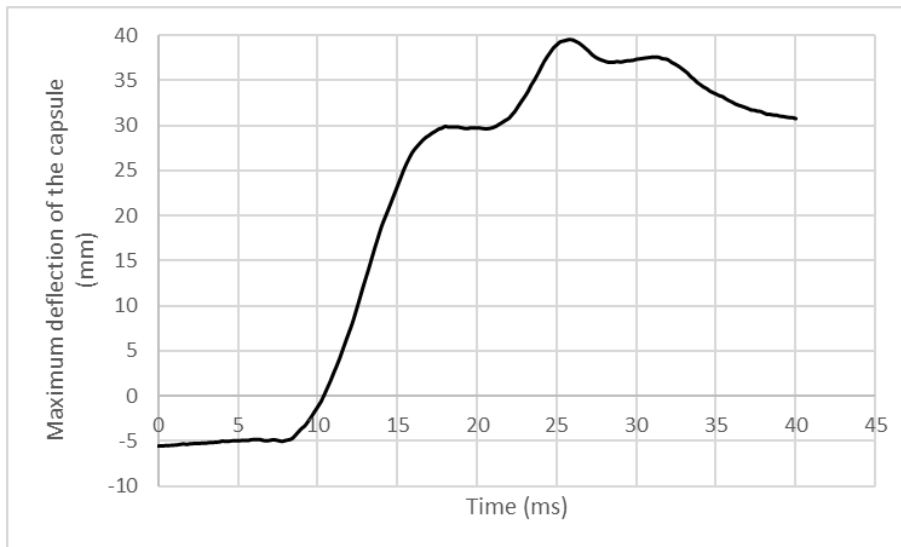

Fig B- 50. Maximum deflection of the capsule of Liver L12 during time

On Liver L12, laceration occurred out of the cameras field. It is difficult to conclude on the mechanism of the laceration, but the creation of the laceration seems to be correlated with the orientation of major principal strain.

In addition to the laceration on the area of interest, other lacerations occurred on the right lobe (Fig B- 51).

Fig B- 51. Presentation of the lacerations on Liver L12

3. Discussion

To understand and quantify the mechanism of the laceration of the Glisson's capsule, this preliminary study proposed a methodology to observe a laceration during deceleration tests on human fresh liver.

This preliminary work makes it possible to study the liver in condition closer to the physiologic one, and to study the ultimate strain on the whole pressurized liver contrary to tensile tests on samples.

It is therefore important to note that as exposed by Matthes et al. (2003), the overpressure was created on segment 4, which represent 22.8% of the injuries due to road accidents. Furthermore, other lacerations occur on segments 1, 6, and 7 which represent 38% of the injuries.

Due to the hydration of the tissues, some areas are highlighted which compromises a good correlation. In addition, during deceleration tests, the surface of the liver can create folds and thus damage the random pattern previously created, which also compromises a good correlation.
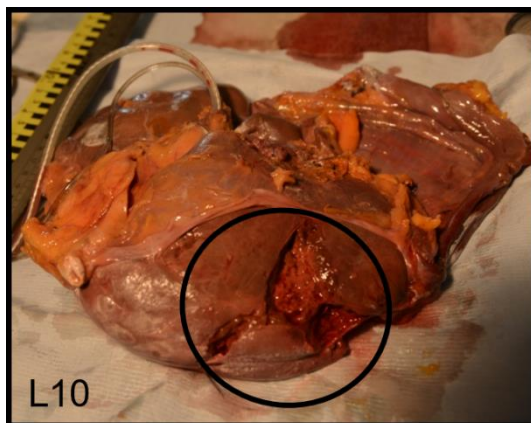
In their study, Brunon et al. (2010), measured the ultimate strain of the capsule through tensile tests on fresh human livers. They found an ultimate stain at 32.2 ± 13.8 %. Their study was carried out on samples composed of parenchyma and capsule, as in our study. This result seems to be in accordance with our study. Indeed, Liver L9 on which no laceration occurs on the area of interest presents a peak of strain around 15 %. Liver L10 has a strain peak around 50%, Liver L11 around 25% and Liver L12 around 35%.

This study considers the physiological state of the liver, thanks to the pressurization system. Moreover, the results were compared to the reference state, the liver in a physiological state. Even if the test protocol is quite easy to reproduce, the creation of the laceration depends on the morphology of the liver, whether the right lobe is prominent or not, the behavior of the liver may change.

In addition, this study must be done on fresh liver, indeed, as explained in Chapter 3, livers preserved with Winckler seem more rigid, which seems to prevent the appearance of laceration.

A limitation of this study is that the anatomy of the liver was not study, thus no link between Part A and Part B can be realized. The liver used in our experimental work cannot be classified in the four morphotypes.

In order to improve the reproducibility of the tests, it may be interesting at first to rethink the fixation box, so that it is easily adaptable to the morphology of each liver, to allow a good support of it back and avoid toggle movement. Moreover, in order for the software to be able to calculate the correlation on the all area of interest, it would be necessary to find uniform lighting on the liver to avoid highlighting areas.

Conclusion

Research question: **Can the ultimate strain of the hepatic capsule be calculated for quasi *in vivo* livers?**

In order to answer this question, an overview of the literature was carried out and highlighted the following questions:

- Has the pressurization of the liver a significant effect on the Glisson capsule?
- Is there an under or an overestimation of the ultimate strain through tensile tests on samples?
- Can an experimental setup reproduce the occurrence of a local laceration and which value is the ultimate strain of the Glisson capsule?

Has the pressurization of the liver a significant effect on the Glisson capsule?

To answer this question, a pressurization system was setup, and the strain state of the Glisson capsule was studied on different configuration: the unpressurized liver, the under, physiologically and over pressurized liver and samples. For the whole liver, as the internal pressure of the liver increases, there is a medio-lateral and cranio-caudal extension of the tissues. When comparing the samples after collection with the *in vivo* state a significant difference is found. Two mechanisms seem to influence the strain state: the gravity and the pre-strain release.

Is there an underestimation or an overestimation of the ultimate strain through tensile tests on samples?

We found out that the strain state of sample after collection, compared to *in vivo* state, shows that the measured tensile ultimate strains may be underestimated due to the gravity effect for sample with a large ratio Length/Width (more than 4) or overestimated due to *in vivo* pre-strain release, for sample with a small ratio Length/Width (less than 3).

Can an experimental setup reproduce the occurrence of a local laceration and which value is the ultimate strain of the Glisson capsule?

Deceleration tests were setup using a pendulum. Even if no laceration on liver embalmed with Winckler was observed, fresh liver showed softer tissue and lacerations were observed on the right lobe. To understand the initiation of these lacerations the strain state, the orientation of the major principal strain, the pressure in the portal vein and in the hepatic artery, as well as the deflection of the capsule were studied. The study of the strain on the right lobe does not allow us to have an accurate value. On 3 tested livers (livers 10,11,12), lacerations occurred in the area of interest during tests for which the maximum major strain reached respectively 45, 25 and 35%. For the liver for which the maximum major strain did not reach more than 15% (liver 9), no laceration was observed in the area of interest.

This study faced several limitations. Due to the hydration of the tissues, some areas are highlighted which compromises a good correlation. In addition, during deceleration tests, the surface of the liver can create folds and thus damage the random pattern previously created, which also compromises a good correlation. Moreover, as no lacerations were observed liver embalmed with Winckler, this study obliges us to have access to fresh or embalmed livers with Safebalm®.

> **To conclude it is important to take into account the pressurization of the vessels and to find the mechanical parameters which fit the behavior of a fresh liver in a numerical model to reproduce laceration on the liver in Part C.**

Reference

Abdel-Misih, Sherif R.Z., and Mark Bloomston. 2010. "Liver Anatomy." Surg Clin North Am 90 (4): 643–53. doi:10.1016/j.suc.2010.04.017.

Abri, B., S. Shams-Vahdati, S. Paknezhad, P. Sepehri-Majd, and S. Alizadeh. 2016. "Blunt Abdominal Trauma and Organ Damage and Its Prognosis." J. Anal Res Clin Med 4 (4): 228–32.

Ahn, Bummo, and Jung Kim. 2010. "Measurement and Characterization of Soft Tissue Behavior with Surface Deformation and Force Response under Large Deformations." Medical Image Analysis 14 (2): 138–48. doi:10.1016/j.media.2009.10.006.

Arvieux, Ch. C, B Rossignol, and G Gueret. 2003. "Les Traumatismes Graves Du Foie," 457–72.

Baker, S. P., B. O'Neill, W. Haddon, and W. B. Long. 1974. "The Injury Severity Score: A Method for Describing Patients with Multiple Injuries and Evaluating Emergency Care." The Journal of Trauma 14 (3): 187–96.

Bohlin, N. I. 1967. "A Statistical Analysis of 28,000 Accident Cases with Emphasis on Occupant Restraint Value." SAE Technical Paper 670925. Warrendale, PA: SAE International. http://papers.sae.org/670925/.

Brown, Jeffrey D., Jacob Rosen, Yoon Sang Kim, Lily Chang, Mika N. Sinanan, and Blake Hannaford. 2003. "In-Vivo and in-Situ Compressive Properties of Porcine Abdominal Soft Tissues." Studies in Health Technology and Informatics 94: 26–32.

Brown, Jeffrey D., Jacob Rosen, Mika N. Sinanan, and Blake Hannaford. 2003. "In-Vivo and Postmortem Compressive Properties of Porcine Abdominal Organs." In Medical Image Computing and Computer-Assisted Intervention - MICCAI 2003, edited by Randy E. Ellis and Terry M. Peters, 238–45. Springer Berlin Heidelberg. http://link.springer.com/chapter/10.1007/978-3-540-39899-8_30.

Brunon, A., K. Bruyère-Garnier, and M. Coret. 2010. "Mechanical Characterization of Liver Capsule through Uniaxial Quasi-Static Tensile Tests until Failure." Journal of Biomechanics 43 (11): 2221–27.

Brunon, A., K. Bruyère-Garnier, and M. Coret. 2011. "Characterization of the Nonlinear Behaviour and the Failure of Human Liver Capsule through Inflation Tests." Journal of the Mechanical Behavior of Biomedical Materials 4 (8): 1572–81.

Carson, Henry J., and Benjamin A. Cook. 2008. "Massive Internal Injury in the Absence of Significant External Injury after Collisions of Passenger Vehicles with Much Larger Vehicles." Journal of Forensic and Legal Medicine 15 (4): 219–22. doi:10.1016/j.jflm.2007.10.008.

Carter, F. J, T. G Frank, P. J Davies, D McLean, and A Cuschieri. 2001. "Measurements and Modelling of the Compliance of Human and Porcine Organs." Medical Image Analysis 5 (4): 231–36. doi:10.1016/S1361-8415(01)00048-2.

Champion, Howard R. 2012. "Abbreviated Injury Scale." In Encyclopedia of Intensive Care Medicine, 1–5. Springer Berlin Heidelberg.

Cheynel, Nicolas. 2007. "Traumatismes Hépatiques. Epidemiologie Lors Des Accidents de La Route et Physiopathologie : Étude Biomécanique Du Comportement Du Foie En Décélération." Université de Bourgogne.

Cheynel, Nicolas, Thierry Serre, Pierre-Jean Arnoux, Patrick Baque, Laurent Benoit, Stephane-Victor Berdah, and Christian Brunet. 2006. "Biomechanic Study of the Human Liver during a Frontal Deceleration." The Journal of Trauma 61 (4): 855–61. doi:10.1097/01.ta.0000196871.19566.92.

Chui, C., E. Kobayashi, X. Chen, T. Hisada, and I. Sakuma. 2007. "Transversely Isotropic Properties of Porcine Liver Tissue: Experiments and Constitutive Modelling." Medical & Biological Engineering & Computing 45 (1): 99–106. doi:10.1007/s11517-006-0137-y.

Chui, Dr C., E. Kobayashi, X. Chen, T. Hisada, and I. Sakuma. 2004. "Combined Compression and Elongation Experiments and Non-Linear Modelling of Liver Tissue for Surgical Simulation." Medical and Biological Engineering and Computing 42 (6): 787–98. doi:10.1007/BF02345212.

Clarke, E. C., S. Cheng, M. Green, R. Sinkus, and L. E. Bilston. 2011. "Using Static Preload with Magnetic Resonance Elastography to Estimate Large Strain Viscoelastic Properties of Bovine Liver." Journal of Biomechanics 44 (13): 2461–65. doi:10.1016/j.jbiomech.2011.06.023.

Conte, Cécile. 2012. "Comportement mécanique du foie en contexte traumatique : Rupture et endommagement des tissus." IFSTTAR: Université Claude Aix-Marseille.

Crandall, J. R., and W. D. Pilkey. 1994. "The Preservation of Human Surrogates for Impact Studies." In , 582–85. Washington, USA: Engineering Research Center, University of DC.

Dan, Diane. 1999. "Caractérisation mécanique du foie humain en situation de choc." Paris: Université Paris 7.

Egorov, V., S. Tsyuryupa, S. Kanilo, M. Kogit, and A. Sarvazyan. 2008. "Soft Tissue Elastometer." Medical Engineering & Physics 30 (2): 206–12. doi:10.1016/j.medengphy.2007.02.007.

Friedman, Z., C. Kugel, J. Hiss, B. Marganit, M. Stein, and S. C. Shapira. 1996. "The Abbreviated Injury Scale. A Valuable Tool for Forensic Documentation of Trauma." The American Journal of Forensic Medicine and Pathology 17 (3): 233–38.

References

Fu, Y. B., and C. K. Chui. 2014. "Modelling and Simulation of Porcine Liver Tissue Indentation Using Finite Element Method and Uniaxial Stress-Strain Data." Journal of Biomechanics 47 (10): 2430–35. doi:10.1016/j.jbiomech.2014.04.009.

Fu, Y. B., C. K. Chui, and C. L. Teo. 2013. "Liver Tissue Characterization from Uniaxial Stress–strain Data Using Probabilistic and Inverse Finite Element Methods." Journal of the Mechanical Behavior of Biomedical Materials 20 (April): 105–12. doi:10.1016/j.jmbbm.2013.01.008.

Gao, Zhan, and Jaydev P. Desai. 2010. "Estimating Zero-Strain States of Very Soft Tissue under Gravity Loading Using Digital Image Correlation." Medical Image Analysis 14 (2): 126–37. doi:10.1016/j.media.2009.11.002.

Gao, Zhan, Kevin Lister, and Jaydev P. Desai. 2010. "Constitutive Modeling of Liver Tissue: Experiment and Theory." Annals of Biomedical Engineering 38 (2): 505–16.

Guyton, Arthur C. 1976. Textbook of Medical Physiology. 5th edition. Philadelphia: W.B. Saunders Company.

Hoff, William S., Michelle Holevar, Kimberly K. Nagy, Lisa Patterson, Jeffrey S. Young, Abenamar Arrillaga, Michael P. Najarian, Carl P. Valenziano, and Eastern Asociation for the Surgery of Trauma. 2002. "Practice Management Guidelines for the Evaluation of Blunt Abdominal Trauma: The East Practice Management Guidelines Work Group." The Journal of Trauma 53 (3): 602–15. doi:10.1097/01.TA.0000025413.43206.97.

Hollenstein, Marc, Alessandro Nava, Davide Valtorta, Jess G. Snedeker, and Edoardo Mazza. 2006. "Mechanical Characterization of the Liver Capsule and Parenchyma." In Biomedical Simulation, edited by Matthias Harders and Gábor Székely, 150–58. Springer Berlin Heidelberg. http://link.springer.com/chapter/10.1007/11790273_17.

Javouhey, E., and M. Chiron. 2003. "Epidemiologie Des Traumatismes Par Accident de La Circulation Chez L'enfant." In Conférences Médecins, 3–16.

Jolly, B. T., and B. Grebing. 1997. "Liver Injuries and Two-Point Shoulder Restraints: Case Report and Discussion." The Journal of Trauma 42 (6): 1144–47.

Jor, J. W.Y., M. P. Nash, P. M. F. Nielsen, and P. J. Hunter. 2011. "Estimating Material Parameters of a Structurally Based Constitutive Relation for Skin Mechanics." Biomech Model Mechanobiol 10: 767–78.

Kerdok, Amy E., Mark P. Ottensmeyer, and Robert D. Howe. 2006. "Effects of Perfusion on the Viscoelastic Characteristics of Liver." Journal of Biomechanics 39 (12): 2221–31. doi:10.1016/j.jbiomech.2005.07.005.

Kim, Jung. 2004. "Virtual Environments for Medical Training : Graphic and Haptic Simulation of Tool-Tissue Interactions." Thesis, Massachusetts Institute of Technology. http://dspace.mit.edu/handle/1721.1/17942.

Kim, Jung, Boon K. Tay, N. Stylopoulos, D. W. Rattner, and M. A. Srinivasan. 2003. "Characterization of Intra-Abdominal Tissues from in Vivo Animal Experiments for Surgical Simulation." In Medical Image Computing and Computer-Assisted Intervention - MICCAI 2003, edited by Randy E. Ellis and Terry M. Peters, 206–13. Springer Berlin Heidelberg. http://link.springer.com/chapter/10.1007/978-3-540-39899-8_26.

Kiss, Miklos Z., Tomy Varghese, and Timothy J. Hall. 2004. "Viscoelastic Characterization of in Vitro Canine Tissue." Physics in Medicine and Biology 49 (18): 4207. doi:10.1088/0031-9155/49/18/002.

Klinich, K. D., P. Bowman, C. A. C. Flannagan, and J. D. Rupp. 2016. "Injury Patterns in Motor-Vehicle Crashes in the United States: 1998-2014." UMTRI-2016-16. Michigan.

Klinich, K. D., CA Flannagan, K Nicholson, LW Schneider, and J. D. Rupp. 2010. "Factors Associated with Abdominal Injury in Frontal Farside, and Nearside Crashes." Stapp Car Crash Journal, 54–73.

Laumon, B. 2002. "Recherches coordonnées sur les traumatismes consécutifs à un accident de la circulation routière, leurs causes et leurs conséquences." Rapport UMRETTE 0205. INRETS: Université Claude Bernard Lyon 1.

Lefevre, Jérémie, Jean-David Zeitoun, and Ariane Chryssostalis. 2007. "Evaluation de la gravité et recherche des complications précoces. Identifier les situations d'urgence et planifier leur prise en charge." In Hépato-gastro enterologie, 3ème ed., 14. Vernazobres-grego.

"Le Registre du Rhône des victimes d'accidents de la circulation routière." 2007.

Lu, Yuan-Chiao, Andrew R. Kemper, and Costin D. Untaroiu. 2014. "Effect of Storage on Tensile Material Properties of Bovine Liver." Journal of the Mechanical Behavior of Biomedical Materials 29 (January): 339–49. doi:10.1016/j.jmbbm.2013.09.022.

Lu, Yuan-Chiao, and Costin D. Untaroiu. 2013. "Effect of Storage Methods on Indentation-Based Material Properties of Abdominal Organs." Proceedings of the Institution of Mechanical Engineers, Part H: Journal of Engineering in Medicine 227 (3): 293–301. doi:10.1177/0954411912468558.

Maass, H., and U. Kühnapfel. 1999. "Noninvasive Measurement of Elastic Properties of Living Tissue." In , 6.

Marchesseau, Stéphanie, Tobias Heimann, Simon Chatelin, Rémy Willinger, and Hervé Delingette. 2010. "Fast Porous Visco-Hyperelastic Soft Tissue Model for Surgery Simulation: Application to Liver Surgery." Progress in Biophysics and Molecular Biology 103 (2-3): 185–96. doi:10.1016/j.pbiomolbio.2010.09.005.

References

Matthes, Gerrit, Dirk Stengel, Julia Seifert, Grit Rademacher, Sven Mutze, and Axel Ekkernkamp. 2003. "Blunt Liver Injuries in Polytrauma: Results from a Cohort Study with the Regular Use of Whole-Body Helical Computed Tomography." World Journal of Surgery 27 (10): 1124–30. doi:10.1007/s00268-003-6981-0.

Mazza, Edoardo, Patrick Grau, Marc Hollenstein, and Michael Bajka. 2008. "Constitutive Modeling of Human Liver Based on in Vivo Measurements." In Medical Image Computing and Computer-Assisted Intervention – MICCAI 2008, edited by Dimitris Metaxas, Leon Axel, Gabor Fichtinger, and Gábor Székely, 726–33. Springer Berlin Heidelberg. http://link.springer.com/chapter/10.1007/978-3-540-85990-1_87.

Melvin, J. W., R. L. Stalnaker, V. L. Roberts, and M. L. Trollope. 1973. "Impact Injury Mechanisms in Abdominal Organs." SAE Technical Paper 730968. Warrendale, PA: SAE International. http://papers.sae.org/730968/.

Menegaux, Fabrice. 2003. "Lésions Abdominales Traumatiques." EM-Consulte. http://www.em-consulte.com/article/13385/lesions-abdominales-traumatiques.

Nasseri, Simin, Lynne E. Bilston, and Nhan Phan-Thien. 2002. "Viscoelastic Properties of Pig Kidney in Shear, Experimental Results and Modelling." Rheologica Acta 41 (1-2): 180–92. doi:10.1007/s003970200017.

Nava, Alessandro, Edoardo Mazza, Oliver Haefner, and Michael Bajka. 2004. "Experimental Observation and Modelling of Preconditioning in Soft Biological Tissues." In Medical Simulation, edited by Stéphane Cotin and Dimitris Metaxas, 1–8. Springer Berlin Heidelberg. http://link.springer.com/chapter/10.1007/978-3-540-25968-8_1.

Nicolle, S., L. Noguer, and J. -F. Palierne. 2012. "Shear Mechanical Properties of the Spleen: Experiment and Analytical Modelling." Journal of the Mechanical Behavior of Biomedical Materials 9: 130–36. doi:10.1016/j.jmbbm.2012.02.005.

Nicolle, S., and J.-F. Palierne. 2010. "Dehydration Effect on the Mechanical Behaviour of Biological Soft Tissues: Observations on Kidney Tissues." Journal of the Mechanical Behavior of Biomedical Materials 3 (8): 630–35. doi:10.1016/j.jmbbm.2010.07.010.

Nicolle, S., P. Vezin, and J.-F. Palierne. 2010. "A Strain-Hardening Bi-Power Law for the Nonlinear Behaviour of Biological Soft Tissues." Journal of Biomechanics 43 (5): 927–32. doi:10.1016/j.jbiomech.2009.11.002.

Ochsner, M. G. 2001. "Factors of Failure for Nonoperative Management of Blunt Liver and Splenic Injuries." World Journal of Surgery 25 (11): 1393–96.

Ohara, T. 1953. "On Comparison of Strengths of the Various Organ-Tissues." J. Kyoto Pref Med Univ 53: 577–97.

ONISR. 2011. La sécurité routière en France. Bilan de l'année 2010.

ONISR. 2012. La sécurité routière en France. Bilan de l'année 2011.

ONISR. 2013. La sécurité routière en France. Bilan de l'accidentalité de l'année 2012.

ONISR. 2015. La Sécurité Routière En France. Bilan de L'accidentalité de L'année 2015.

Ottensmeyer, Mark Peter. 2001. "Minimally Invasive Instrument for in Vivo Measurement of Solid Organ Mechanical Impedance." Thesis, Massachusetts Institute of Technology. http://dspace.mit.edu/handle/1721.1/8858.

Palanca, Marco, Gianluca Tozzi, and Luca Cristofolini. 2016. "The Use of Digital Image Correlation in the Biomechanical Area: A Review." International Biomechanics 3 (1): 1–21.

Pervin, Farhana, Weinong W. Chen, and Tusit Weerasooriya. 2011. "Dynamic Compressive Response of Bovine Liver Tissues." Journal of the Mechanical Behavior of Biomedical Materials 4 (1): 76–84. doi:10.1016/j.jmbbm.2010.09.007.

Pukacki, F., T. Jankowski, M. Gabriel, G. Oszkinis, Z. Krasinski, and S. Zapalski. 2000. "The Mechanical Properties of Fresh and Cryopreserved Arterial Homografts." European Journal of Vascular and Endovascular Surgery 20 (1): 21–24. doi:10.1053/ejvs.2000.1120.

Rachev, A, and S.E. Greenwald. 2003. "Residual Strains in Conduit Arteries." Journal of Biomechanics 36: 661–70.

Raghunathan, S., D. Evans, and Jessica L. Sparks. 2010. "Poroviscoelastic Modeling of Liver Biomechanical Response in Unconfined Compression." Annals of Biomedical Engineering 38 (5): 1789–1800. doi:0.1007/s10439-010-9957-x.

Rausch, M. K., N. Famaey, T. O. Shultz, W. Bothe, C. D. Miller, and E. Kuhl. 2013. "Mechanics of the Mitral Valve." Biomechanics and Modeling in Mechanobiology 12 (5): 1053–71.

Rausch, M. K., and E. Kuhl. 2013. "On the Effect of Prestrain and Residual Stress in Thin Biological Membranes." Journal of the Mechanics and Physics of Solids 61: 1955–69.

Roan, Esra, and Kumar Vemaganti. 2007. "The Nonlinear Material Properties of Liver Tissue Determined from No-Slip Uniaxial Compression Experiments." Journal of Biomechanical Engineering 129 (3): 450–56. doi:10.1115/1.2720928.

Rosen, Jacob, Jeffrey D. Brown, Smita De, Mika Sinanan, and Blake Hannaford. 2008. "Biomechanical Properties of Abdominal Organs in Vivo and Postmortem under Compression Loads." Journal of Biomechanical Engineering 130 (2): 021020. doi:10.1115/1.2898712.

Rouiller, Ch. 1964. The Liver: Morphology, Bio-Chemistry, Physiology. Academic Press. Vol. 2. New-York, NY, USA.

Sakuma, Ichiro, Yosuke Nishimura, Chee Kong Chui, Etsuko Kobayashi, Hiroshi Inada, Xian Chen, and Toshiaki Hisada. 2003. "In Vitro Measurement of Mechanical Properties of Liver Tissue under Compression and Elongation Using a New Test Piece Holding Method with Surgical Glue." In Surgery Simulation and Soft Tissue Modeling, edited by Nicholas Ayache and Hervé Delingette, 284–92. Springer Berlin Heidelberg. http://link.springer.com/chapter/10.1007/3-540-45015-7_27.

Samur, Evren, Mert Sedef, Cagatay Basdogan, Levent Avtan, and Oktay Duzgun. 2007. "A Robotic Indenter for Minimally Invasive Measurement and Characterization of Soft Tissue Response." Medical Image Analysis 11 (4): 361–73. doi:10.1016/j.media.2007.04.001.

Santago, Anthony C. 2010. "Characterizing the Biomechanical Response of the Liver." Blacksburg, Virginia: Virginia Polytechnic Institute and State University.

Saraf, H., K. T. Ramesh, A. M. Lennon, A. C. Merkle, and J. C. Roberts. 2007a. "Mechanical Properties of Soft Human Tissues under Dynamic Loading." Journal of Biomechanics 40 (9): 1960–67. doi:10.1016/j.jbiomech.2006.09.021.

———. 2007b. "Measurement of the Dynamic Bulk and Shear Response of Soft Human Tissues." Experimental Mechanics 47 (3): 439–49. doi:10.1007/s11340-007-9052-x.

Schwartz, Jean-Marc, Marc Denninger, Denis Rancourt, Christian Moisan, and Denis Laurendeau. 2005. "Modelling Liver Tissue Properties Using a Non-Linear Visco-Elastic Model for Surgery Simulation." Medical Image Analysis 9 (2): 103–12. doi:10.1016/j.media.2004.11.002.

Seifert, Thomas. 2003. "Identification of Material Parameters Using Instrumented Identation Test Data."

Snedeker, J. G., P. Niederer, F. R. Schmidlin, M. Farshad, C. K. Demetropoulos, J. B. Lee, and K. H. Yang. 2005. "Strain-Rate Dependent Material Properties of the Porcine and Human Kidney Capsule." Journal of Biomechanics 38 (5): 1011–21. doi:10.1016/j.jbiomech.2004.05.036.

Sparks, Jessica L., John H. Bolte, Rebecca B. Dupaix, Kenneth H. Jones, Steven M. Steinberg, Rodney G. Herriott, Jason A. Stammen, and Bruce R. Donnelly. 2007. "Using Pressure to Predict Liver Injury Risk from Blunt Impact." Stapp Car Crash Journal 51 (October): 401–32.

Sparks, Jessica L., and Rebecca B. Dupaix. 2008. "Constitutive Modeling of Rate-Dependent Stress-Strain Behavior of Human Liver in Blunt Impact Loading." Annals of Biomedical Engineering 36 (11): 1883–92. doi:10.1007/s10439-008-9555-3.

Stingl, J., V. Báĉa, P. Ĉech, J. Kovanda, H. Kovandová, V. Mandys, J. Rejmontová, and B. Sosna. 2002. "Morphology and Some Biomechanical Properties of Human Liver and Spleen." Surgical and Radiologic Anatomy 24 (5): 285–89. doi:10.1007/s00276-002-0054-1.

Tamura, Atsutaka, Kiyoshi Omori, Kazuo Miki, Jong B. Lee, King H. Yang, and Albert I. King. 2002. "Mechanical Characterization of Porcine Abdominal Organs." Stapp Car Crash Journal 46 (November): 55–69.

Tay, Boon K., Jung Kim, and Mandayam A. Srinivasan. 2006. "In Vivo Mechanical Behavior of Intra-Abdominal Organs." IEEE Transactions on Bio-Medical Engineering 53 (11): 2129–38. doi:10.1109/TBME.2006.879474.

Tinkoff, Glen, Thomas J. Esposito, James Reed, Patrick Kilgo, John Fildes, Michael Pasquale, and J. Wayne Meredith. 2008. "American Association for the Surgery of Trauma Organ Injury Scale I: Spleen, Liver, and Kidney, Validation Based on the National Trauma Data Bank." Journal of the American College of Surgeons 207 (5): 646–55. doi:10.1016/j.jamcollsurg.2008.06.342.

Uehara, H. 1995. "A Study on the Mechanical Properties of the Kidney, Liver and Spleen, by Means of Tensile Stress Test with Variable Strain Velocity." J. of Kyoto Pref. Univ. of Med., no. 104: 439–51.

Umale, Sagar, Simon Chatelin, Nicolas Bourdet, Caroline Deck, Michele Diana, Parag Dhumane, Luc Soler, Jacques Marescaux, and Remy Willinger. 2011. "Experimental in Vitro Mechanical Characterization of Porcine Glisson's Capsule and Hepatic Veins." Journal of Biomechanics 44 (9): 1678–83. doi:10.1016/j.jbiomech.2011.03.029.

Umale, Sagar, Caroline Deck, Nicolas Bourdet, Parag Dhumane, Luc Soler, Jacques Marescaux, and Remy Willinger. 2013. "Experimental Mechanical Characterization of Abdominal Organs: Liver, Kidney & Spleen." Journal of the Mechanical Behavior of Biomedical Materials 17 (January): 22–33. doi:10.1016/j.jmbbm.2012.07.010.

Umut Ozcan, M., Sina Ocal, Cagatay Basdogan, Gulen Dogusoy, and Yaman Tokat. 2011. "Characterization of Frequency-Dependent Material Properties of Human Liver and Its Pathologies Using an Impact Hammer." Medical Image Analysis 15 (1): 45–52. doi:10.1016/j.media.2010.06.010.

Winckler, Georges. 1964. Manuel D'anatomie Topographique et Fonctionnelle : Par Georges Winckler. Masson et Cie Niort, impr. Soulisse et Cassegrain.

Wu, J. Z., R. G. Dong, and W. P. Smutz. 2004. "Elimination of the Friction Effects in Unconfined Compression Tests of Biomaterials and Soft Tissues." Proceedings of the Institution of Mechanical Engineers. Part H, Journal of Engineering in Medicine 218 (1): 35–40.

Yarpuzlu, Berkay, Mehmet Ayyildiz, Olgu Enis Tok, Ranan Gulhan Aktas, and Cagatay Basdogan. 2014. "Correlation between the Mechanical and Histological Properties of Liver Tissue." Journal of the Mechanical Behavior of Biomedical Materials 29 (January): 403–16. doi:10.1016/j.jmbbm.2013.09.016.

Yeh, W. C., Li, P. C., Jeng, Y. M., Hsu, H. C., Kuo, P. L., Li, M. L., ... & Lee, P. H. (2002). Elastic modulus measurements of human liver and correlation with pathology. *Ultrasound in medicine & biology*, *28*(4), 467-474.

Part C: Numerical finite elements models of the liver

In order to improve the safety of passengers during road accident, numerical models of the whole body have been developed. An accurate description of both the mechanical behavior and the geometry of these models can help for an accurate assessment of injury risk using these models. Concerning the mechanical behavior of organ like liver, the knowledge of the mechanical behavior of hepatic tissues in the physiological condition is important. The mechanical parameters in physiological conditions have been studied. Moreover, those models tend to be more and more detailed, with the distinction of all the organs and the vessels.

Does the morphology of the liver influence the response of numerical models?

In this part, we first review the literature on numerical models of the human body and especially on the liver.

In Chapter 2, we reproduce the deceleration test realized in Part B, Chapter 4 with a generical models created by Conte (2012). Finally, the third and last chapter of this part will be the study of the numerical models implemented with each morphotype previously identified.

Chapter 1: Literature review on numerical models of the liver

Table of contents

1. Human body modelling for injury risk prediction

1.1. Human body models

Numerical models of the human body for injury risk prediction have been developed over the decades mainly for applications in the field of road safety. In these first human body models developed (Huang et al., 1994)., the majority of the organs were simplified and only the region of interest was finely meshed.

With the increasing of the computing power, ore detailed human body models were developed, with a more detailed anatomy obtained from direct frozen slices or clinical imaging.

From 2000S, several human body models for injury risk prediction can be listed;

- the Total HUman Model for Safety (THUMS) (Iwamoto et al., 2002; Maeno and Hasegawa, 2001), which was developed and in parallel with the computing power tested by Toyota and some universities;
- the HUman MOdel for Safety (HUMOS) (Robin, 2001; Behr et al, 2003).
- the H-Model (Haug, 2001) was developed by ESI Software and the Hong-Ik University;
- the WSU human models from the Wayne State University (Zhao and Narwani, 2005).
- The Global Human Body Models Consortium (GHBMC) (Vavalle et al, 2013)

Human body models were also developed for injury risk prediction in the field of forensic medicine (Milanowicz and Kedzior, 2017).

1.2. Abdomen and liver models

To study more accurately the injury mechanisms of the abdomen under dynamic loading, detailed finite elements models of the abdomino-pelvic segment have emerged. The Wayne State University proposed a finite element model of the human abdomen (WSUHAM) (Lee and Yang, 2001) and analyzed the injury mechanisms due to the seatbelt (Foster et al., 2006). Snedeker et al. (2007) developed a finite element model of the abdomen to predict the renal injuries. At the Laboratory of Applied Biomechanics in Marseille, a finite element model of the abdomino-pelvic segment, presented in Fig. C- 1, was proposed by Labé (2008).

Fig. C- 1. MELBA model (Labe, 2008)

More recently, Conte (2012) proposed a vascularized model of the liver, which was validated against compression tests.

Many other liver models were also developed for virtual surgery (Delingette and Ayache, 2005; Marchesseau et al, 2010). This type of models may need a real-time response. In that case, material properties must be simplified, which penalizing the modeling of the damage and rupture of the hepatic tissues.

2. Modelling of the mechanical behavior of the hepatic tissues

2.1. Parenchyma

2.1.1. Hyperelastic behavior

A hyperelastic or Green elastic material is a type of constitutive model for ideally elastic material for which stress-strain relationship derives from a strain energy density function ψ.

$$T_i = \frac{\partial \psi}{\lambda_i},$$

With
ψ, the strain energy density function
λ, the elongation
$\underline{\underline{T}}$, the Lagrangian strain tensor

This function can be described thanks to the invariant of the right Cauchy deformation tensor $\underline{\underline{B}}$.

$$I_1 = tr(\underline{\underline{B}}),$$

$$I_2 = \frac{I_1^2 - tr(\underline{\underline{B}}^2)}{2},$$

$$I_3 = \det\left(\underline{\underline{B}}\right) = 1,$$

With $\left|\begin{array}{l} \underline{\underline{B}}, \text{the right Cauchy deformation tensor} \\ I_1, I_2, I_3, \text{the invariant of } \underline{\underline{B}} \end{array}\right.$

Most models rely on simplistic assumptions of isotropy and incompressibility. The strain energy ψ, can be defined as follow:

- Polynomial, in which ψ is a polynomial of the invariants of $\underline{\underline{B}}$. The two most used laws are the Mooney Rivlin law, as done by Fu and Chui (2014):

$$\psi = C_{10}(I_1 - 3) + C_{01}(I_2 - 3),$$

With $\left|\begin{array}{l} \psi, \text{the strain energy density function} \\ I_1, I_2, \text{the invariant of the Cauchy deformation tensor} \\ C_{10}, C_{01}, \text{empirically determined material constants:} \\ \quad 2(C_{01} + C_{10}) = \mu_0, \text{the initial shear modulus} \\ \quad 4(C_{10} + C_{01}) = {E}/{1 + \nu}, E \text{ the elastic modulus and } \nu \text{ the} \\ \quad \text{Poisson's ratio} \end{array}\right.$

- And the Ogden law used by Chang and Hannaford (2015):

$$\psi = \sum_p \frac{\mu_p}{\alpha_p}(\lambda_1^{\alpha_p} + \lambda_2^{\alpha_p} + \lambda_3^{\alpha_p} - 3),$$

With $\left|\begin{array}{l} \psi, \text{the strain energy density function} \\ \lambda_i, \text{the principal stretches} \\ \mu_p, \alpha_p, \text{material constants:} \\ \quad {\left(\sum_p ({\mu_p}/{\alpha_p})\right)}/{2} = \mu_0, \text{the initial shear} \\ \quad \text{modulus[1]} \\ \quad \mu_0 . {2(1 + \nu)}/{3(1 - 2\nu)} = K, \text{the bulk} \\ \quad \text{modulus[2]} \end{array}\right.$

- Exponential used by Carter et al. (2001):

---

[1] Shear modulus: Shear modulus or rigidity is defined as the ratio of shear stress to the shear strain.
Shear stress: It is the component of stress coplanar with a material cross section.
Shear strain: it is defined as a change in angle.
[2] Bulk modulus: It is a measure of how incompressible the object is. It is defined as the ratio of the infinitesimal pressure increase to the resulting relative decrease of the volume.

$$\sigma(\lambda) = \mu \left(\frac{1}{\lambda^2} - \lambda \right) \exp \left[\gamma(\lambda + \frac{1}{\lambda} - 1) \right],$$

With
$\begin{array}{l} \sigma, \text{ the normal stress} \\ \mu, \text{ the shear modulus} \\ \gamma, \quad \text{a} \quad \text{dimensionless} \\ \text{parameter} \end{array}$

- Logarithmic and polynomial to describe the hepatic lobules behavior as done by Chui et al. (2007):

$$\psi = \frac{-C_1}{2} \ln(1 - u) + \frac{q}{2},$$
with

$$u = \frac{1}{2} C_2 (I_1 - 3)^2 + \frac{1}{2} C_3 (I_4 - 1)^2 + C_4 (I_1 - 3)(I_4 - 1)$$
$$q = C_5 (I_1 - 3)^2 + C_6 (I_4 - 1)^2 + 2C_7 (I_1 - 3)(I_4 - 1)$$

With
$\begin{array}{l} \psi, \text{ the strain energy density function} \\ C_i, \text{ the parameters of the law} \\ I_1, I_4, \text{ invariants of the Cauchy deformation tensor} \\ (I_4 \text{ is the square of the component of } \underline{\underline{B}} \text{ in the} \\ \text{principal direction}) \end{array}$

2.1.2. Viscoelastic behavior

Linear viscoelasticity is used to represent materials with a high proportion of water, which exhibit a linear voluminal behavior under axial stress. A complex shear modulus G* is introduced to express the response of the material to oscillatory stress. This law is for example used for the linear viscoelastic behavior of the porcine liver for shear tests (Nicolle et al., 2010).

Quasi-linear viscoelasticity assumes that the mechanical behavior of the material can be decoupled into a time-dependent linear viscoelastic relaxation response and a time-independent elastic response (Ahn and Kim, 2010; Tamura et al., 2002).

Under impact conditions, it is necessary to describe the effects of viscosity over time. Some authors rely on a thermodynamic approach, and then the liver is modeled as a second-order Mooney-Rivlin hyperelastic material whose viscoelastic component is implemented by second-order Prony series[1]. We speak of a generalized Maxwell model (Taylor et al., 2009).

---

[1] Prony's method: It extracts valuable information from a uniformly sampled signal and builds a series of damped complex exponentials or sinusoids.

2.1.3. Poro-elastic

Although some authors consider the poroelastic behavior of the hepatic tissue to be negligible when loading at high speed (Dan, 1999), others have decided to take it into account in their models (Jordan et al., 2009; Marchesseau et al., 2010; Raghunathan et al., 2010; Sparks et al., 2007). The parenchyma is then considered as a mixture between an incompressible porous solid matrix and a mobile interstitial fluid[1]. The behavior of the solid phase is then represented by a hyperelastic or hyper-viscoelastic law and the fluid follows a Darcy law.

2.2. Glisson capsule

The Glisson capsule can be modeled by a Pointing-Thomson model as in HUMOS or MELBA (Table C- 1). This law is based on a Kelvin-Voigt model and the viscosity is based on Navier's equations[2].

Table C- 1. Parameters for the behavior law of the hepatic capsule in HUMOS (Arnoux et al., 2001) and MELBA (Labe, 2008)

	HUMOS	MELBA
Density (g/mm³)	0.001	0.0011
Young modulus[3] (MPa)	0.532	0.05
Poisson's ratio[4]	0.436	0.3
Initial shear modulus	5	0
Internal pressure	Voluminal viscoelastic model	No internal pressure

Tensile tests report an hyperelastic behavior of the hepatic capsule (Brunon et al., 2010, 2011; Umale et al., 2011). Hooke's law can therefore be chosen in order to modelise the capsule mechanical behavior as proposed by Conte (2012) (Table C- 2).

---

[1] Interstitial fluid: It is a solution that bathes and surrounds the tissues cells of multicellular animals.

[2] Navier's equations: They described the physics of many phenomena of scientific and engineering interest. They described the motion of viscous fluid substances.

[3] The Young modulus: It is a measure of the stiffness of a solid material. It defines the relationship between stress and strain in a material.

[4] Poisson's ratio: It is the amount of transversal expansion divided by the amount of axial compression.

Table C- 2. Parameters for the elastic behavior of the hepatic capsule

	Conte (2012)
Density (g/mm³)	0.0011
Young modulus	17
Poisson's ratio	0.49

2.3. Hepatic vessels

Only few models take into account the vascularization of the liver. Indeed, even if the models of the human body take into account the main vascular network, the ramifications within an organ are not modeled.

The mechanical behavior of the main vessels (vena cava, portal vein) are modeled by a Pointing Thomson law as in Labe (2008), or Conte (2012) (Table C- 3):

$$\dot{\sigma} = K\dot{\varepsilon} - \left(\frac{E + E_t}{\nu}\sigma\right) + (\frac{\dot{E}E_t}{\nu}\varepsilon),$$

With $\begin{vmatrix} \sigma, \text{ the stress} \\ \varepsilon, \text{ the strain} \\ \nu, \text{ the Poisson's ratio} \\ E, \text{ the young modulus, and } E_t, \text{ the tangential} \\ \text{young modulus} \\ K = E/3(1 - 2\nu) \end{vmatrix}$

Table C- 3. Parameters for the Pointing Thomson law for the mechanical behavior of the main hepatic vessels

	Density (g/mm³)	E (MPa)	ν	E_1 (MPa)	E_2(MPa)	E_t (MPa)	ν_t
MELBA (Labé, 2008)	0.0011	4	0.49	0.02	0.01	5	0.45
Conte (2012)	0.0011	4.2	0.49	0.02	0.01	5	0.15

In Conte (2012), the intrahepatic vessels were modeled by an elastic law (Table C- 4).

Table C- 4. Parameters for the elastic law for the intrahepatic vessels

	Conte (2012)
Density (g/mm³)	0.0011
Young modulus (MPa)	0.01
Poisson's ratio	0.49

Due to difficulty of geometrical reconstruction of the hepatic artery, it has never been taken into account in liver models.

2.4. Diaphragm

To describe the mechanical behavior of the diaphragm, Labe choose a Hooke's law. with the Young modulus and Poisson's ratio reported in Table C- 5.

Table C- 5. Parameters for the Hooke's law for the diaphragm

Parameters	Values
ρ	0.1875 g.mm^{-3}
E	2 MPa
ν	0.45

3. Synthesis and problematics

Before obtaining models of the full human body or the abdomen, it is important to study each organ separately. The purpose of this part will be to **reproduce the deceleration tests of Part B, Chapter 4.**

The models tend to be more and more realistic, so it is important to **found out if the morphology of the liver has an influence on the numerical model.**

Chapter 2: Modelling of a standard vascularized liver for the simulation of a deceleration test

Table of contents

In this preliminary study on numerical modeling, we focus our work on only one liver of Part B. We choose liver L9, which has no laceration on the area of interest but for which all the parameters where set up as the acceleration and the pressure. As no information on the anatomy of the liver were recorded during experimental works, Liver L9 cannot be classified in one morphotype.

1. Geometry and meshes of the standard liver

In this preliminary study on numerical modeling, we focus our work on only one liver of Part B. We choose liver L9, which has no laceration on the area of interest but for which all the parameters where set up as the acceleration and the pressure. As no information on the anatomy of the liver were recorded during experimental works, Liver L9 cannot be classified in one morphotype.

1.1. Geometry sources

A standard model of the liver was developed on the basis of the external geometry used by Conte (2012), previously acquired by Labe (2008) for the abdomino-pelvic model MELBA, on a man around thirty years old. The internal geometry (intra-hepatic vessels) of the standard model of the liver was reconstructed from an injected CT-scan provided by the Radiology department of Hôpital Nord of Marseille (Conte, 2012) thanks to Intrasense.

1.2. Mesh characteristics

All the parts of this numerical models were previously meshed using the hypermesh® software by Conte (2012).

The parenchyma was meshed with tetrahedral elements (Fig. C- 2). We obtained a mesh with 141 617 nodes and 754 138 elements TETRA.

The size of the elements varies from 0.44 to 10.87 mm. The volume mesh obtained is of good quality as the aspect ratio[1] of the elements is less than 3.78 and the internal angles are between 13.7° and 129.3°, with 89 elements of internal angle lesser than 20° and 90 elements greater than 120°.

The Glisson capsule is meshed with shell triangular elements (Fig. C- 2). We obtained a mesh with 8758 nodes and 17448 shell elements.

The size of the elements varies from 1.16 to 6.36 mm. The surface mesh obtained is of good quality because the aspect ratio of the elements is less than 2.83 and the internal angles are between 24.3° and 112.1°.

The intrahepatic vessels are meshed generation by generation with triangular shell elements (Fig. C- 2). For the first generation, the target mesh size was 1.5 mm, for the second generation the target mesh size was 1 mm, and for the other generation, the target

---

[1] Aspect ratio: It is the ratio between the length of the largest side of an element and the smallest side. For 3D elements, the ratio is defined as the maximum of the aspect ratio calculated on each face. For a quality mesh, it is recommended that this ratio does not exceed 5.

mesh size was 0.7 mm. We obtained a mesh with 9 087 nodes and 18 166 shell elements for the portal vein and 22 621 nodes and 45 230 shell elements for the vena cava.

Fig. C- 2. Standard liver model A) Mesh of the parenchyma, B) mesh of the hepatic capsule C) Mesh of the intrahepatic vessel in anterior view

The size of the elements varies from 0.72 to 10.13 mm for the vena cava and from 0.53 to 3.03 mm for the portal vein. The surface mesh obtained is of good quality because the aspect ratio of the elements is less than 5.0 for the vena cava and 4.49 for the portal vein and the internal angles are between 13.56° and 140.48°, with 44 elements of internal angle lesser than 20° and 45 elements greater than 120° for the vena cava, and between 13.91° and 128.81°, with 2 elements of internal angle lesser than 20° and 3 elements greater than 120°, for the portal vein.

2. Material properties

2.1. Parenchyma

To describe the mechanical behavior of the parenchyma, we have chosen to place the parenchyma in the formalism of the thermodynamics of continuous media and we described the strain energy density function according to the Ogden law.

$$\text{Ogden law: } \psi = \sum_p \frac{\mu_p}{\alpha_p}(3\lambda^{\alpha_p} - 3), \; p \in [1,5]$$

$$\text{Mooney-Rivlin law: } \psi = C_1(I_1 - 3) + C_2(I_1 - 3)^2,$$

$$
\begin{aligned}
\alpha_1 &= 4 &&; \mu_1 = 4C_1 \\
\alpha_2 &= -4 &&; \mu_2 = 0 \\
\alpha_3 &= 2 &&; \mu_3 = \frac{\mu_1}{2} + 3\mu_4 \\
\alpha_4 &= -2 &&; \mu_4 = -4C_2
\end{aligned}
$$

With
ψ, the strain energy density function
λ_i, the principal stretches
μ_p, α_p, material constants for the Ogden law
C_1, C_2, empirically determined material constants for the Mooney-Rivlin law
I_1, the first invariant of the Cauchy deformation tensor

The parameters used for the parenchyma were determined by optimization in §6.

2.2. Other constituents of the liver

To describe the mechanical behavior of the Glisson capsule, we have chosen the same elastic law as in Conte (2012). The parameters are exposed in Chapter 1 §2.2.

The same Hooke's law as in Conte (2012) was chosen to describe the mechanical behavior of the walls of the hepatic vessels. The parameters are exposed in Chapter 1 §2.3.

Finally, to describe the mechanical behavior of the diaphragm, we have chosen the same Hooke's law as in Labe (2008). The parameters are exposed in Chapter 1 §2.4.

3. Loading and boundary conditions for the simulation of a deceleration test

3.1. Modelling of the fixation frame and impacted plate

In order to reproduce the deceleration tests exposed in Part B, Chapter 4, different parts of the fixation rig were modeled (Fig. C- 3):

- A plate on the back of the liver;
- A plate with a hole on the front of the liver;
- A diaphragm holding bar.

These parts are considered as rigid bodies.

Fig. C- 3. Presentation of the numerical model

3.2. Management of the interactions

In our model there are two types of interactions:

Adhesions are observed when two objects remain fixed relative to each other during the deformation. This is the case between the parenchyma and the Glisson capsule, as well as between the parenchyma and the walls of the vessels. This type of interaction is represented by a continuous mesh. The nodes at the interface of the two constituents are thus common to the two constituents. The advantage of the method is that it does not make the calculation more complicated. On the other hand, two constituents bonded by adhesion, cannot be dissociated in the rest of the calculation.

The frictionless contacts are observed when the structures are mobile relative to one another. This is the case for the Glisson capsule and the plates, as well as for the diaphragm and the Glisson capsule. To model these interactions, interfaces of types 7 and 11, which prevent the structures from interpenetrating during the calculation, will be implemented. These types of interface are exposed Appendix C-1. It is then necessary to define a penetration gap, set at 0.3 mm in our study.

3.3. Fluid modelling

In order to model the blood, several solutions may be envisaged, such as the creation of voluminal elements to which a quasi-zero Young's modulus and a Poisson's ration of 0.5 are attributed to represent an incompressible fluid. This first solution poses problems during large deformation. Thus, another solution is to use the Arbitrary Lagrangian Eularian theory to model the fluid-structure interaction.

In our study, we decided to simplify this problem by modeling the fluid by the pressure exerted by the fluid on the wall. To do so, a pressure function, presented in Fig. C- 4, was implemented.

Fig. C- 4. Fluid pressure time-histories recorded during the deceleration test on Liver L9 (PartB; Chapter 4; §2.1) and imposed to the model

4. Optimization of the parenchyma properties

4.1. Starting point

Conte (2012) proposes a method in order to adjust the mechanical properties of the liver. In one previous study (Conte, 2009) she highlighted that the behavior law of the Glisson capsule does not influence the response of the model. Thus, only parameters of the behavior law of the parenchyma is studied here.

The experimental tests used to validate the numerical model of Conte (2012), were carried out on livers embalmed with Winckler solution. In our study, the deceleration tests were carried out on livers embalmed with Safebalm®. We have seen in Part B, Chapter 3, that these two types of embalming seem to have different effects on the parenchyma. In addition, visually, the tissues embalmed with safebalm® seem more flexible. So, an adjustment of the material properties is needed.

To realize this adjustment of the parenchyma material properties, we took as a starting point the properties defined by Conte (2012), which are exposed in Table C- 6.

Table C- 6. Properties of the hepatic parenchyma (Conte, 2012)

ρ	0.0011 g.mm^{-3}		
ν	0.4501		
α_1	4	μ_1	0.7126
α_2	0	μ_2	0
α_3	2	μ_3	-1.723
α_4	-2	μ_4	-0.6931
α_5	0	μ_5	0

In her study, Conte (2012) argues that the parameters influencing the most the model response are the strain potentials C_1, C_2, that are represented by μ_1, and μ_4 in the Ogden law, as well as the Poisson's ratio.

4.2. Methodology

First, we studied the influence of the different parameters of the numerical response of the standard liver model.

For this analysis, the criteria compared were:

- Time histories of the distance between the center point of the bulbous portion of the liver and the plate during the deceleration test of liver L9. (Fig. C- 6).
- Time histories of the maximal major and minor principal strains during the deceleration test of Liver L9.

Secondly, we performed an optimization of the Ogden law parameters.

The $\sum_i \alpha_i \mu_i$ was set equal to 0.0114. As the different μ_i are linked, we only reportes the value of μ_1. The parametric analysis was divided in three steps in order to find the optimized values of ν and μ_1 (Fig. C- 5).

Fig. C- 5. Parametric analysis for optimized values of v and μ_1

In this optimization, two criteria were considered: the peak of the maximum major principal strain and the peak of the maximum minor principal strain.

Fig. C- 6. Deflection of the capsule A) at t=0, B) at the maximum of deflection.

4.3. Results on the influence of the Poisson's ratio

It is observed that the Poisson's ratio has only a minimal effect when considering the distance from the center point of the bulbous portion of the liver to the plate (Fig. C- 7).

Considering the principal strains, the influence of the Poisson's ratio is not simple to analyze, but it seems that a lower value of the Poisson's ratio gives a response closer to the experimental data (Fig. C- 8 & Fig. C- 9).

Fig. C- 7. Influence of the Poisson's ratio (mu1=0.5626; mu4=-0.6931) on the distance from the center point of the bulbous portion of the liver to the plate

Fig. C- 8. Influence of the Poisson's ratio (mu1=0.5626; mu4=-0.6931) on the maximal major principal strain

Fig. C- 9. Influence of the Poisson's ratio (mu1=0.5626; mu4=-0.6931) on the maximal minor principal strain

4.4. Results on the influence of the Ogden law parameters

The Ogden law is characterized by the following equation: $\sum_i \alpha_i \mu_i$, in order to meet the eligibility requirements of the Ogden law, this equation must be positive. Moreover, the different μ_i, are linked. Thus, for μ_1 fixed, we studied different values of $\sum_i \alpha_i \mu_i$ (Fig. C-10).

Fig. C- 10. Influence of the $\sum_i \alpha_i \mu_i$ in Ogden equation (mu1=0.4126; nu=0.4501) on the distance from the center point of the bulbous portion of the liver to the plate

It is observed that the lower the value of $\sum_i \alpha_i \mu_i$ is, the more the response of the numerical model refers to the experimental response. However, it is observed that a value too low leads to numerical. The minimal acceptable value is 0.0114.

To test the influence of the parameters of the Ogden law, for a $\sum_i \alpha_i \mu_i$ fixed, we studied five values of μ_1 (Fig. C- 11).

It is observed that the values of the different μ_i, do not influence the distance from the center point of the bulbous portion of the liver to the plate.

Fig. C- 11. Influence of μ_1 (nu=0.4501, $\sum_i \alpha_i \mu_i = 0.2206$) on the distance from the center point of the bulbous portion of the liver to the plate

Considering the principal strains, the influence of the parameters of the Ogden law is not clear and further investigation must be carried out (Fig. C- 12 & Fig. C- 13).

Fig. C- 12. Influence of the Ogden parameters (nu=0.4501, $\sum_i \alpha_i \mu_i = 0.2206$) on the maximal major principal strain

Fig. C- 13. Influence of the Ogden parameters (nu=0.4501, $\sum_i \alpha_i \mu_i = 0.2206$) on the maximal minor principal strain

4.5. Results on the optimization of the Ogden law parameters

Table C- 7 summarizes the results in terms of maximum values and errors between numerical and experimental responses.

Time-histories of the maximal principal strains obtained with optimized values of v and μ_1 are presented on Fig. C- 14.

Strain patterns are presented in In Fig. C- 15., At t=16ms, right after the contact between the plate and the Glisson capsule, we can see that the strain field seems equivalent, as in most of the area the major principal strain is around 7%. Moreover, as observed in the experiment, the maximum major principal strain computed is in the area of contact between the Glisson capsule and the plate.

Table C- 7. Comparison of the major and minor principal strain for the optimized parameters and the experimental test of Liver L9.

	Nu_0.321 et Mu1_0.31		Experimental
	Value	Error	
Major principal strain (%)	45.65	21.04	57.81
Minor principal strain (%)	12.73	0.04	12.73

Fig. C- 14. Comparison of experimental and numerical (nu=0.321; mu1=0.31) curves of the major and minor principal strain

Fig. C- 15. Comparison of the major principal strain pattern, on the numerical model and the experimental test, at t=16 ms.

In Fig. C- 16, at t=24ms, at the peak strain, we also can see that the strain field seems to be equivalent, as in most of the area the major principal strain is around 15%. Moreover, in both cases, the maximum major principal strain is located in a very small area.

Fig. C- 16. Comparison of the major principal strain pattern, on the numerical model and the experimental test, at t=24 ms.

To synthetize, the material parameters used for the parenchyma in the following of the study are presented in Table C- 8.

Table C- 8. Parenchyma material properties used for the study

ρ	0.0011 g.mm^{-3}		
ν	0.321		
α_1	4	μ_1	0.31
α_2	0	μ_2	0
α_3	2	μ_3	-0.9325
α_4	-2	μ_4	-0.3625
α_5	0	μ_5	0

Chapter 3: Influence of the morphology on finite elements models

Table of contents

1. Numerical models of the four liver morphotypes

The four morphotypes of livers highlighted in Part A, from the reconstruction of 78 CT-scans of healthy adults were modelized in order to study the influence of the liver geometry on its numerical response (Fig. C- 17).

Fig. C- 17. Representative geometries of the four liver morphotypes, A) external geometries, B) vessels geometries

As for the model of the standard liver, parenchymas were meshed with tetrahedral elements, the four Glisson capsule and intrahepatic vessels were meshed with triangular shell elements.

All information on meshes are given in Appendix C-1 for each morphotype.

The material properties used in this study are the same as in Part C, Chapter 2. The parenchyma takes the optimized values (Table C- 9).

Table C- 9. Parameters for the Ogden law for the parenchyma

Parameters	Values
ρ	0.0011 g.mm^{-3}
ν	0.321
α_1	0.31
α_2	0
α_3	-0,9325
α_4	-0,3625
α_5	0
μ_1	4
μ_2	0
μ_3	2
μ_4	-2
μ_5	0

2. Numerical responses of the four liver morphotypes under deceleration test

2.1. Morphotype 1

The model of the morphotype 1 is illustrated in Fig. C- 18.

Fig. C- 18. General view of the numerical model of morphotype 1

Table C- 10 summarizes the peaks for the curves of the maximal major principal strain and the maximal minor principal strain obtained experimentally, with the standard numerical model and with the model of the liver morphotype 1.

Table C- 10. Comparison of the maximum major and minor principal strain of morphotype 1, generical model and experimental deceleration test of Liver L9

	Morphotype 1	Generic model		Experimental	
		Value	Difference	Value	Difference
Major principal strain (%)	38.13	45.65	16,5%	57.81	34,0%
Minor principal strain (%)	17.61	12.73	38.3%	12.73	38.3%

The time-histories of the principal strains obtained experimentally, numerically with the standard liver model and with the model of the liver morphotype 1 are presented in Fig. C- 19.

Fig. C- 19. Comparison of experimental deceleration test of Liver L9, generical and morphotype 1 numerical curves of the major and minor principal strain

The contact between the plate and the capsule happened at t=14m, the peak of strain happened at t=26ms (Fig. C- 20 & **Fig. C- 21**).

Fig. C- 20. Major principal strain pattern at the contact between the plate and the capsule A) for Morphotype 1 numerical model, B) for generical model

Fig. C- 21. Major principal strain pattern at the peak of strain, A) for Morphotype 1 numerical model, B) for generical model

2.2. Morphotype 2

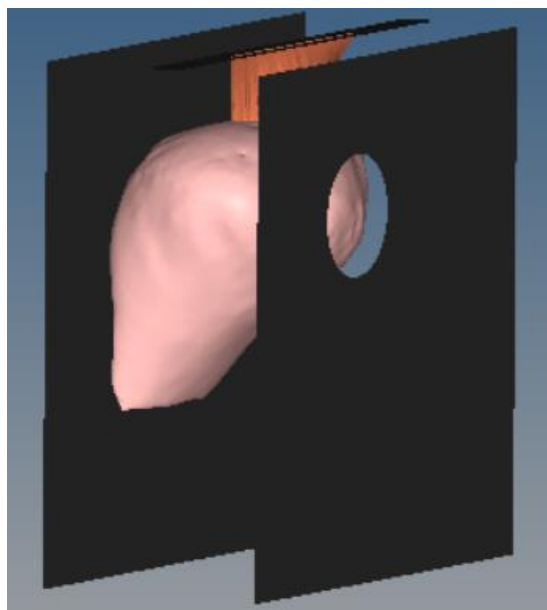The model of the morphotype 2 is illustrated in Fig. C- 22.

Fig. C- 22. General view of the numerical model of morphotype 2

Table C- 11 summarizes the peaks for the curves of the maximal major principal strain and the maximal minor principal strain obtained experimentally, with the standard numerical model and with the model of the liver morphotype 2.

Table C- 11. Comparison of the maximum major and minor principal strain of morphotype 2, generical model and experimental deceleration test of Liver L9

	Morphotype 2	Generic model		Experimental	
		Value	Difference	Value	Difference
Major principal strain (%)	43.45	45.65	4.8%	57.81	24.8%
Minor principal strain (%)	16.85	12.73	32.4%	12.73	32.4%

The time-histories of the principal strains obtained experimentally, numerically with the standard liver model and with the model of the liver morphotype 2 are presented in Fig. C- 23.
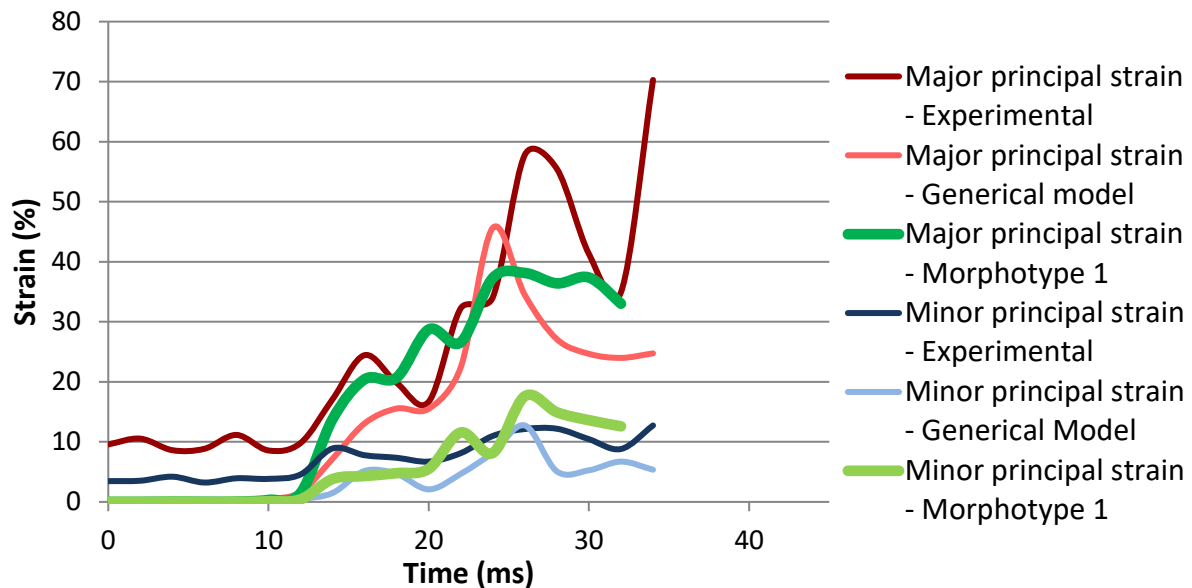

Fig. C- 23. Comparison of experimental deceleration test of Liver L9, generical and morphotype 2 numerical curves of the major and minor principal strain

The contact between the plate and the capsule happened at t=12ms, the peak of strain happened at t=24ms (Fig. C- 24 & Fig. C- 25).
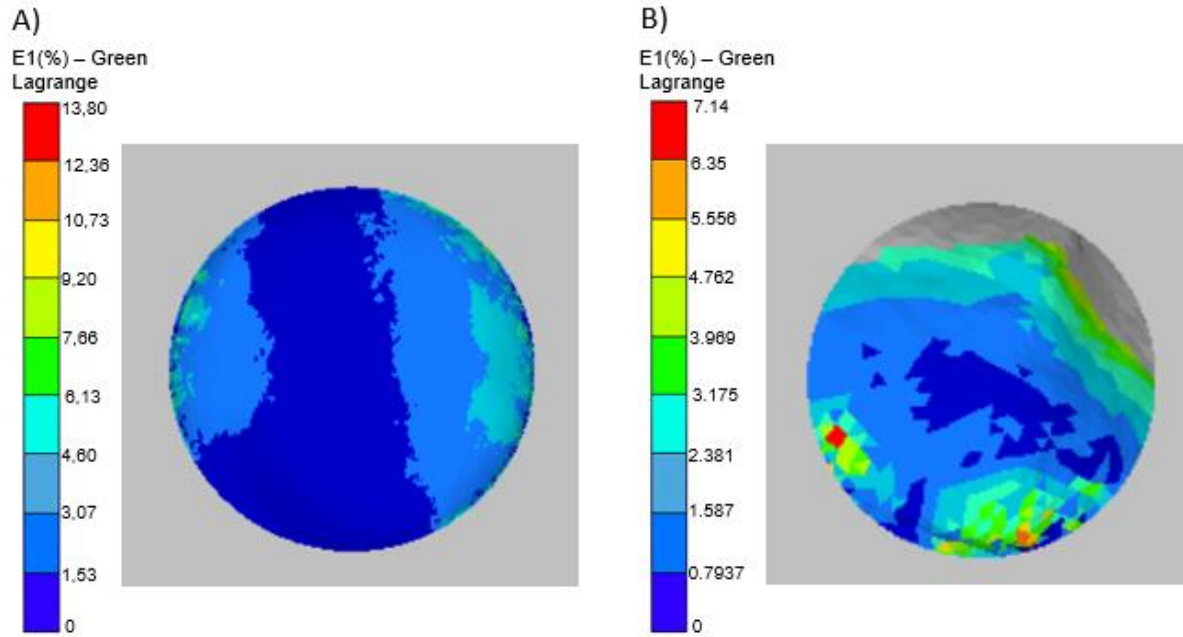

Fig. C- 24. Major principal strain pattern at the contact between the plate and the capsule A) for Morphotype 2 numerical model, B) for generical model

Fig. C- 25. Major principal strain pattern at the peak of strain, A) for Morphotype 2 numerical model, B) for generical model

2.3. Morphotype 3

The model of the morphotype 3 is illustrated in Fig. C- 26.

Fig. C- 26. General view of the numerical model of morphotype 3

Table C- 12 summarizes the peaks for the curves of the maximal major principal strain and the maximal minor principal strain obtained experimentally, with the standard numerical model and with the model of the liver morphotype 3.

Table C- 12. Comparison of the maximum major and minor principal strain of morphotype 3, generical model and experimental deceleration test of Liver L9

Morphotype 3		Generic model		Experimental	
		Value	Difference	Value	Difference
Major principal strain (%)	27.79	45.65	39.1%	57.81	51.9%
Minor principal strain (%)	9.62	12.73	24.4%	12.73	24.4%

The time-histories of the principal strains obtained experimentally, numerically with the standard liver model and with the model of the liver morphotype 3 are presented in Fig. C- 27.

Fig. C- 27. Comparison of experimental deceleration test of Liver L9, generical and morphotype 3 numerical curves of the major and minor principal strain

The contact between the plate and the capsule happened at t=10ms, the peak of strain happened at t=32ms (Fig. C- 28 & Fig. C- 29).

Fig. C- 28. Major principal strain pattern at the contact between the plate and the capsule A) for Morphotype 3 numerical model, B) for generical model
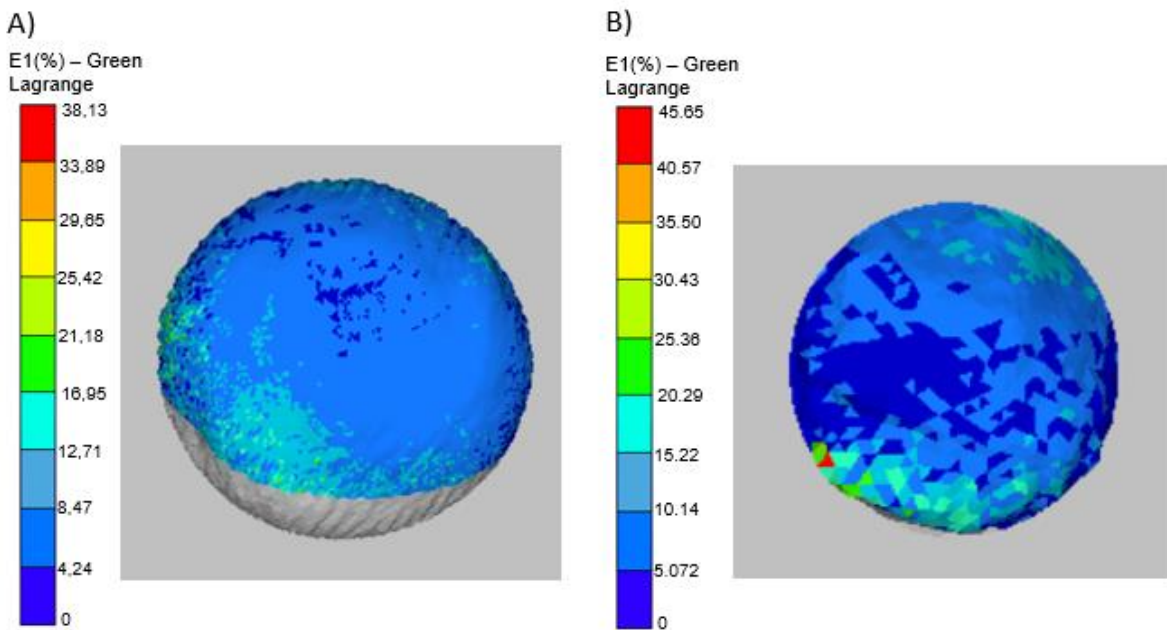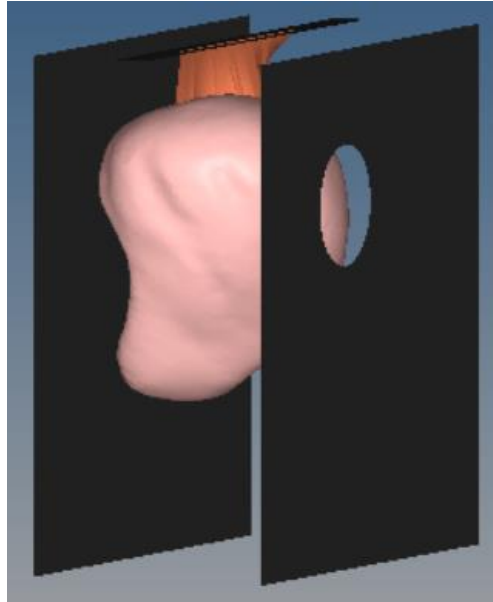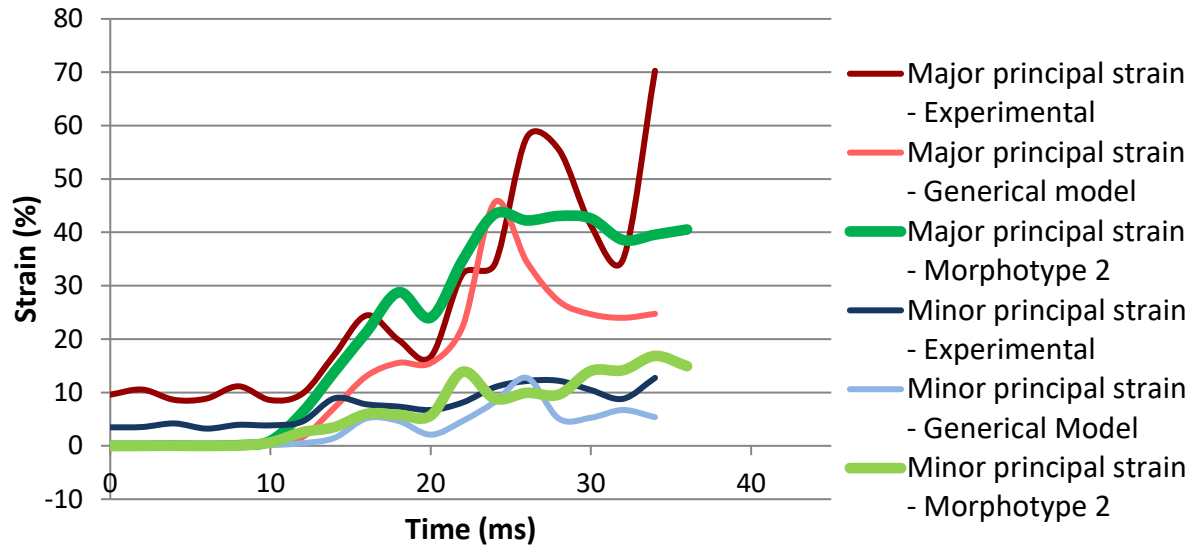

Fig. C- 29. Major principal strain pattern at the peak of strain, A) for Morphotype 3 numerical model, B) for generical model

To compare the numerical results with the experimental ones, we work on the area visible in the reference state. Thus, a part of the capsule is not considered as it become visible due to the movement of the liver.

2.4. Morphotype 4

The model of the morphotype 4 is illustrated in Fig. C- 30.

Fig. C- 30. General view of the numerical model of morphotype 4

Table C- 13 summarizes the peaks for the curves of the maximal major principal strain and the maximal minor principal strain obtained experimentally, with the standard numerical model and with the model of the liver morphotype 4.

Table C- 13. Comparison of the maximum major and minor principal strain of morphotype 4, generical model and experimental deceleration test of Liver L9

	Morphotype 4	Generic model		Experimental	
		Value	Difference	Value	Difference
Major principal strain (%)	35.11	45.65	23.1%	57.81	39.3%
Minor principal strain (%)	18.62	12.73	46.3%	12.73	46.3%

The time-histories of the principal strains obtained experimentally, numerically with the standard liver model and with the model of the liver morphotype 4 are presented in Fig. C- 31.

Fig. C- 31. Comparison of experimental deceleration test of Liver L9, generical and morphotype 4 numerical curves of the major and minor principal strain

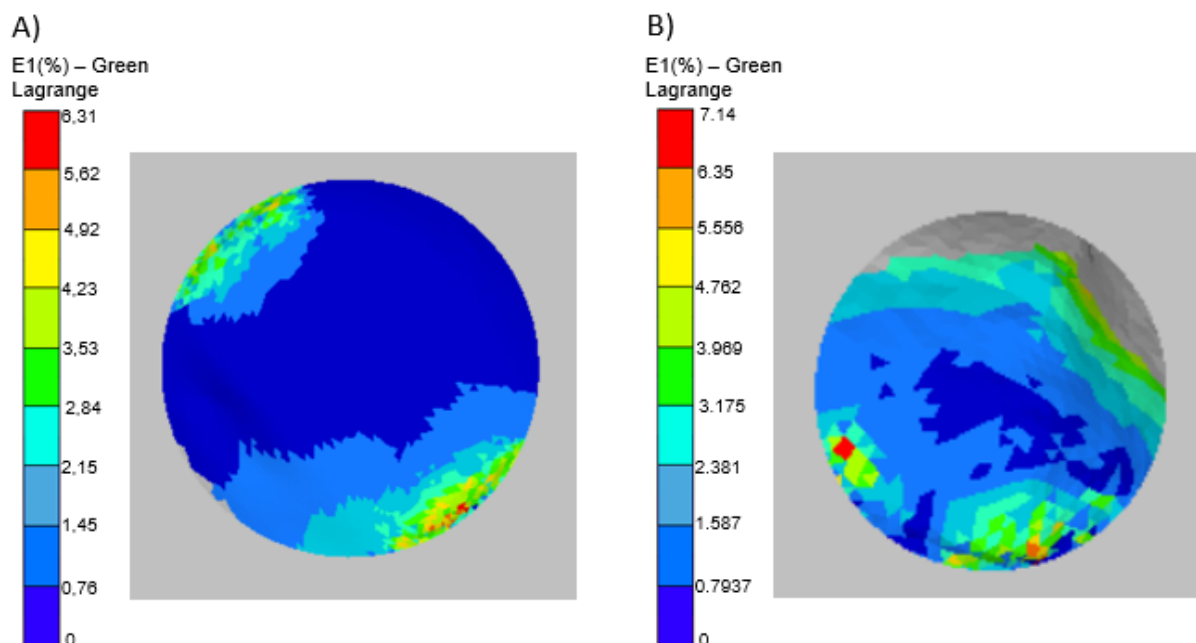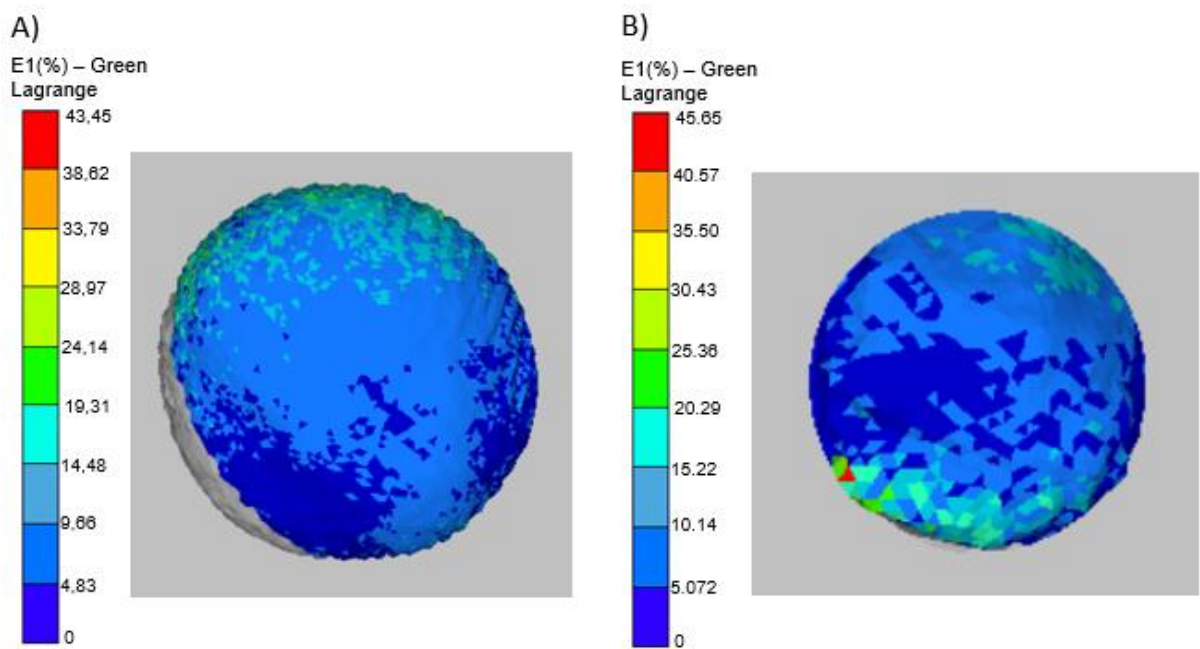The contact between the plate and the capsule happened at t=14ms, the peak of strain happened at t=24ms (Fig. C- 32 & Fig. C- 33).

Fig. C- 32. Major principal strain pattern at the contact between the plate and the capsule A) for Morphotype 4 numerical model, B) for generical model

Fig. C- 33. Major principal strain pattern at the peak of strain, A) for Morphotype 4 numerical model, B) for generical model
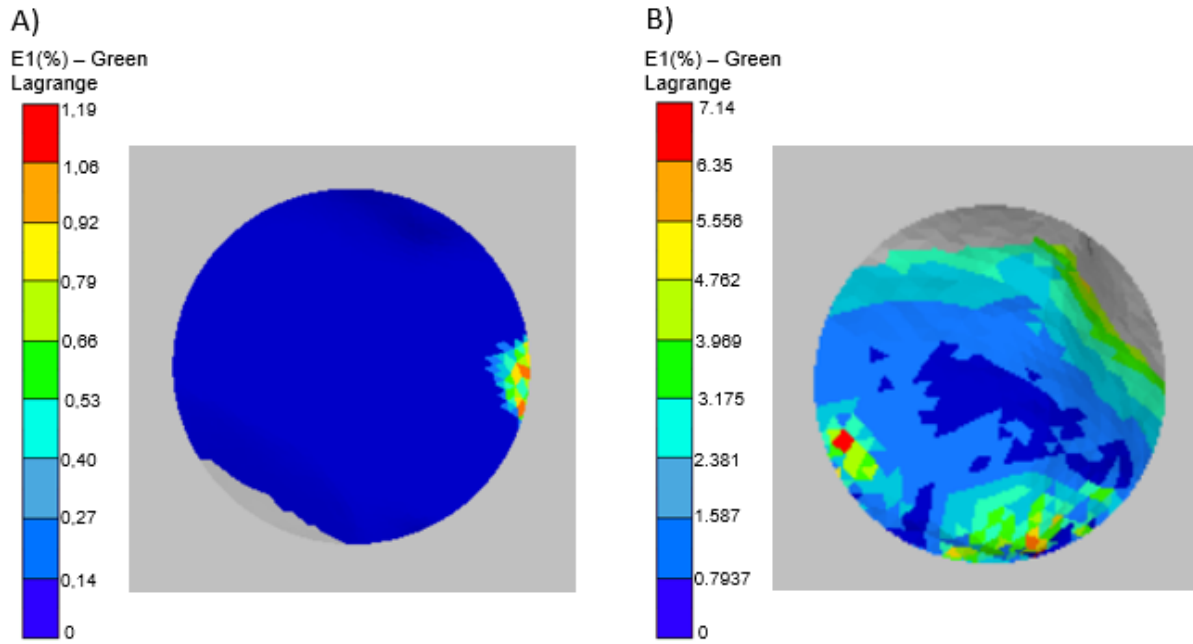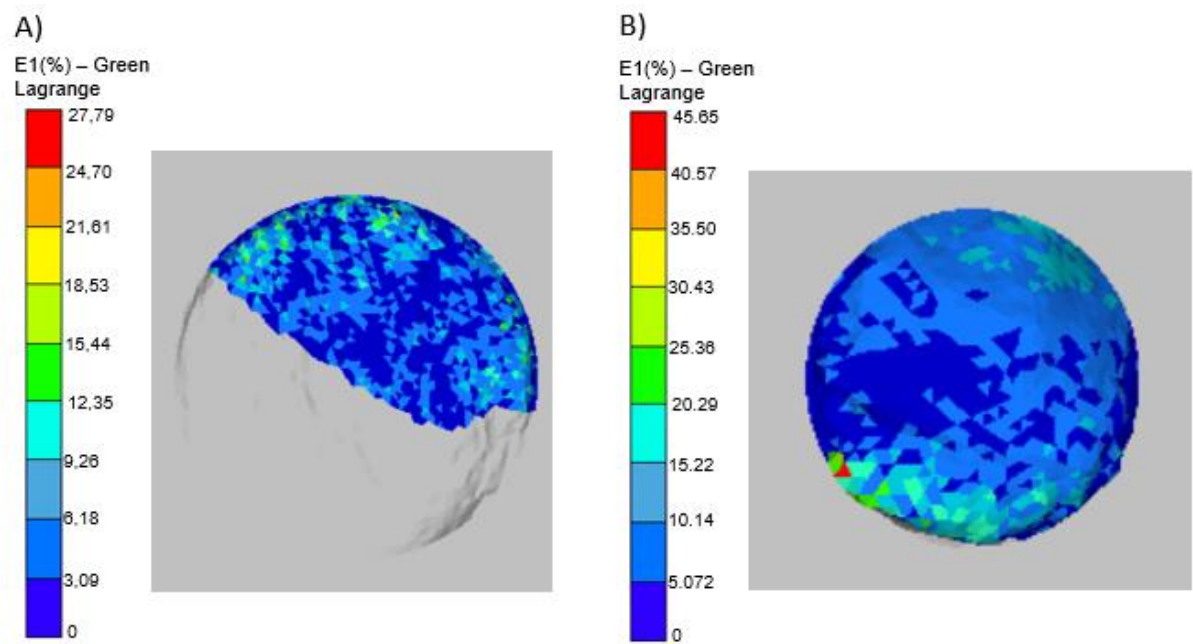
To compare the numerical results with the experimental ones, we work on the area visible in the reference state. Thus, a part of the capsule is not considered as it become visible due to the movement of the liver.

3. Discussion

This study points out that more than mechanical properties, the geometry of the model has a strong influence on the response.

Other authors pointed out this influence in other applications. Indeed, according to Niemeyer et al. (2012), who study over 300 geometries on lumbar spine, geometry has a profound effect on the simulated biomechanics of the lumbar spine. Moreover, in their study, Schoell et al. (2015), worked on age- and sex- specific FE models with change of geometry and mechanical properties. They pointed out that both, geometry and material properties change with age and sex resulting in different responses of the thorax.

Except for Morphotype 3, the volume seemed correlated to the peak of strain. The small peak of strain of Morphotype 3 can be explain by the fact that due to liver movement, only a small part can be analyzed.

As explained in Part B, Chapter 3, lesions appeared when the strain is over 20%. Thus, lesions should appear on those models. It would be interesting to improve our models with the simulation of the rupture to better understand the mechanisms of lesion.

Conclusion

Research question: **Does the morphology of the liver influence the response of numerical models?**

An overview of the literature was carried out and our previous work give us central theme with different key points:

- Modification of a generic model of the liver to reproduce deceleration tests;
- The optimization of the material properties;
- The implementation of the different morphotypes in the generic model.

In Part B, In Chapter 4, deceleration tests were carried out in a physiological condition. It seemed interesting to: **modify a generic model of the liver to reproduce these deceleration tests**.

A first simulation of the deceleration test was performed using a standard liver model, previously developed by Conte (2012) The diaphragm was added and boundary conditions (fixation box, holed plate) modeled using rigid bodies. Loading of the liver was simulated applying the internal pressure measured onto the vessels' wall and applying the measured deceleration to the fixation box

The maximum deflection of the capsule during the test and the maximum major and minor principals' strains on the area of the Glisson's capsule were studied. With our numerical model, we had to: **optimized the material properties.**

Properties of the Glisson's capsule, the vessels and the fixation device were fixed as previous studies pointed out that the properties of the parenchyma have the most influence on the response. A parametric study was carried out, principally on nu and mu1. We compared the maximum deflection experimental and numerical curves, as well as the maximum of major principal strain and the maximum of minor principal strain between experimental and numerical data. This analysis allowed us to find the best fit to reproduce our experimental work.

Finally, as we found out the existence of four morphotypes, it seemed interesting to: **implement the different morphotypes in the generic model.**

The implementation of the four morphotypes on the generic models pointed out the importance of both, the material properties and the geometry in the response of numerical models.

To conclude, the geometry of the liver, and more generally of the organs, should be taken into account **to have a more accurate response of the organ through impact.**

Reference

Ahn, Bummo, and Jung Kim. 2010. "Measurement and Characterization of Soft Tissue Behavior with Surface Deformation and Force Response under Large Deformations." Medical Image Analysis 14 (2): 138–48. doi:10.1016/j.media.2009.10.006.

Arnoux, P. J., L. Thollon, and K. Kayvantash. 2001. "The RADIOSS Human Model for Safety (HUMOS). Model Presentation and Guideline." In Mecalog SARL. Antony, France.

Behr, M., Arnoux, P.J., Serre, T., Bidal, S., Kang, H.S., Thollon, L., Cavallero, C., Kayvantash, K., Brunet, C., 2003. A Human Model for Road Safety: From Geometrical Acquisition to Model Validation with Radioss. Computer Methods in Biomechanics and Biomedical Engineering 6, 263–273. https://doi.org/10.1080/10255840310001606080

Brunon, A., K. Bruyère-Garnier, and M. Coret. 2010. "Mechanical Characterization of Liver Capsule through Uniaxial Quasi-Static Tensile Tests until Failure." Journal of Biomechanics 43 (11): 2221–27.

Brunon, A., K. Bruyère-Garnier, and M. Coret. 2011. "Characterization of the Nonlinear Behaviour and the Failure of Human Liver Capsule through Inflation Tests." Journal of the Mechanical Behavior of Biomedical Materials 4 (8): 1572–81.

Carter, F. J, T. G Frank, P. J Davies, D McLean, and A Cuschieri. 2001. "Measurements and Modelling of the Compliance of Human and Porcine Organs." Medical Image Analysis 5 (4): 231–36. doi:10.1016/S1361-8415(01)00048-2.

Cheng, L., & Hannaford, B. (2015). Finite Element Analysis for evaluating liver tissue damage due to mechanical compression. *Journal of biomechanics*, *48*(6), 948-955.

Chui, C., E. Kobayashi, X. Chen, T. Hisada, and I. Sakuma. 2007. "Transversely Isotropic Properties of Porcine Liver Tissue: Experiments and Constitutive Modelling." Medical & Biological Engineering & Computing 45 (1): 99–106. doi:10.1007/s11517-006-0137-y.

Conte, Cécile. 2012. "Comportement mécanique du foie en contexte traumatique : Rupture et endommagement des tissus." IFSTTAR: Université Claude Aix-Marseille.

Conte, Cécile, Catherine Masson, Nicolas Cheynel, and Pierre-Jean Arnoux. 2009. "On Liver Modelling under Trauma Situations." Journal of Biological Physics and Chemistry 9 (4): pp167–70.

Dan, Diane. 1999. "Caractérisation mécanique du foie humain en situation de choc." Paris: Université Paris 7.

Delingette, H., and N. Ayache. 2005. "Hepatic Surgery Simulation." In ACM, 48(2):31–36.

Foster, C. D., W. N. Hardy, K. H. Yang, A. I King, and S. Hashimoto. 2006. "High-Speed Seatbelt Pretensioner Loading of the Abdomen." Stapp Car Crash Journal 50: 27–51.

Fu, Y. B., & Chui, C. K. (2014). Modelling and simulation of porcine liver tissue indentation using finite element method and uniaxial stress–strain data. *Journal of biomechanics*, *47*(10), 2430-2435.

Haug, E. (2001, November). H-model overview description. In *Proceedings of the Twenty-Ninth International Workshop on Human Subjects for Injury Biomechanics Research.*Huang, Y., A. King, and J. Cavanaugh. 1994. "Finite Element Modeling of Gross Motion of Human Cadavers in Side Impact." In SAE Technical Paper, 19. doi:10.4271/942207.

Iwamoto, M., Y. Kisanuki, I. Watanabe, K. Furusu, K. Miki, and J. Hasegawa. 2002. "Development of a Finite Element Model of the Total Human Model for Safety (THUMS) and Application to Injury Reconstruction." In Proceedings of the 2002 International Research Council on Biomechanics of Injury, 31–42. Munich, Germany.

Jansova, M., L. Hyncik, H. Cechova, J. Toczyski, D. Gierczycka-Zbrozek, and P. Baudrit. 2015. "Evaluation of Human Thorax FE Model in Various Impact Scenarios." Applied and Computational Mechanics 9 (1): 5–20.

Jordan, P., S. Socrate, T. E. Zickler, and R. D. Howe. 2009. "Constitutive Modeling of Porcine Liver in Indentation Using 3D Ultrasound Imaging." Journal of the Mechanical Behavior of Biomedical Materials 2 (2): 192–201. doi:10.1016/j.jmbbm.2008.08.006.

Labe, Alice. 2008. "Etude Des Mécanismes Lésionnels de La Région Abdomino-Pelvienne : Applications À La Traumatologie Virtuelle et À La Sécurité Routière." Aix Marseille 2. http://www.theses.fr/2008AIX22031.

Lee, J.B., and K.H. Yang. 2001. "Development of a Finite Element Model of the Human Abdomen." Stapp Car Crash Journal 45: 79–100.

Maeno, T., and J. Hasegawa. 2001. "DEVELOPMENT OF A FINITE ELEMENT MODEL OF THE TOTAL HUMAN MODEL FOR SAFETY (THUMS) AND APPLICATION TO CAR-PEDESTRIAN IMPACTS." In Proceedings of 17th International ESV Conference, 1–10.

Marchesseau, Stéphanie, Tobias Heimann, Simon Chatelin, Rémy Willinger, and Hervé Delingette. 2010. "Fast Porous Visco-Hyperelastic Soft Tissue Model for Surgery Simulation: Application to Liver Surgery." Progress in Biophysics and Molecular Biology 103 (2-3): 185–96. doi:10.1016/j.pbiomolbio.2010.09.005.

Meier, U., O. López, C. Monserrat, M. C. Juan, and M. Alcañiz. 2005. "Real-Time Deformable Models for Surgery Simulation: A Survey." Computer Methods and Programs in Biomedicine 77 (3): 183–97. doi:10.1016/j.cmpb.2004.11.002.

Milanowicz, M., and K. Kedzior. 2017. "Active Numerical Model of Human Body for Reconstruction of Falls from Height." Forensic Science International 270: 223–31. doi:https://doi.org/10.1016/j.forsciint.2016.10.009.

Reference

Nicolle, S., P. Vezin, and J.-F. Palierne. 2010. "A Strain-Hardening Bi-Power Law for the Nonlinear Behaviour of Biological Soft Tissues." Journal of Biomechanics 43 (5): 927–32. doi:10.1016/j.jbiomech.2009.11.002.

Niemeyer, F., Wilke, H. J., & Schmidt, H. (2012). Geometry strongly influences the response of numerical models of the lumbar spine—a probabilistic finite element analysis. *Journal of biomechanics*, *45*(8), 1414-1423.

Raghunathan, S., D. Evans, and Jessica L. Sparks. 2010. "Poroviscoelastic Modeling of Liver Biomechanical Response in Unconfined Compression." Annals of Biomedical Engineering 38 (5): 1789–1800. doi:0.1007/s10439-010-9957-x.

Robin, S. 2001. "HUMOS: Human Model for Safety–a Joint Effort towards the Development of Refined Human-like Car Occupant Models." In 17th International Technical Conference on the Enhanced Safety Vehicle, 297.

Schoell, S. L., Weaver, A. A., Vavalle, N. A., & Stitzel, J. D. (2015). Age-and sex-specific thorax finite element model development and simulation. *Traffic injury prevention*, *16*(sup1), S57-S65.

Snedeker, Jess G., Brent B. Barnstuble, Paul A. Iaizzo, Mehdi Farshad, Peter Niederer, and Franz R. Schmidlin. 2007. "A Comprehensive Renal Injury Concept Based on a Validated Finite Element Model of the Human Abdomen." The Journal of Trauma 62 (5): 1240–49. doi:10.1097/01.ta.0000215531.05677.19.

Sparks, Jessica L., John H. Bolte, Rebecca B. Dupaix, Kenneth H. Jones, Steven M. Steinberg, Rodney G. Herriott, Jason A. Stammen, and Bruce R. Donnelly. 2007. "Using Pressure to Predict Liver Injury Risk from Blunt Impact." Stapp Car Crash Journal 51 (October): 401–32.

Spitzer, V., M.J. Ackerman, A.L. Scherzinger, and D. Whitlock. 1996. "The Visible Human Male: A Technical Report." JAMIA 3: 118–30.

Tamura, Atsutaka, Kiyoshi Omori, Kazuo Miki, Jong B. Lee, King H. Yang, and Albert I. King. 2002. "Mechanical Characterization of Porcine Abdominal Organs." Stapp Car Crash Journal 46 (November): 55–69.

Taylor, Z. A., O. Comas, M. Cheng, J. Passenger, D. J. Hawkes, D. Atkinson, and S. Ourselin. 2009. "On Modelling of Anisotropic Viscoelasticity for Soft Tissue Simulation: Numerical Solution and GPU Execution." Medical Image Analysis 13 (2): 234–44. doi:10.1016/j.media.2008.10.001.

Terzopoulos, D., and K. Fleischer. 1988. "Deformable Models." The Visual Computer 4: 306–31.

Umale, Sagar, Simon Chatelin, Nicolas Bourdet, Caroline Deck, Michele Diana, Parag Dhumane, Luc Soler, Jacques Marescaux, and Remy Willinger. 2011. "Experimental in

Vitro Mechanical Characterization of Porcine Glisson's Capsule and Hepatic Veins." Journal of Biomechanics 44 (9): 1678–83. doi:10.1016/j.jbiomech.2011.03.029.

Vavalle, N.A., D.P. Moreno, A.C. Rhyne, J.D. Stitzel, and F.S. Gayzik. 2013. "Lateral Impact Validation of a Geometrically Accurate Full Body Finite Element Model for Blunt Injury Prediction." Annals of Biomedical Engineering 41 (3): 497–512.

Zhao, J., and G. Narwani. 2005. "DEVELOPMENT OF A HUMAN BODY FINITE ELEMENT MODEL FOR RESTRAINT SYSTEM R&D APPLICATIONS." In The 19th International Technical Conference on the Enhanced Safety of Vehicles (ESV).

CONCLUSION AND PERSPECTIVES

The study of the variability of the liver geometry from scanner of 78 patients allowed to define four morphotypes. Each of these morphotypes was associated to more global characteristics of a person: his age and his thoracic circumference. A small liver slightly covered by the ribcage, with a moderate development of the left lobe was associated to women under the age of 50, with an abdominal perimeter not exceeding 85 cm and a thoracic perimeter not exceeding 75 cm. A large liver partially covered by the ribcage, with a small development of the left lobe was associated with women under the age of 50, with an abdominal perimeter exceeding 85 cm and a thoracic perimeter around 75 cm. A large liver partially covered by the ribcage with a moderate development of the left lobe was associated with men around the age of 50, with an abdominal perimeter exceeding 85 cm and a thoracic perimeter exceeding 75 cm. Finally, a small liver completely covered by the ribcage with a large development of the left lobe was associated with women over the age of 50, with an abdominal perimeter exceeding 85 cm and a thoracic perimeter not exceeding 75 cm.

It would be interesting to add more characteristics to the study as the height and the weight of the individuals. Moreover, another study to determine the influence of the operator on the placement of the different points, which determine the characteristics length of the liver, must be carried out.

The second objective of the thesis was to bring new experimental data on the mechanical behavior of the liver. In order to develop and validate numerical models of the liver, isolated organs tests are useful for completing full body tests. They make possible to better control the boundary conditions, specifically to reproduce *in vivo* conditions, and offer the possibility of observing the organ more easily. The first experimental test that we conducted allowed to evaluate the strain state of the Glisson capsule by 3D digital image correlation according to different levels of pressurization of the liver and on isolated samples. We found out that pressurization have a significant effect on the state strain of the capsule. We highlighted that ultimate strain obtained by tests on isolated sample may be underestimated due to initial gravity effect for samples with a large ratio (Length/Width) and overestimated due to the pre-strain release on sample with a small ratio (Length/Width). The second experimental theist that we conducted aimed at identifying the local ultimate strain during a frontal impact of the liver through deceleration tests. In this test, the right lobe of the liver impacts on the holed plate that over-pressurized locally the capsule up to rupture. The preservation of the livers in Winckler seemed to reduce the variability of the liver mechanical response, and lacerations could be observed only on livers preserved with Safebalm®.

It would be interesting to reproduce these deceleration tests and record the real pressure in the liver. Moreover, for further deceleration tests, the fixation box must be improving to better maintain the liver during the tests and avoid the pendulum movement of the liver. Finally, the pressurization tests must be followed by traction test on the samples to determine the ultimate strain on samples.

In a third part, a generic numerical model of the liver was used to simulate the deceleration tests performed in the experimental part. This generic liver was established by Conte (2012) in previous study on the liver. As this previous work was validated thanks to experimental work carried out on livers preserved with Winckler, an optimization phase was needed to determine material properties from validation data obtained on a liver preserved with Safebalm ®. Then to highlight the importance of the morphology on the mechanical response of the liver, the different liver-types corresponding to the different morphotypes identified in the first part were modeled. This study pointed out that both, the material properties and the geometry of the organ is important to have an accurate numerical model.

In a previous study, Studer et al (2015) pointed out the existence of three morphotypes of spleen and they found out a connection between a type of spleen and a type of liver. Thus, "cupped" shape spleens are linked with a large liver partially covered by the ribcage, with small development of the left lobe, and "convex" shape spleen as well as "flat" shape spleen are linked with a small liver slightly covered by the ribcage, with a moderate development of the left lobe, or a large liver partially covered by the ribcage, with a moderate development of the left lobe, or a small liver completely covered by the ribcage with a large development of the left lobe. Then, a total of seven models could be developed to represent the different spleen-liver system of the overall population. The identification of the morphology of the different organs of the abdominal segment and these modelling can help to identify possible over-risks of abdominal injuries in case of road accident.

APPENDIX

APPENDIX C-1: Information about numerical models of the four morphotypes

The four parenchyma were meshed with tetra elements. Information on meshes is given in Table AC- 1 & Table AC- 2 for each morphotype

Table AC- 1. Information on the mesh of each morphotype parenchyma

	Number of nodes	Number of elements (TETRA)	Size of elements (mm)	Angles between elements (°)	Aspect ratio
Morphotype 1	336 770	1 683 857	0.03 – 11.39	7.27 – 163.82	10.44
Morphotype 2	230 745	1 152 477	0.03 – 11.45	5.53 – 153.77	7.35
Morphotype 3	207 509	1 061 234	0.10 – 10.92	5.68 – 156.97	5.61
Morphotype 4	206 227	1 036 676	0.05 – 8.77	6.75 – 163.88	6.96

Table AC- 2. Distribution of the size of the volume elements for each morphotype

Percentile	minimum	5th	10th	25th	50th	75th	90th	95th	maximum
Morphotype 1	0.03	0.54	0.60	0.74	0.93	1.23	1.69	2.10	10.83
Morphtoype 2	0.03	0.72	0.80	0.95	1.18	1.51	2.02	2.47	11.45
Morphotype 3	0.10	0.68	0.80	1.03	1.35	1.75	2.25	2.63	10.92
Morphotype 4	0.05	0.63	0.71	0.87	1.09	1.39	1.82	2.16	8.77

Even if the aspect ratio is over 5, the number of elements involved represent 0%. Thus, the quality of the mesh is considered good.

The four Glisson capsules were meshed with shell triangular elements. Information on meshes is given in Table AC- 3 & Table AC- 4 for each morphotype.

Table AC- 3. Information on the mesh of each morphotype Glisson capsule

	Number of nodes	Number of elements (TRIA)	Size of elements (mm)	Angles between elements (°)	Aspect ratio
Morphotype 1	76 566	152 835	0.07 – 4.26	11.68 – 141.35	4.97
Morphotype 2	50 387	100 539	0.1 – 4.43	11.63 – 141.33	4.98
Morphotype 3	35 253	70 314	0.3 – 6.09	5.68 – 156.97	4.99
Morphotype 4	38 459	76 688	0.1 – 4.09	11.33 – 141;65	4.99

Table AC- 4. Distribution of the size of the volume elements for each morphotype

Percentile	minimum	5th	10th	25th	50th	75th	90th	95th	maximum
Morphotype 1	0.07	0.63	0.69	0.81	0.96	1.15	1.32	1.44	4.26
Morphtoype 2	0.1	0.93	1.01	1.15	1.30	1.43	1.56	1.65	4.43
Morphotype 3	0.3	1.24	1.33	1.49	1.67	1.83	1.98	2.10	6.09
Morphotype 4	0.1	0.87	0.95	1.09	1.25	1.41	1.55	1.66	4.09

The four intrahepatic vessels were meshed with shell triangular elements. Information on meshes is given in Table AC- 5 & Table AC- 6 for each morphotype.

Table AC- 5. Information on the mesh of each morphotype intrahepatic vessel

		Number of nodes	Number of elements (TRIA)	Size of elements (mm)	Angles between elements (°)	Aspect ratio
Morphotype 1	Vena cava	18 891	37 778	1	10.95 – 139.70	4.99
	Portal vein	13 818	27 635	1	11.04 – 140.60	4.97
Morphotype 2	Vena cava	13 565	27 126	1	11.55 – 139.13	4.99
	Portal vein	12 186	24 368	1	11.17 – 140.28	4.97
Morphotype 3	Vena cava	15 924	31 837	1	11.27 – 141.05	5.00
	Portal vein	7 479	14 938	1	11.39 – 140.77	4.99
Morphotype 4	Vena cava	18 357	36 710	1	11.20 – 140.67	4.99
	Portal vein	9 727	19 450	1	11.21 – 139.53	4.98

Table AC- 6. Distribution of the size of the volume elements for each morphotype

Percentile		minimum	5th	10th	25th	50th	75th	90th	95th	maximum
Morphotype 1	Vena cava	0.04	0.57	0.65	0.76	0.89	1.04	1.19	1.33	5.63
	Portal vein	0.06	0.51	0.61	0.73	0.85	0.98	1.10	1.19	3.78
Morphtoype 2	Vena cava	0.04	0.76	0.86	1.01	1.15	1.30	1.45	1.56	6.00
	Portal vein	0.1	0.65	0.79	0.94	1.08	1.21	1.37	1.48	4.05

Morphotype 3	Vena cava	0.12	0.50	0.62	0.87	1.07	1.27	1.44	1.55	4.54
	Portal vein	0.17	0.45	0.54	0.76	1.00	1.21	1.41	1.53	4.59
Morphotype 4	Vena cava	0.07	0.45	0.57	0.82	1.02	1.17	1.34	1.48	3.53
	Portal vein	0.1	0.59	0.75	0.91	1.04	1.17	1.30	1.39	4.58